Editors' choice

# Dinosaur "mummification": Clay templating in a fluvial setting preserves three-dimensional integument renderings after carcass desiccation

EVAN T. SAITTA, PAUL C. SERENO, DANIEL VIDAL, MARIA CIUDAD REAL, TYLER M. KEILLOR, LAUREN BOP, STEPHANIE L. BAUMGART, AIDAN BURDICK, VIKTOR J. RADERMACHER, THOMAS G. KAYE, LAURE DUSSUBIEUX, EVAN MAXEY, ALEXANDER S. FILATOV, and XINQI CHEN

Saitta, E.T., Sereno, P.C., Vidal, D., Ciudad Real, M., Keillor, T.M., Bop, L., Baumgart, S.L., Burdick, A., Radermacher, V.J., Kaye, T.G., Dussubieux, L., Maxey, E., Filatov, A.S., and Chen, X. 2026. Dinosaur "mummification": Clay templating in a fluvial setting preserves three-dimensional integument renderings after carcass desiccation. *Acta Palaeontologica Polonica* 71 (3): 535–579.

Dinosaur "mummies" preserve large areas of three-dimensional, wrinkled, desiccated integument renderings enveloping articulated skeletons. The majority of dinosaur "mummies" are "duck-billed" hadrosaurids in desiccated death poses that were buried in Late Cretaceous fluvial sandstones, such as in the Lance and Hell Creek formations of western North America, and unlike the lacustrine, marshy, or shallow marine sediments of many Konservat-Lagerstätten. Although first described in 1912, the structural and chemical nature of these renderings and the steps leading to their formation have only recently begun to be explored in detail. Hypotheses about the mode and mechanism of "mummy" preservation have varied widely, from simple impressions in sediment to near-pristine retention of organic tissues or biomolecules. Two newly described "mummies" of the Late Cretaceous hadrosaurid *Edmontosaurus annectens* were subjected to a wide range of modern structural and chemical analyses. These specimens come from a several-kilometer region in east-central Wyoming, USA, near the top of the Maastrichtian Lance Formation that has produced multiple of the best-preserved "mummy" dinosaurs over the course of the last century. These two "mummies" preserve exceptional integument renderings, including skin/scales, tail spikes, and hooves. We characterized how the three-dimensional form of the integument is preserved and whether any original tissue structure or organic biomolecules remain. We find little evidence for any endogenous organic preservation or internal tissue structure. Instead, these "mummies" likely desiccated sub-aerially for a period of time before rapid burial and infilling of the carcass by fluvial sands. Next, organic decay induced preservation of their outermost integumentary surface largely via microbially induced clay templating (a < 1 mm, predominantly kaolinite/partly illite, external "death mask"). In places, microbially induced precipitation of iron compounds (e.g., pyrite) as stains/concretions occurred, although some of these precipitates might also appear during or be altered by late-stage weathering (e.g., iron oxides, manganese oxides). Dinosaur "mummies" are rare examples of high-fidelity mineral templating of soft tissues in Mesozoic animals, a taphonomic mode better studied in far older, invertebrate fossils of Paleozoic or Precambrian marine Lagerstätten. The "mummies" are also closely associated with fossil plant material, suggesting that the sediments were not organic-limited. Future work should characterize variation in the composition of fossilized dinosaur integument, determine if any endogenous organic or inorganic compounds from the integument preserve in other "mummies", determine which mineral precipitates are early-stage and induced by decay versus late-stage and induced by subsurface oxidative weathering, and look for bacterial biomarkers (e.g., hopanoids) in the integument template.

Key words: Dinosauria, *Edmontosaurus*, clay templating, integument rendering, dinosaur mummification, taphonomy, Late Cretaceous.

*Evan T. Saitta [evansaitta@gmail.com; ORCID: https://orcid.org/0000-0002-9306-9060] and Laure Dussubieux [ldussubieux@fieldmuseum.org; ORCID: https://orcid.org/0000-0002-9334-8131], Integrative Research Center, Field Museum of Natural History, 1400 S Lake Shore Dr, Chicago, 60605 IL, USA.*

*Paul C. Sereno [dinosaur@uchicago.edu; ORCID: https://orcid.org/0000-0001-7958-3701], Department of Organismal Biology & Anatomy, University of Chicago, Anatomy Bldg, 1027 E 57th St, Chicago, 60637 IL, USA; Committee on Evolutionary Biology, Chicago, IL, USA.*

*Daniel Vidal [dvidal@uchicago.edu; ORCID: https://orcid.org/0000-0002-6054-1357] and Maria Ciudad Real [paleobiologa@gmail.com; ORCID: https://orcid.org/0009-0007-8342-0658], Grupo de Biología Evolutiva, UNED, Paseo Senda del Rey 9, 28040 Madrid, Spain.*

*Tyler M. Keillor [tkeillor@uchicago.edu; ORCID: https://orcid.org/0009-0001-4830-2513] and Lauren Bop [conroy1@uchicago.edu; ORCID: https://orcid.org/0000-0002-2799-4792], Department of Organismal Biology & Anatomy, University of Chicago, Anatomy Bldg, 1027 E 57th St, Chicago, 60605 IL, USA.*

*Stephanie L. Baumgart [sbaumgart@ufl.edu; ORCID: https://orcid.org/0000-0001-9534-7389], Department of Physiology and Aging, University of Florida College of Medicine, 1345 Center Drive, Gainesville, 32610 FL, USA.*

*Aidan Burdick [aidanburdick2026@u.northwestern.edu; ORCID: https://orcid.org/0000-0002-1551-8975], Department of Earth and Planetary Sciences, Northwestern University, 2145 Sheridan Road, Evanston, 60208 IL, USA.*

*Viktor J. Radermacher [viktor.radermacher@wits.ac.za; ORCID: https://orcid.org/0000-0001-6524-7811], Evolutionary Studies Institute, University of the Witwatersrand, 1 Jan Smuts Avenue, Braamfontein, Johannesburg, 2000, South Africa; Karoo Origins Fossil Centre, Graaff-Reinet, South Africa; Department of Earth & Environmental Sciences, University of Minnesota, Minnesota, USA.*

*Thomas G. Kaye [tom@tomkaye.com; ORCID: https://orcid.org/0000-0001-7996-618X], Foundation for Scientific Advancement, 7023 Alhambra Dr, Sierra Vista, AZ 85658, USA.*

*Evan Maxey [emaxey@anl.gov; ORCID: https://orcid.org/0000-0001-7519-5277], Argonne National Laboratory, 9700 S. Cass Avenue, Lemont, 60439 IL, USA.*

*Alexander S. Filatov [afilatov@uchicago.edu; ORCID: https://orcid.org/0000-0002-8378-1994], Department of Chemistry and James Franck Institute, University of Chicago, 5735 S Ellis Ave, Chicago, 60637 IL, USA.*

*Xinqi Chen [xchen@northwestern.edu; ORCID: https://orcid.org/0000-0003-0413-4893], Keck Interdisciplinary Surface Science (Keck-II) Center, NUANCE Center, Northwestern University, 2145 Sheridan Road, Evanston, 60208 IL, USA.*

Received 3 March 2026, accepted 1 June 2026, published online 14 September 2026.



# Introduction

## Dinosaur "mummies" and the concept of "skin impressions"

Osborn's seminal 1912 paper on the fossilized skeleton of a "duckbill" dinosaur established the term dinosaur "mummy" (Osborn 1912: 41) for those rare fossil skeletons associated with extensive integument renderings, which he termed "skin impressions". Despite widespread usage, both of Osborn's terms have serious drawbacks when directly applied to the fossil record. A "mummy" is popularly thought of as a human or animal with integument and other soft tissues preserved via an embalming process invented in ancient Egypt. The term has gained broader application to include humans or animals with soft tissues preserved by various mechanisms that halt decay, such as desiccation, freezing, or some combination of human and natural agencies (Carpenter 2007). By this broader definition, the oldest human mummies predate those in Egypt by several millennia (Lynnerup 2007).

Applying the "mummy" concept considerably farther back in time to a duckbill dinosaur begs a further question: what if a desiccated mummy lost all original organic content in decay or subsequent diagenesis? What if no tissue layers or any original biomolecules remain? More than a century ago, Osborn (1912: 35, 41) anticipated this circumstance, describing an "extremely thin 'impression layer'" composed of "clayey elements" that made a "perfect cast of all the epidermal markings". Osborn did not believe any of the original integument was preserved: "This is invariably an impression cast, for there is no indication of the preservation of the epidermis itself."

"Skin impression", by Osborn's own account, does not accurately describe either the original dehydrated tissues or his inferred cast. True integument impressions are true negative relief surfaces generated by physically pressing integument into soft, fine-grained sediment (Currie et al. 1991; Sereno et al. 2026). Although Osborn (1912: 46) came to describe the integument rendering as an "impression-cast", "skin impression" is the term that would be regularly adopted by subsequent paleontologists.

In this paper, we use "mummy" to describe a fossilized skeleton associated with extensive integument renderings, no matter how they were generated. We use "integument rendering" rather than "skin impressions" to denote negative or positive relief fossils in the sense that they are generated by soft tissue integument. Using the term "rendering" in place of "impression" acknowledges the presence of a version, or facsimile of the surface, of integument without implying anything about its genesis, the presence or absence of internal structure, or its material composition (Sereno et al. 2026). In the century that has elapsed since Osborn's (1912) paper, the structural and chemical nature of the integument renderings of dinosaur "mummies" and their stepwise formation have yet to be sufficiently clarified. We perform an array of analyses (Table 1) on two newly described "duckbill mummies" of *Edmontosaurus annectens*, both of which come from the upper portion of the Lance Formation (Maastrichtian) very near the area in east-central Wyoming that yielded Osborn's "mummy" (Sereno et al. 2026).

## Past dinosaur "mummification" hypotheses

*Sternberg's musings*.—The first recognized *Edmontosaurus* "mummy" (AMNH 5060) was found in 1908 by the Sternberg family in the Lance Creek area of eastern Wyoming (Sternberg 1909), only a few kilometers from the two specimens studied here (Sereno et al. 2026). Charles H. Sternberg, fossil collector extraordinaire, proposed a death and burial scenario for the specimen. The earliest taphonomic pathway proposed involved a "float and bloat" scenario. In a popular account of the discovery, Sternberg (1909: 274–276) suggested that the animal died in deep water and that the carcass became bloated by gas during decay, floated in the currents, eventually ruptured and sank to the river bottom for burial. He suggested that the close adherence of the skin to many parts of the skeleton was due either to gas escape or sediment compaction during burial (Sternberg 1909; see also Sternberg 1970), with a lively account of how the beast may have "broken its neck" or "choked to death or drowned", its "front limbs stretched out as if imploring aid, while the hind limbs in a convulsive effort were drawn up and folded against the abdomen" (Sternberg 1909: 274–276). He accurately described the enveloping matrix as sandstone but also claimed that it had special preservation potential as an antiseptic peat bog. He described the skeleton as coming to rest on a river bottom of mud.

The position and pose of the skeleton, the form and close adherence of integument to underlying bone, and the nature of the surrounding sediment offer abundant evidence contrary to almost every aspect of this scenario. The supine position with the carcass resting on one side of its ribcage, outstretched forelimbs, hyper-flexed neck and hind limbs, and lack of any evidence of injury or scavenging all suggest the typical position of a carcass that has succumbed to drought, quite possibly on a dry riverbed (Carpenter 2007). The wrinkling of the thin integument of the torso is clear evidence of subaerial desiccation, and the surrounding massive sandstone, which lacks appreciable mud or mud horizons, suggests rapid burial by ensuing floodwaters.

*Osborn's desiccation-flood cycle*.—Later, Osborn (1911, 1912) critiqued Sternberg's scenario along the lines suggested above. He remarked that the AMNH mummy suffered a "natural death" (Osborn 1912: 41) outside of water (e.g., in a dried riverbed during a drought). He proposed that this death was followed by desiccation under sun exposure, eliminating the more decay prone tissues, such as muscle and internal organs, while shrinking the now wrinkled, folded, and "leathery" skin onto the bones. Only later was the carcass modestly transported and buried by annual floodwaters at the end of the dry season (Osborn 1911, 1912).

There is a common taphonomy in dry habitats for large-bodied vertebrates, including humans, that involves rapid deflation and dehydration. In this sense, the early taphonomy of dinosaur "mummies" might in some ways be similar to natural human mummies, with skin desiccating and becoming better stabilized over long periods of time through the action of dehydration reactions and cross-linking of dermal proteins such as collagen (Jones et al. 2016), a sort of natural analogy to artificial tanning processes (Covington 2009).

Osborn (1911, 1912) cited the presence of sufficient clay elements in the otherwise poorly cemented sandstone matrix to have generated a replacement cast of the outer margin of the integument. He observed the thin, fragile lamina composing the fossil integument, much of which he noted was lost inadvertently during excavation. We support most of Osborn's (1911, 1912) insightful description and interpretations, although we question the genesis of the integument lamina as a replacement cast. It is Osborn's (1911, 1912) taphonomic hypothesis that has largely influenced subsequent interpretations (Manning 2008).

*Carpenter's mass death, drought-flood cycle*.—Carpenter (1987, 2007) highlighted additional details on drought-related mass death assemblages in seasonally dry and flooded habitats. As drought proceeds, animals are drawn to shrinking riverways, some dying on the dry riverbed within the channel. This allows rapid burial upon the return of floodwaters with minimal or no transport. The overabundance of carcasses in drought-related death, in addition, overwhelms the limited scavenging that otherwise may commence prior to or immediately after death. Subsequent research has shown the prevalence of a cyclic monsoonal weather system for coastal habitats along the North American Seaway in the Late Cretaceous (Fricke et al. 2010). Note that the terminology around what constitutes "rapid burial" can be inconsistent across publications, conflating the time between death and burial (which can be offset by a prolonged period of subaerial desiccation prior to flooding) with the rate of sedimentation during burial itself. Herein, we refer to the latter—"rapid" means that sedimentation rate was high during burial, albeit delayed after death.

Carpenter (2007) described post-burial phases of mummification in some detail, although differing from the conclusions we draw below. He drew on the literature of biofilms during decay of the skin to suggest the deposition of minerals by bacteria, describing a "halo of mineralization" (Carpenter 2007: 13) exterior to the mummy, which was then infilled with sand. He regarded the minerals most likely involved to be groundwater-transported carbonates, including iron carbonates, deposited in an anaerobic setting. Carpenter (2007) did not have direct access to the specimens or thin sections of the integument renderings, and he did not connect biofilms with the deposition of a clay template, unlike Sereno et al. (2026). We did not find evidence to support the creation of such a mineralized integument halo subsequently infilled by sand.

Recently, Drumheller et al. (2022) challenged the limited-scavenging model, using the evidence of vertebrate feeding preserved in the fossilized integument rendering of the Hell Creek Formation (Maastrichtian) of North Dakota *Edmontosaurus* "mummy" ("Dakota", NDGS 2000, formerly MRF-03) to suggest that incomplete scavenging might

also promote the escape of decomposition-related gasses and fluids out of the carcass, enhancing desiccation of the integument prior to rapid burial.

*"Wet environment" mummification hypothesis*.—Manning (2008) and Manning et al. (2009) described the "mummification" process in two hadrosaurid specimens, the first a subadult specimen of *Brachylophosaurus canadensis* ("Leonardo" JRF 115H) from the Judith River Formation (Campanian) of Montana and the second an adult specimen of *Edmontosaurus* cf. *annectens* ("Dakota", NDGS 2000) from the Hell Creek Formation (Maastrichtian) of North Dakota. "Wet environment mummification" was proposed for the *Brachylophosaurus* "mummy", because of the lack of evidence of "an arid environment" according to Manning (2008: 131–132). The authors revert to Sternberg's (1909) suggestion that wrinkling of the integument rendering was caused by sediment compression after burial in a massive sandstone at or immediately following death (see also Lingham-Soliar 2014), which in our view is implausible. The integument rendering itself was described as an "integument trace" or "integument boundary" but not characterized in terms of thickness or composition. It seems at some point, carbonate deposition occurred around much of the skeleton.

At face value from published images, the *Brachylophosaurus* "mummy" is very similar to those of *Edmontosaurus*, showing a high degree of articulation, cervical and caudal hyperextension, integument wrinkling and close association to underlying bone, and the absence of scavenging. Subaerial desiccation is the obvious explanation for these features, followed by rapid burial in a channel with infilling of a breached carcass by a massive influx of sand sediment. There appears to be no basis for erecting a new pattern of "wet environment" mummification.

For the *Edmontosaurus* mummy, Manning et al. (2009) suggested it was buried on the margins of a sandy river channel. They described a "skin thickness" of 2.5 and 3.5 mm, which indeed would be very thin were it to represent the full integument of a multi-ton herbivore. They described "mineralized soft-tissue structures" in the "skin envelope" and "ungual phalanx sheath," including the differentiation of the epidermis, also said to measure about 3.5 mm in thickness, as well as individual skin cells (Manning et al. 2009: 3433).

Considering the same *Edmontosaurus* mummy, Drumheller et al. (2022) accepted the replacement-cast hypothesis (sensu Sereno et al. 2026), adding evidence of modest scavenging of the carcass. They suggested an "alternate fossilization pathway" involving a longer subaerial duration of "weeks or months, until sediment from the adjacent river buried the remains" (Drumheller et al. 2022: 18), rather than immediate burial. The preservation of integument renderings on the mid-section of the tail (scales, spikes) and CT scan of the manus (Drumheller et al. 2022: figs. 3 and 8) look very similar to those we obtained for our mummies (Sereno et al. 2026)—there is little evidence of preserved layers inside the thin, external envelope of the integument rendering. We await fuller description of the composition of the integument rendering and a detailed comparison of internal and external matrix to know how closely NDGS 2000 resembles the new Lance Formation UCRC "mummies".

*Organic retention hypotheses*.—Hypotheses proposed to explain dinosaur "mummification" have broadened over time. On one extreme, the fossilized integument has been described as simple molds and casts in the sediment rather than the preserved skin itself or even a unique sedimentological layer. Such fossils would be lacking in original, endogenous compounds and be entirely inorganic. On the other extreme, there have been recent trends in molecular taphonomy to propose diverse biomolecular signatures and histological structures in dinosaur "mummy" integument. The fossilized integument rendering of "mummies", such as *Edmontosaurus* (NDGS 2000), has been proposed to preserve not just the external morphology of scales, but also subdermal tissue structures under histological thin section as well as endogenous "keratin" amino acids or even proteins (Manning et al. 2009).

Similarly, Barbi et al. (2019) suggested carbonaceous preservation of the stratum corneum layer in an *Edmontosaurus* specimen from Alberta, Canada (UALVP 53290), with small patches of fossilized skin preserved predominantly as carbonyl and even containing cellular structures. However, they also noted that the integument layer was enriched in iron and kaolinite laminae and that the cellular structures are surrounded by calcium carbonate with iron inside.

Other fossil hadrosaur integument rendering specimens (e.g., YPMPU 016969) have likewise been suggested to preserve extensive organic material (Fabbri et al. 2020) through oxidative cross-linking and polymerization of biomacromolecules (e.g., between proteins and lipids), rather than unaltered proteins. These "protein fossilization products" are said to allow for the preservation of organic extracellular matrix, dermal cells, and blood vessels (Wiemann et al. 2018). These cross-linked polymers are formed from chemical reactions that could occur under relatively oxic, subaerial exposure and desiccation of the skin. All of these hypotheses imply that the fossil integument of these dinosaur "mummies" should consist predominantly of organic material, rich in C and N.

## Is there pervasive biomolecular or histological preservation in "mummy" dinosaurs?

We are skeptical of the evidence used to make claims of extreme biomolecular and histological preservation in the integument of "mummy" dinosaurs (see Sereno et al. 2026). Namely, we are not fully convinced that (i) the majority, or even prominent percentage, of the fossilized integument is preserved organically, (ii) that histological features such as cells and vessels preserve, and (iii) that relatively intact amino acids or polypeptides preserve.

Using samples of integument near the ungual sheath, Manning et al. (2009) employed backscattered electron microscopy (BSE), scanning electron microscopy (SEM), electron microprobe analysis (EMP), Fourier-transform infrared spectroscopy (FTIR), amino acid analysis, and pyrolysis gas chromatography-mass spectrometry (Py-GC/MS). However, structures reported to "closely resemble" aggregates of cells in shape and size under electron microscopy (see Manning et al. 2009: fig. 2c, d) are not clearly demarcated in their images, nor are they apparent to us. When interpreting microscopic structural data from fossils, care must be taken not to falsely describe patterns that are not there (e.g., the Bertazzo et al. 2015 report of dinosaur erythrocytes can have their full range of morphologies reproduced through thermally degraded, pliable turkey skin when examined under electron microscopy Saitta and Vinther 2019). Their EMP results showing prevalent calcite (see Manning et al. 2009: fig. 3) would not be consistent with the hypothesis that subdermal histological structures preserve. The FTIR bands suggested to be amide bands on sediment grains found near the ungual sheath (see Manning et al. 2009: fig. 4a, b), like other claims of amide bands in infrared spectra of other fossils (e.g., Surmik et al. 2016), are likely inconclusive of endogenous proteins (Saitta et al. 2019b). Indeed, their amino acid results show that the sediment, ungual sheath, and integument rendering all have somewhat similar amino acid relative compositional profiles to each other, although this is difficult to judge in their log-transformed plot that omits some samples (see Manning et al. 2009: fig. 5a).

These profiles do not match those of more robustly supported endogenous, thermally stable amino acids from closed-system eggshell (Saitta et al. 2024). Rather, Manning et al. (2009) report unstable Asx or Ser at similar or greater concentrations to some of the more stable Glx, Gly, Ala, or Val in many of their samples. Furthermore, the high values of Gly/Ala used as evidence of keratin or collagen (see Manning et al. 2009: fig. 5b) are only seen in one of their integument rendering samples. The second highest value comes from one of the sediment controls. All the other integument samples that would be predicted to have high Gly/Ala under their hypothesis, instead have low values similar to the sediment or fossil plant material. Although the Py-GC/MS suggests that there may be a larger set of n-alkanes/alkenes in the integument rendering than in the surrounding sediment (see Manning et al. 2009: fig. 6), the two pyrograms have many shared compounds that could also be derived from an organic consolidant applied to the specimen or from other laboratory/environmental contaminants. More crucially, the integument rendering pyrogram lacks any of the highly diagnostic pyrolysis products known to come from reptilian/avian β-"keratin" as reported in Saitta et al. (2017).

Barbi et al. (2019) likewise used a variety of methods, including light microscopy, SEM/BSE, EDS, FTIR, scanning transmission X-ray microscopy (STXM), and X-ray near edge spectroscopy (XANES). However, we again caution against overinterpretation of superficial, microscopic visual similarities to modern, fresh tissues under thin section (see Barbi et al. 2019: fig. 2); laminae do not necessarily indicate stratified dermal or epidermal tissue preservation, but could instead derive from other sources, such as aluminosilicate clays. Indeed, their thin sections show large silicate grains amid finer material in the fossilized integument rendering, and their proposed carbonaceous layers have similar backscatter electron intensities (i.e., similar atomic number) as the embedding resin (see Barbi et al. 2019: fig. 3).

Carbon-rich regions (see Barbi et al. 2019: fig. 4) may be due to cracks in the sample, in which the embedding resin has infiltrated, rather than the aluminosilicates that predominate in the matrix (see Barbi et al. 2019: fig. 5). In addition to the lack of specificity of the proposed FTIR bands (see Barbi et al. 2019: table 1), we also caution that the STXM/XANES evidence of carbonyls would likewise not be specific enough to infer histological preservation of the integument, and what appear to us to most clearly be the actual fragments of microtomed material from the sample may be predominantly iron sulfides, iron oxides, or other inorganic compounds, such as carbonates (see Barbi et al. 2019: figs. 10–14). As Barbi et al. (2019) note, some of these spectroscopic signatures could also indicate kaolinite clay presence. It is difficult to infer how the microtomed STXM images precisely relate to the different regions of the fossil sample that are more clearly presented in embedded, thin sections of the figured micrographs. We also note that carbonyls could come from a variety of carbonaceous compounds, and we should consider a variety of possible sources, including consolidants applied during field excavation or laboratory preparation and embedding media applied for thin sectioning.

Fabbri et al. (2020) used petrographic thin sectioning, followed by SEM, EDS, and Raman spectroscopy on a small (~6 $cm^2$) patch of integument rendering from the flank region of a partial hadrosaur skeleton. They concluded the preservation of melanosomes, as well as blood vessels and dermal cells, within an organic extracellular matrix consisting of "protein fossilization products". However, we propose an alternative interpretation (Fig. 1). The area that they identify as the organic dermis shows a somewhat platy texture under SEM (see Fabbri et al. 2020: fig. 2), which could also be consistent with aluminosilicates. Furthermore, many of the elemental signatures under EDS are shared between their purported dermis layer and the external matrix (see Fabbri et al. 2020: fig. 3)—the most obvious difference being the larger size and greater number of the silicate grains in the external matrix versus a more uniform calcium signal internally, consistent with early calcium carbonate cementation after burial that replaced tissues as they decayed. The only strong C signal is localized near their interpreted melanosomes rather than throughout their purported organically preserved dermis. Even then, some C signal could derive from carbonates as well as organic resin polymers

used to embed the sample within any cracks in their sample. Possible cracking is consistent with the fact that the carbon-rich line is observed cross-cutting mineral phases (presumably carbonate and aluminosilicate) in their EDS maps. Finally, Raman signatures hypothesized to derive from amides and N-rich heterocycles representing "protein fossilization products" (see Fabbri et al. 2020: fig. 4) have alternatively been interpreted as quasi-periodic spectral artefacts (Alleon et al. 2021; note that it is unclear if an edge filter was used to obtain this Raman data).

Despite the concerns detailed above, biomolecular preservation of melanin or melanosomes in some dinosaur "mummies" is worthy of consideration (Fabbri et al. 2020). Melanin biopolymers can indeed preserve in exceptional depositional environments from many localities (Roy et al. 2020; Vinther 2020). A three-dimensional ankylosaur "mummy" of *Borealopelta* preserves skeletal articulation, fossilized "keratin" sheathing of the osteoderms, and organic melanin (Brown et al. 2017). The specimen retains organosulfur signatures consistent with phaeomelanin countershading. The sheathing was hypothesized at the time to preserve via calcium phosphates based on UV fluorescence imaging, but its elemental composition could also be consistent with presence of iron carbonates (see their supplemental EDS maps), which may help to explain their non-fluorescence in certain regions (Brown 2017).

## Dinosaur "mummies" vs. other fossilized "keratinous" integument

Dinosaur "mummies" are rare, highly complete, and articulated skeletons that preserve large patches of associated or articulated integument in three dimensions, which may include scales (Bell 2014), crests (Osborn 1911, 1912), spikes (Horner 1984; Sereno et al. 2026), combs (Bell et al. 2014), ungual sheaths (Drumheller et al. 2022; Sereno et al. 2026), and rhamphotheca (e.g., LACM 23502, Morris 1970; SMF R 4036, Uhl 2020; El Atfy and Uhl 2021). Often, the carcass is in a supine position with the ribcage opening upward and forelimbs sprawled to either side. The depth of the skeleton and sediment wedge engulfing the carcass can exceed one meter in vertical depth (Uhl 2020; Drumheller et al. 2022; Sereno et al. 2026). Most often, these "mummies" are hadrosaurid "duckbills" (Davis 2014). "Mummy" ceratopsians are rarer (e.g., *Triceratops*, "Lane", HMNS 2006.1743). Ankylosaur "mummies" are also rare, such as *Borealopelta* (TMP 2011.033.0001), whose carcass, unlike those of other dinosaur "mummies", was washed out to sea and preserved in a carbonate concretion within Alberta oil sands of the Clearwater Formation (Brown et al. 2017). Less extensive, scaly integument patches also preserve in a variety of other non-avian dinosaurs, including sauropods (Pittman et al. 2022), ceratopsians (Bell et al. 2022), theropods (Hendrickx et al. 2022), ankylosaurs (Arbour and Evans 2017), and stegosaurs (Christiansen and Tschopp 2010). Generally

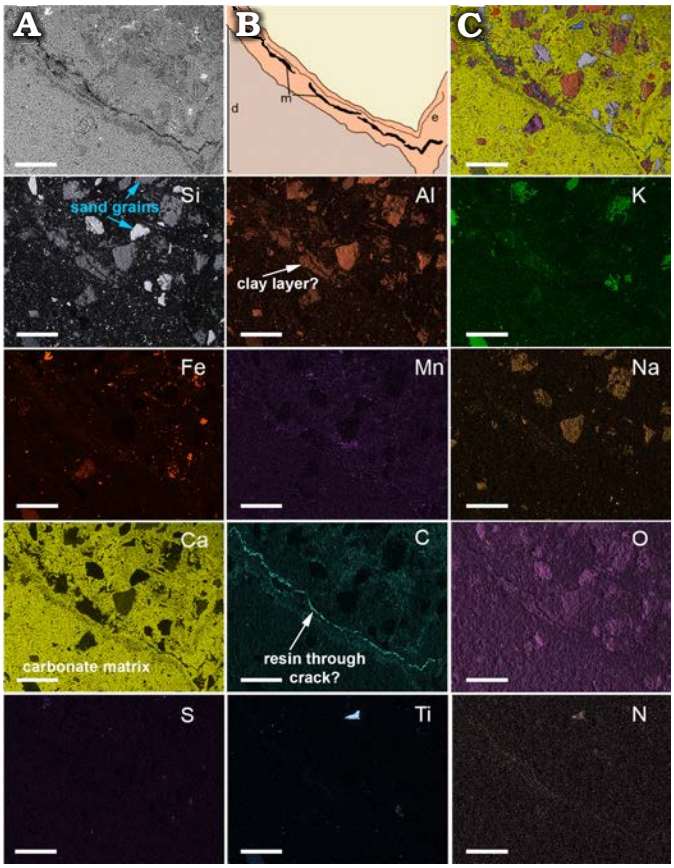


Fig. 1. Our alternative interpretation for Fabbri et al. (2020) thin-sectioned hadrosaur fossil integument rendering (YPMPU 016969, from Montana, USA, Late Cretaceous). Photograph (**A**), interpretive drawing (d, e, m, the original interpretations of dermis, epidermis, and melanin, respectively) (**B**), and layered EDS map (**C**). Element maps of Si, Al, K, Fe, Mn, Na, Ca, C, O, S, Ti, and N, consistent in color between the layered map and the single-element maps. Figure after Fabbri et al. (2020: fig. 3) with permission from RightsLink/John Wiley and Sons. We instead interpret the thin section as larger sand grains external to a partially preserved clay template, with extensive carbonate cementation (unlike the uncemented UCRC hadrosaur "mummies" Sereno et al. 2026). A crack in the clay layer exposes the embedding resin (Chinsamy and Raath 1992) as a carbon signature (likewise seen in the UCRC hadrosaur "mummies" below). Scale bars 200 μm. Panel labeling follows Fabbri et al. (2020).

speaking, preservation of soft tissue structures is still an extremely rare phenomenon.

Most vertebrate skeletons are preserved within a relatively thin layer, concentrated by gravity in the throes of decay and disarticulation, followed by sediment compaction. Coming typically from comparatively better-oxygenated, terrestrial, high-energy fluvial sands (Uhl 2020), dinosaur "mummies" differ in preservation from the quiescent, fine-grained environments more conducive to soft tissue preservation. These exceptionally preserved, two-dimensional "compression fossils" are slab-bound and extremely thin (Parry et al. 2018). They are typically found in low-oxygen, low-energy lacustrine or shallow marine Konservat-Lagerstätten such as those preserving the Jehol (Xu et al. 2020), Solnhoffen (Barthel 1970), or Crato (Martill et al. 2007) biotas.

*Organic preservation of integument*.—Exceptional fossilization occurs when soft tissues preserve in addition to biomineralized tissues (Parry et al. 2018) such as the apatite of vertebrate bone and teeth or the calcite of eggshell. Soft tissues can be preserved either organically or inorganically.

In organic soft tissue preservation, thermodynamically unstable bonds break into lower energy states, such as the hydrolysis of proteins (Saitta et al. 2024), while more stable organic material can cross-link, polymerize, saturate, aromatize, and lose reactive functional groups to reach diagenetic stability (Vandenbroucke and Largeau 2007). The best example of organic material that can not only preserve at the molecular level but also preserve some anatomical details of the vertebrate integumentary tissues they derive from is melanin in compression fossils from Konservat-Lagerstätten such as Jehol, preserving not just morphological details of dinosaur feathers (Saitta et al. 2018b), but also their original pigment-based coloration (Roy et al. 2020). Fine-grain, low-energy, and hypoxic/anoxic/euxinic environments are more likely to preserve fossil melanin from vertebrate integument (Vinther 2020).

*Inorganic preservation of integument*.—While melanin pigment is ubiquitous across vertebrate integument and capable of fossilizing in rare depositional environments, vertebrate integument need not be preserved organically to persist in the fossil record. Authigenic mineralization induced through microbial decay of organics can preserve even microscopic details of tissues, such as vertebrate muscle fibers (Briggs et al. 1993) or feces (Qvarnström et al. 2016) replicated as calcium phosphate. Integument, especially, can be preserved in exceptional circumstances via phosphatization (e.g., Saitta et al. 2018a; He et al. 2023), explaining why the integument of vertebrate compression fossils from localities such as Jehol can be visualized readily under fluorescence imaging (e.g., Mayr et al. 2016).

Feather fibers of the Cretaceous dinosaur *Shuvuuia deserti*, were found in xeric, aeolian, poorly cemented sand with large pore size—somewhat like dinosaur "mummies" deposited in terrestrial, relatively more oxygen-bearing, sandy, and sometimes poorly cemented sediments, but which differ in coming from aeolian, as opposed to fluvial, sands. *Shuvuuia deserti* feathers are very clearly preserved predominantly as calcium phosphate based on energy dispersive X-ray spectroscopy (EDS) and time-of-flight secondary ion mass spectrometry (TOF-SIMS), possibly with some lesser aluminosilicate contribution (Saitta et al. 2018a). There is uncertainty as to how much of this phosphatic preservation is precipitated from exogenous ions during decay of organic material versus how much is driven by in vivo calcification of integumentary structures (Blakey et al. 1963). Both true mammalian α-keratins and "reptilian" corneous β-proteins (i.e., β-"keratins") (Holthaus et al. 2018) can be calcified in vivo to alter the material properties of these tissues for biomechanical purposes (Earland et al. 1962; Blakey et al. 1963; Pautard 1964; Blakey and Lockwood 1968; Szewciw et al. 2010). Furthermore, "hard" keratins such as hoof sheaths can incorporate many sorts of trace elements (e.g., Mg, K, Ca, P, Cu, Zn, Na, Fe) in vivo (Baggott et al. 1988), which would themselves be capable of preserving in the geologic record.

## Our evidence-based approach

With reference to one early adult and one late juvenile *Edmontosaurus annectens* "mummy" (UCRC PV30 and UCRC PV31, respectively) originally described by Sereno et al. (2026), we aim to answer several key questions using a battery of structural and chemical analytic techniques, including multiple forms of microscopy, spectroscopy, and spectrometry:

(i) How does the sediment matrix within and outside a dinosaur "mummy" compare?

(ii) What are the structure and composition of integument renderings?

(iii) Are any original tissue structures or biomolecules preserved?

(iv) Do various integument renderings (e.g., scale, spike, hoof) differ in preservation?

(v) How might these integument renderings form?

Table 1 details the methods used: laser diffraction grain size analysis (LGSA), light microscopy (LM), stereophotogrammetry (SPG; i.e., structure from motion photogrammetry) and white light scanning, micro-computed X-ray tomography (micro-CT) and clinical CT, laser-stimulated fluorescence photography (LSF), portable X-ray fluorescence (pXRF), synchrotron XRF (sXRF), backscatter electron microscopy (BSE), energy dispersive X-ray spectroscopy (EDS), laser ablation-inductively coupled plasma-mass spectrometry (LA-ICP-MS), time-of-flight secondary ion mass spectrometry (TOF-SIMS), and X-ray diffraction (XRD).

*Institutional abbreviations*.—AMNH, American Museum of Natural History, New York, USA; ANL, Argonne National Laboratory, Lemont, USA; FMNH, Field Museum of Natural History, Chicago, USA; FSA, Foundation for Scientific Advancement, Sierra Vista, USA; JRF, Judith River Foundation, Malta, USA; HMNS, Houston Museum of Natural Science, USA; LACM, Natural History Museum of Los Angeles, USA; LU, Loyola University, Chicago, USA; MRF, Marmarth Research Foundation, Marmarth, North Dakota, USA; NDGS, North Dakota Geological Survey, Bismarck, USA; NU, Northwestern University, Evanston, USA; SMF, Naturmuseum Senckenberg, Frankfurt, Germany; TMP, Royal Tyrrell Museum of Palaeontology, Drumheller, Canada; UALVP, University of Alberta Laboratory for Vertebrate Palaeontology, Edmonton, Alberta, Canada; UCRC, University of Chicago Research Collection, USA; UIUC, University of Illinois Urbana-Champaign, USA; YPMPU, Yale Peabody Museum of Natural History, Princeton University Collection, New Haven, USA.

*Other abbreviations*.—BSE, back-scattered electron microscopy; CT, computed tomography (clinical and micro);

Table 1. Summary of 11 methods employed, institutional location of laboratory analysis, analytic focus, controls used for the analysis, and fossil specimens tested. The control of sediment matrix may include associated fossil plant matter within the matrix.

| No. | Method | Institution | Analytic focus | Control(s) | Specimens |
|---|---|---|---|---|---|
| 1 | laser diffraction grain size analysis (LGSA), oven ashing | NU | grain size distribution, organic fraction | ashed, non-ashed | UCRC PV30<br>UCRC PV31 |
| 2 | stereophotogrammetry (SPG), white light scanning | UC | macrostructure, coloration | sediment matrix | UCRC PV30<br>UCRC PV31 |
| 3 | light microscopy (LM): digital, optical, and polarized | UC LU | microstructure, birefringence | sediment matrix, modern tissues | UCRC PV30<br>UCRC PV31 |
| 4 | clinical and micro-computed tomography (CT) | UC | internal structure, electron density | sediment matrix | UCRC PV30 |
| 5 | laser-stimulated fluorescence (LSF) | FSA | structure, fluorescence | sediment matrix | UCRC PV30 |
| 6 | portable X-ray fluorescence (pXRF) | FMNH | elemental composition (higher versatility, lower power) | sediment matrix | UCRC PV30 |
| 7 | synchrotron X-ray fluorescence (sXRF) | ANL | elemental composition, localization (lower versatility, higher power) | sediment matrix | UCRC PV30 |
| 8 | back-scattered electron microscopy (BSE), energy-dispersive X-ray spectroscopy (EDS) | UC | ultrastructure, elemental composition, localization | sediment matrix | UCRC PV30<br>UCRC PV31 |
| 9 | laser ablation-inductively coupled plasma-mass spectrometry (LA-ICP-MS) | FMNH | elemental composition, depth profile | sediment matrix | UCRC PV30 |
| 10 | time-of-flight secondary ion mass spectrometry (TOF-SIMS) | NU | molecular composition, localization | sediment matrix | UCRC PV30 |
| 11 | X-ray diffraction (XRD) | UIUC UC | phase composition | sediment matrix | UCRC PV30 |

EDS, energy-dispersive X-ray spectroscopy; LA-ICP-MS, laser ablation-inductively coupled plasma-mass spectrometry; LGSA, laser diffraction grain size analysis; LM, light microscopy (digital, optical, polarized); LSF, laser-stimulated fluorescence; pXRF, portable X-ray fluorescence; SPG, stereophotogrammetry; sXRF, synchrotron X-ray fluorescence; TOF-SIMS, time-of-flight secondary ion mass spectrometry; XRD, X-ray diffraction.

# Material and methods

*Modern integument sampling and histology*.—For comparison to the *Edmontosaurus annectens* integument, extant diapsid tissues were examined. We sampled chicken (*Gallus gallus*) claw and skin as well as alligator (*Alligator mississippiensis*) claw and scute from the UCRC frozen collection. For histologic thin sectioning, we sampled the midline crest of a male Doria's angle-headed lizard (*Gonocephalus doriae*, FMNH H:249773) from Borneo, a structure analogous to *Edmontosaurus annectens* tail spikes (Sereno et al. 2026). The *Gonocephalus doriae* specimen had originally been fixed in formalin and was stored in ethanol at the FMNH. The midline crest above the head and neck was dissected off and then further cut into three anteroposterior pieces, which were kept in ethanol. The posterior piece was then placed into a plastic cassette and embedded in paraffin wax at the Human Tissue Resource Center (HTRC)-Histology and IHC Core of the University of Chicago. After setting, a microtome was used to cut away the excess wax laterally to reveal more medial layers containing the midsagittal spikes. At this point, serial sectioning of 20-µm thickness was carried out along the sagittal plane. The middle portion of the dissected neck was instead cut into 10-µm thick sections along the dorsal (i.e., coronal or frontal) plane. The thin sections were then placed onto glass microcopy slides and stained with hematoxylin and eosin for visualization under the Dino-Lite Digital Microscope (Dino-Lite MS08B stand; illuminated from below with a Dino-Lite MSAK827 LED light source). A sagittal section was also imaged with the Nikon Eclipse LV150N optical microscope at Loyola University for higher resolution.

*Fossil integument sampling and thin sectioning.—Early adult "mummy" samples:* Small areas of integument were sampled from the early adult *Edmontosaurus annectens* (UCRC PV30) "mummy" in several locations and in different manners:

(i) A small oval flake (~15 mm major axis) from the postero-dorsal edge of a mid-tail spike and a small amount of its sediment matrix was removed along a crack. This flake underwent BSE/EDS, TOF-SIMS, portable XRF, and LA-ICP-MS. Ultimately, the flake was consumed during XRD clay analysis.

(ii) A mid-tail spike was sampled and prepared by hand in three dimensions. The surrounding matrix on both lateral surfaces was completely removed using standard paleontology preparation tools for photography and micro-CT scanning.

(iii) Posterior to the 3D-prepared spike above, another spike and two articulated half spikes were stabilized at their surface with Epotek 301 epoxy. This stabilized block of spikes was then separated from the rest of the specimen using a pneumatic air scribe. We used an iPhone 14 for stereophotogrammetry of the block, which was then micro-CT scanned. Next, we sent the block to Spectrum Petrographics (Vancouver, Washington, USA), where it was vacuum embedded in Epotek 301 epoxy and cut into five 30-µm microprobe polished transverse thin sections. These thin sections were spaced semi-evenly from anterior to posterior along

the complete spike within the block (L9L 001 AE anterior end, L9L 002 AQ anterior quarter, L9L 003 C center, L9L 004 PQ posterior quarter, L9L 005 PE posterior end). An additional 150-µm microprobe polished transverse thin section was produced for LSF and XRD at the anterior quarter (AQ). The thin sections underwent light microscopy (including polarized light microscopy), BSE/EDS, TOF-SIMS, LSF, and XRD clay analysis (University of Illinois Urbana-Champaign, USA). In the process of removing this spike block, a single basement scale along the ventral edge of the block separated off and was collected as its own sample for BSE/EDS (SOM 1; Supplementary Online Material available at http://app.pan.pl/SOM/app71-Saitta_etal_SOM.pdf).

(iv) A separated jacket containing the right hoof-bearing right pes underwent clinical CT scanning at the University of Chicago, USA hospital.

(v) A disarticulated, heavily glued block of wrinkled integument rendering found between the hindlimbs was studied using light microscopy and portable XRF.

(vi) We also sampled dark staining material on the lateral scales of the tail. A small block of integument rendering separated near the base of the tail during excavation, when the jackets were separated for removal. We analyzed this block using synchrotron XRF and portable XRF. This block was also further subsampled with a pin vise to obtain a sample of darker black staining and a sample of orange staining on the scales. These subsamples were then examined with light microscopy and BSE/EDS.

We also took samples from the matrix of the early adult *Edmontosaurus* (UCRC PV30) "mummy":

(i) A large ironstone concretion at the tip of the tail (final dozen caudal vertebrae) was sampled using a pneumatic air scribe to retrieve a small flake. This flake was examined with light microscopy and BSE/EDS. Finally, this ironstone flake was powdered and examined with XRD (University of Chicago, USA).

(ii) A small flake of naturally crumbling, black plant material found beneath the tail at the location where the spikes were removed (as described above) was collected. The flake was examined with light microscopy, BSE/EDS, and TOF-SIMS.

(iii) Sandy sediment matrix samples from the right pes were taken at three sites for laser diffraction grain size analysis: internal to a hoof sheath, external but close to the hoof sheath, and external and far from the hoof sheath. Also analyzed was bulk sediment saved during preparation of the specimen with unknown precise location.

*Late juvenile "mummy" samples*: The late juvenile *Edmontosaurus* (UCRC PV31) "mummy" had its integument rendering sampled with a pin vise at a natural break over the scapula. The sample was stabilized and affixed to an aluminum electron microscopy stub using B-72, and then analyzed with BSE/EDS.

Sandy sediment matrix samples were taken of the matrix in three sites for laser diffraction grain size analysis: internal to the integument rendering layer, external but close to the integument rendering layer, and external and far from the integument rendering layer. Also analyzed was bulk sediment saved during preparation of the specimen with unknown precise location.

*Laser diffraction grain size analysis*.—Laser diffraction grain size analysis was performed at Northwestern University, using a Malvern Mastersizer hydro 3000 on three sediment sampling locations for each of the two UCRC *Edmontosaurus annectens* "mummies" (internal to the integument, external but close to the integument, and external but far from the integument). Each run used about 0.9 g of sediment, placed directly into the equipment with no pretreatment and then sonicated for 30 seconds in water. A second set of replicate samples were analyzed as before, but underwent a pre-treatment of oven ashing at 500°C for 20.5 hours prior to loading into the Malvern Mastersizer in order to estimate the percentage organic fraction based on weight change before and after ashing. All results are reported as averages of 5 measurements per sample.

*Photogrammetry and white light scanning*.—Photogrammetry was performed using a 3rd generation iPhone SE (typical settings: 3.99 focal length, F/1.8 F-stop, 50–64 ISO, ~1/60–1/120 shutter, 28 mm focal) and a Fujifilm X-T4 digital camera (typical settings: 16 focal length, F/7.1 F-stop, 5000 ISO, ~1/60 shutter, 24 mm focal) for the early adult *Edmontosaurus annectens* (UCRC PV30) "mummy". The tail model contained 656 pictures, while the foot model contained 304 pictures. Photogrammetry of the late juvenile *Edmontosaurus annectens* (UCRC PV31) "mummy" utilized only the Fujifilm X-T4 digital camera and its model contained 629 pictures. Pictures were overlapping as is standard for photogrammetry digitizing protocols (Mallison 2014). They were taken without additional external light sources (e.g., ring flash), excepting the laboratory ceiling lamps, to maximize the amount of detail on the scale renderings. All pictures were processed in Agisoft Metashape (post-2.0 versions), which aligned the photos and generated the 3D models from the depth maps. Final models were decimated to 10 million polygons for high resolution and 4 million polygons for medium resolution. Models were scaled to millimeters.

Surface morphology and color were captured using handheld light scanner (Artec Spider I) and reconstructed in Artec Studio (v17.0), provided by University of Minnesota, Makovicky Lab. Photogrammetry and white light models were supplemented with photographs taken with an iPhone 14.

*Light microscopy*.—Light microscopy was performed with three pieces of equipment on both UCRC *Edmontosaurus annectens* "mummy" specimens. These included: a Dino-Lite Edge AM73915MZTL (10–~140×; 5.0MP; USB 3.0) Digital Microscope with a calibrated scalebar feature, a Nikon Eclipse LV150N optical microscope (with plane polarized, cross polarized, and lambda polarized light options) at Loyola University (images stitched with Nikon NIS software), and a Zeiss Axioscope with polarization

at the Department of Organismal Biology & Anatomy, University of Chicago, USA.

*Computed X-ray tomography*.—Both micro-CT and hospital-based CT scanning was performed. Micro-CT scanning occurred at the Department of Organismal Biology & Anatomy, University of Chicago, USA on all removed spikes of the early adult *Edmontosaurus annectens* "mummy", while the hospital-based CT scanning occurred at University of Chicago Medical Center (i.e., UChicago Medicine, USA) on the ironstone concretion-covered tail tip and foot of the early adult *Edmontosaurus annectens* (UCRC PV30) "mummy".

*Laser-stimulated fluorescence photography*.—LSF was performed at the Foundation for Scientific Advancement in Sierra Vista, Arizona, USA, using a modified version of the methodology of Kaye et al. (2015). The 150-µm thin section (AQ, anterior quarter) of the early adult *Edmontosaurus annectens* (UCRC PV30) "mummy" spike was illuminated with a 405 nm, 500 mw violet laser diode and imaged with a digital camera in a dark room. A long pass blocking filter was fitted to the objective of the camera to prevent image saturation by the laser. The image was post-processed in Photoshop CC 2016 for sharpness, color balance, and saturation.

*Portable X-ray fluorescence*.—pXRF analysis was carried out with a Thermo Scientific Niton XL3t Goldd+ spectrometer at the Elemental Analysis Facility at the Field Museum of Natural History in Chicago, Illinois, USA. Samples studied using portable XRF were the flake from the early adult *Edmontosaurus annectens* (UCRC PV30) "mummy" spike, the large isolated integument rendering block between the legs of UCRC PV30, the small integument rendering block that separated between the tail and hip jacket of UCRC PV30. This instrument utilizes a tube with a silver anode and a geometrically optimized large area drift detector. All samples were analyzed using the "Test All Geo" mode (acquisition time of 180 s per sample) with different filters and parameters corresponding to four preset analytical measurement conditions (i.e., beam/filter modes) defined in the software: Main (40 kV and 100 µA), Low (25 kV and 100 µA), Light (15 kV and 200 µA), and High (50 kV and 100 µA).

*Synchrotron XRF*.—Synchrotron XRF was performed on a small block of integument rendering from the early adult *Edmontosaurus annectens* (UCRC PV30) "mummy" that separated between the tail and hip jacket at the Advanced Photon Source of Argonne National Laboratory in Lemont, Illinois, USA. sXRF parameters were as follows: 9.92 keV energy, 30 µm beam size, Vortex ME4 detector, 50 µm scanning step, and ~50 ms dwell time. As for the geometry, the detector was 90 degrees to the incident beam with a 40 mm long aluminum collimator and ~15 mm clearance to sample, while the sample was 45° to incident beam.

*Electron microscopy and energy dispersive X-ray spectroscopy*.—BSE and EDS were performed in the Department of the Geophysical Sciences at the University of Chicago, USA at the FIB-SEM, on the early adult *Edmontosaurus annectens* thin-sectioned spike (15 kV beam), the early adult *Edmontosaurus annectens* spike flake, dark and orange stains, ironstone concretion (30 kV beam), and associated plant matter (20 kV beam), as well as the integument rendering from the late juvenile *Edmontosaurus annectens* (15 kV for a large montage image, 30 kV for the smaller mapped region). The analysis used a TESCAN LYRA3 field-emission scanning electron microscope. The thin section (L9L 005 PE) from the posterior end of the early adult *Edmontosaurus annectens* "mummy" spike was examined and the region of interest with the glass side down (i.e., uncovered analytical side up). All samples were affixed to a microscopy stub with carbon tape on their bottom side to position within the chamber. The general region of interest was demarcated using two strips of copper tape for the early adult *Edmontosaurus annectens* "mummy" spike thin section and no coating was applied to the surface of any sample. The chamber was then pumped down to partial vacuum (i.e., low vacuum mode).

A scintillator-type backscattered electron detector was used to image the sample. Elemental maps were produced by energy-dispersive X-ray spectroscopy by raster imaging the slide with Oxford Instruments X-Max-80 silicon drift x-detectors. Data was analyzed with Aztec software.

*Laser ablation-inductively coupled plasma-mass spectrometry*.—LA-ICP-MS was carried out at the Elemental Analysis Facility at the Field Museum of Natural History in Chicago, USA, with a Thermo ICAP Q Inductively Coupled Plasma-Mass Spectrometer (ICP-MS) connected to an ESI-Elemental Scientific Lasers NW213 laser for direct introduction of solid samples. We analysed the early adult *Edmontosaurus* spike flake. Sand matrix from nearby (i.e., dorsal to) this sampled spike flake was also analyzed as a control. The parameters of the ICP-MS, as described below, are optimized to ensure a stable signal with a maximum intensity over the full range of masses of the elements and to minimize oxides and double ionized species formation ($XO^+/X^+$ and $X^{++}/X^+ < 1$ to 2%). For that purpose, the argon flows, the RF power, the torch position, the lenses, the mirror and the detector voltages are adjusted using an auto-optimization procedure.

To improve sensitivity, helium was used as a gas carrier in the laser setup. We used the scan line analysis mode with a laser beam diameter of 60 µm, operating at 60% of the laser's energy and at a pulse frequency of 20 Hz. Measurements were set to 60 s and were corrected from a blank signal that was recorded in the absence of ablation. The internal standard used was isotope $^{29}Si$. Concentrations for major elements, including silica, were calculated under the assumption that the sum of the major and minor element concentrations in weight percentage is equal to 100% (Gratuze 1999). Three different external standards were used to measure major, minor, and trace elements. The first external standard was a standard reference material (SRM) manufactured by NIST called SRM 610, a soda-lime-silica glass doped with trace elements in the range of 500 ppm. Certified values are

available for a very limited number of elements within it, and concentrations from Pearce et al. (1997) were used for the other elements. The second series of external standards was manufactured by Corning and are called Glass B and D, which are glasses that match compositions of ancient glass (see Brill 1999: vol. 2: 544). Data is presented in the main text as an average across multiple sites on a sample (i.e., dinosaur spike or sediment matrix) and is rounded to the nearest ppm. The limit of detection is different from one element to another—close to the ppb level for the rare earth elements, but higher for other elements (SOM 1).

*Time-of-flight secondary ion mass spectrometry*.—TOF-SIMS was performed at the Northwestern University Atomic and Nanoscale Characterization Experimental Center (Evanston, Illinois, USA) on the early adult *Edmontosaurus* spike flake, spike thin section, sediment matrix, and associated plant material. Measurements were performed using an IONTOF TOF.SIMS M6 instrument equipped with a 30 kV Bi primary ion source. Data were acquired in both positive and negative ion modes to capture complementary chemical information.

For spectral acquisition, analyses were conducted over a 200×200 μm raster area using a 128×128 pixel resolution under random raster mode. A cycle time of 100 μs was employed, with one shot per pixel and one frame per patch. For chemical imaging (mapping), measurements were performed over a larger 500×500 μm area with 512×512 pixels, also in random raster mode, maintaining one shot per pixel and one frame per patch. Measurements were conducted on both as-received surfaces and etched surfaces. Surface cleaning/etching was performed using a 500 eV oxygen ion beam for 30 seconds prior to analysis of the etched condition.

*X-ray diffraction*.—Clay analysis was performed at the Illinois State Geological Survey, University of Illinois Urbana-Champaign, USA X-ray Diffraction (XRD) Laboratory. XRD bulk analysis on the AQ (anterior quarter) 150-μm thin section (~2.54 cm diameter beam was centered on the external matrix immediately adjacent to the integument template) and clay mineral analysis (< 2 μm) from oriented XRD patterns on the spike flake were performed.

For the clay fraction (< 2 μm) of the spike flake analyzed with oriented XRD patterns, the spike was disaggregated in deionized water, stirred in an electronic mixer to suspend clays, allowed to settle, salt-containing solution poured off, and stirred again to get the < 2 μm grains in solution after larger particles settle. Eye droppers were used to transfer the < 2 μm grains to a glass slide, air dried, and saturated by ethylene glycol to orient the clay particles. The data was step-scanned and collected from 2° to 34° 2θ (1° per minute fixed rate, 0.02° 2θ step size). Basal diffraction intensities (d001) of these concentrated clays obtained from the oriented and ethylene glycol saturated films were compared to each other. The analysis was semi-quantitatively calculated from major clay mineral intensities (i.e., smectite, mica, chlorite, and kaolinite).

The thin section was analyzed with an X-ray beam that covered the central area of the slide (~2.54 cm). The data was step-scanned and collected from 5° to 70° 2θ (1° per minute fixed rate, 0.02° 2θ step size). These results are also semi-quantitative and based on the reference intensity ratio (RIR) method. Corundum is the reference standard. All the phase intensities quantified were recalculated (i.e., normalized) using the ratio of $\text{Intensity}_{\text{phase}}/\text{Intensity}_{\text{corundum}}$. Non-clay phases of the external matrix (e.g., quartz, feldspars) were detected. The average concentrations of these mineral phases within the area scanned by the beam are reported. Clay particle orientation impacts their overall peak intensity. Unlike the clay fraction in ethylene glycol, the ability to detect clays in other arrangements is very limited, and this is exacerbated by their low concentrations.

Additional X-ray powder diffraction was performed at the University of Chicago, Gordon Center for Integrative Sciences, on the sample of the ironstone concretion at the tip of the tail of the early adult *Edmontosaurus annectens* (UCRC PV30) "mummy" in order to better characterize the mineral phases within dark precipitates of the specimen. The ironstone concretion was wrapped in weighing paper and foil and then powdered using a hammer. The analysis was performed on a Rigaku SmartLab X-ray diffractometer equipped with a HyPix-3000 detector and Cross-Beam-Optics (CBO). The powder was supported on a zero-background sample holder (single crystal silicon). The measurement was done using a parallel beam selected through the CBO optics using Cu Kα radiation (1.54186 Å). Scans were measured as θ/2θ scans in the range of 10–100° 2θ with the step size of 0.02° and the counting rate of 3° per minute. An incident slit of 0.5 mm and receiving slit of 16 mm were utilized. The measurement was done twice and averaged. The tube was energized at 44 mA and 40 kV. The data collection and analysis was completed in the SmartLab Studio II software package (v.4.4.241.0).

# Results

Below, we describe the results of analyses on the two UCRC *Edmontosaurus annectens* "mummies", their associated sediment, and modern controls. Raw online supplemental data beyond that presented in SOM 1 can be found through Zenodo [Saitta, E. (2026). Online Data for "Dinosaur 'mummification': Clay templating in a fluvial setting preserves three-dimensional integument renderings after carcass desiccation" [Data set, https://doi.org/10.5281/zenodo.20617258]. CT, stereophotogrammetry, and white light scanning files are available on MorphoSource (https://www.morphosource.org/projects/000863152?locale=en).

*Laser diffraction grain size analysis*.—The sediment matrix in both specimens is predominantly sand, with lesser

Table 2. Summary statistics of grain size distributions and estimated organic fraction in the two UCRC *Edmontosaurus annectens* "mummies". Percentages and distributions are based on the frequency of a given particle size that passes in front of the laser (i.e., % by number of particles). Clay % values greater than that of the internal sediment are highlighted in grey. NA, samples that were not oven ashed do not have a calculated organic %.

| Specimen | Oven ashed? | Sample (average of 5 measurements) | Clay % (< 2 μm) | Grain size (μm) | | | | | | Organic % (wt change of ash) |
|---|---|---|---|---|---|---|---|---|---|---|
| | | | | $10^{th}$ percentile | | median | | $90^{th}$ percentile | | |
| Late juvenile *Edmontosaurus annectens* (UCRC PV31) | no | internal | 1.80% | 18.7 | silt | 131 | sand | 252 | sand | NA |
| | | external adjacent | 2.04% | 17.7 | silt | 98.9 | sand | 190 | sand | NA |
| | | external distant | 1.69% | 19.0 | silt | 125 | sand | 227 | sand | NA |
| | | bulk matrix from preparation | 1.06% | 54.7 | sand | 160 | sand | 281 | sand | NA |
| | yes | internal | 0.00% | 31.0 | silt | 136 | sand | 254 | sand | 1.42% |
| | | external adjacent | 0.00% | 40.5 | silt | 112 | sand | 210 | sand | 1.29% |
| | | external distant | 0.00% | 45.3 | silt | 133 | sand | 234 | sand | 1.50% |
| | | bulk matrix from preparation | 0.00% | 81.1 | sand | 165 | sand | 287 | sand | 1.23% |
| Early adult *Edmontosaurus annectens* (UCRC PV30) | no | internal | 2.00% | 12.1 | silt | 85.1 | sand | 164 | sand | NA |
| | | external adjacent | 2.23% | 11.5 | silt | 83.0 | sand | 157 | sand | NA |
| | | external distant | 2.24% | 13.2 | silt | 92.7 | sand | 163 | sand | NA |
| | | bulk matrix from preparation | 2.23% | 17.9 | silt | 138 | sand | 248 | sand | NA |
| | yes | internal | 0.99% | 22.3 | silt | 99.7 | sand | 179 | sand | 1.50% |
| | | external adjacent | 1.32% | 18.5 | silt | 90.9 | sand | 164 | sand | 2.74% |
| | | external distant | 1.34% | 22.9 | silt | 100 | sand | 171 | sand | 1.15% |
| | | bulk matrix from preparation | 0.42% | 35.1 | silt | 155 | sand | 299 | sand | 1.28% |

amounts of silt (Table 2). No special treatment was required of the matrix prior to analysis, such as acidic dissolution of carbonates, suggesting minimal cementation. Clay content is relatively small and less than 3% as measured by number of particles that pass in front of the laser. While clay concentration might be slightly higher external to the integument rendering layer than internal to the integument rendering layer, the sample size is too limited to say with much certainty. The late juvenile appears to have slightly coarser grain distributions in its matrix than does the early adult *Edmontosaurus annectens*. Organic fraction, either sedimentary organics (e.g., fossil plant matter) or applied organic polymers/glues, is also low, at less than 3% by weight in both specimens as estimated through oven ashing. Note that the shift toward large grain size distributions could be due to a loss of small organic particles and/or fusion of clay particles during the oven treatment.

*Photogrammetry and white light scanning.*—When examining the specimens at the macroscopic scale (Figs. 2, 3), both UCRC *Edmontosaurus annectens* "mummy" specimens consist of integument rendering layers that are mostly pale or off-white (Fig. 2D, see also Sereno et al. 2026). This is especially so in the late juvenile UCRC PV31, where both the sediment and the integument rendering have hardly any dark coloration (Fig. $3B_1$). There are putative pale to orange-colored subspherical structures in the sediment that might be clay rip-up clasts around the late juvenile (Fig. $3B_2$, $B_4$), especially lower on the carcass, consistent with high-energy, rapid sedimentation (also see below, where they are present near putative fossil burrows). Possible faint laminations in the sediment of the late juvenile (Fig. $3B_3$, $B_5$), especially numerous near the hips and the ribcage towards the top, might indicate that sediment began to slow after initial deposition of the carcass. Likewise, much of the integument rendering in the early adult UCRC PV30 is relatively light, like the sediment, (Fig. 2) but slightly tanner in color than in the juvenile (Fig. 3). There is occasional orange to black staining sporadically, and sometimes finely, dispersed along the integument rendering of the early adult, with a large ironstone concretion at the tip of the tail (Fig. 2A).

Exceptional anatomical detail of the integument rendering is preserved at the macroscopic level, including skin folds and wrinkles (Fig. $3A_1$, $A_2$), shrinkage around the bones, articulation of the tail spikes in the early adult (Fig. 2B), a dorsal crest in the juvenile (Fig. $3A_3$, $A_4$, $B_1$), and hooves on the early adult (Fig. 2C) (see also Sereno et al. 2026).

*Light microscopy.*—The pale coloration of the integument rendering can be seen on both UCRC specimens at the microscopic level (Figs. 4–6), with occasional flecks of darker compounds dispersed in the early adult *Edmontosaurus annectens* (Fig. 4C).

The exceptional anatomical detail continues at the microscopic level, with surface striations preserved on the early adult hooves and spikes (Fig. 4A, B) and scales as small as ~0.5 mm in diameter preserved in the creases of skin folds on the juvenile (Fig. 6A, B). The cross sections of the integument rendering, spike, and hoof layers on both specimens is extremely thin, less than 1 mm, and sometimes ~200 μm in cross section (Figs. 4D, F, 6C, D).

The sediment matrix is extremely similar under petrographic thin section both externally and internally to the thin fossil integument rendering layer (Fig. 4E). Sub-angular, not well-sorted, predominantly sand-sized grains have almost no cementation, with large pore spaces (i.e., clast dominant), although some grains show some contact dissolution. There is some variability in the color of the grains, indicative of different compositions, and cross-polarized light microscopy

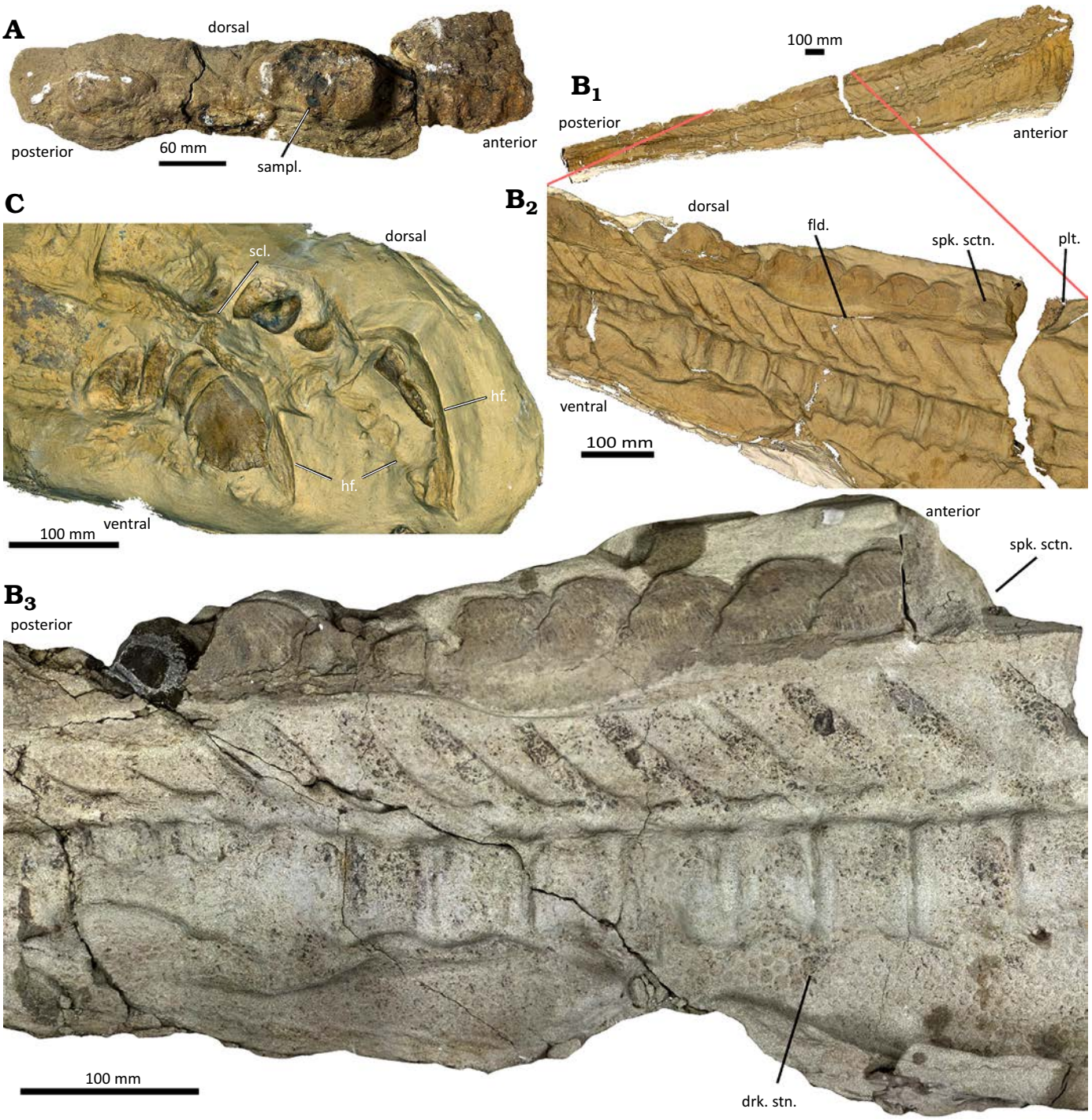


Fig. 2. The early adult *Edmontosaurus annectens* (Marsh, 1892) "mummy" (UCRC PV30 from Wyoming, USA, Late Cretaceous), revealing morphology and coloration. Macroscopic images of ironstone concretion at tail tip (**A**), the tail (**B**), and foot (**C**). $B_1$, $B_2$, the white light scans recorded prior to the removal of the spike block for thin sectioning. A black plant material was revealed underneath the spike that was previously removed and physically prepared in three dimensions. $B_3$, close up showing coloration of the scales and sediment matrix after removal of spike block for thin sectioning. Abbreviations: drk. stn., dark staining material on the scales, different from the applied consolidants; fld., sharp fold in the integument rendering ventral to spikes due to shrink-wrapping during desiccation; hf., hoof; plt., plant material under tail revealed after removal of the three dimensionally prepared spike; sampl., sampling location of ironstone tail tip concretion; scl., scales of the foot; spk. sctn., spike block that was removed and thin sectioned.

(Fig. 4G, H) shows that a few of the grains show birefringence consistent with carbonates (e.g., dolomite or calcite).

It is useful to compare the thickness of this fossil integument rendering layer to histology of modern "reptile"-like scales. In particular, the midsagittal spikes of *Gonocephalus doriae* (Fig. 5A–C) are highly anatomically analogous in shape and imbrication to the tail spikes of *Edmontosaurus annectens* (Fig. 5D) (Sereno et al. 2026). The outermost, highly "keratinized" epidermal layer is likewise very thin. However note that these spikes are ~2–3 mm long anteroposteriorly

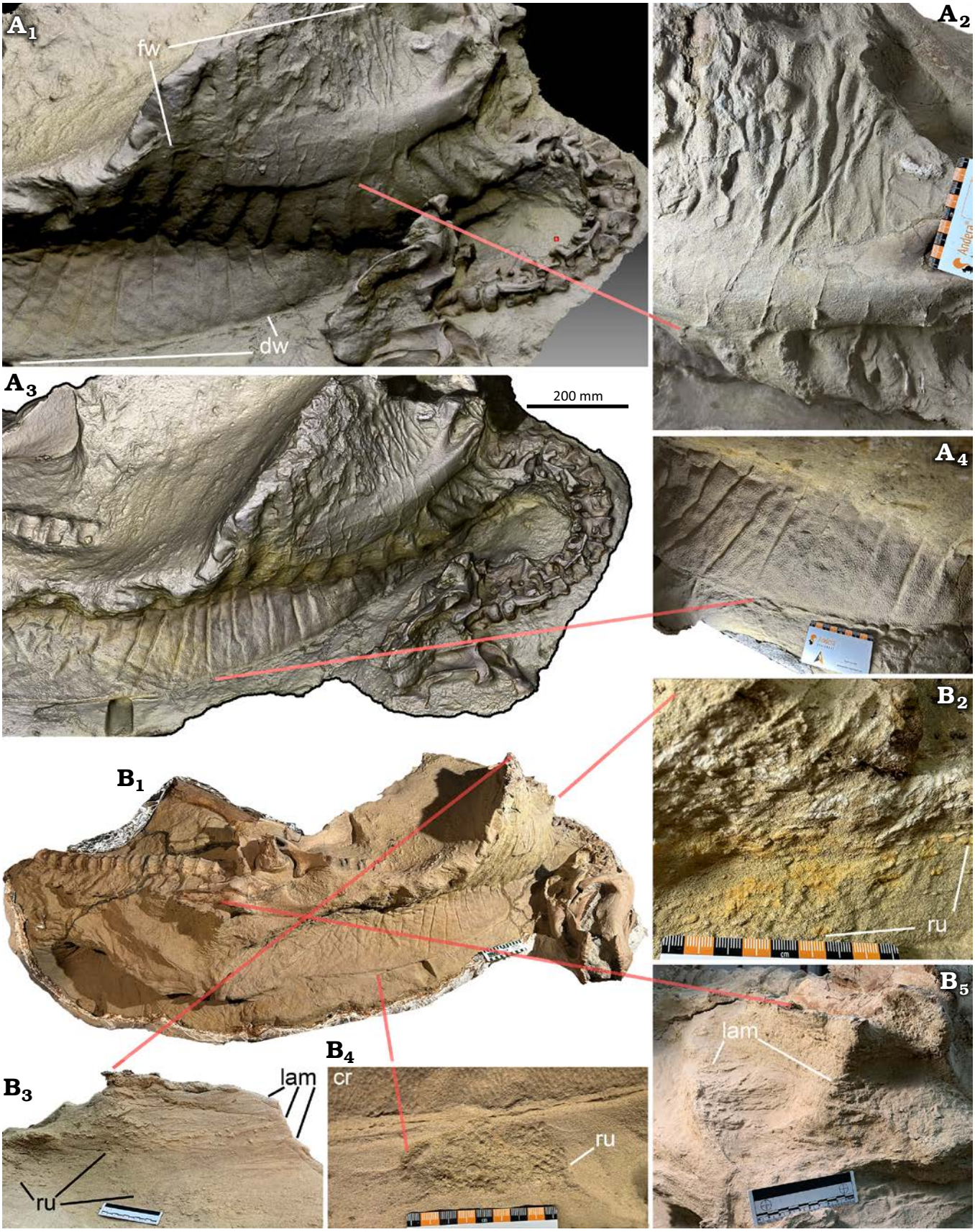


Fig. 3. The late juvenile *Edmontosaurus annectens* (Marsh, 1892) "mummy" (UCRC PV31 from Wyoming, USA, Late Cretaceous), revealing morphology and coloration. **A**. Photogrammetry model showing the deep folded wrinkles of the dorsal crest and fine wrinkles over the scapula and ribs. $A_1$, general view (note that the small red dot is an Agisoft Metashape software measuring marker used to generate the scale bar in $A_3$); $A_2$, close up of the fine wrinkles →

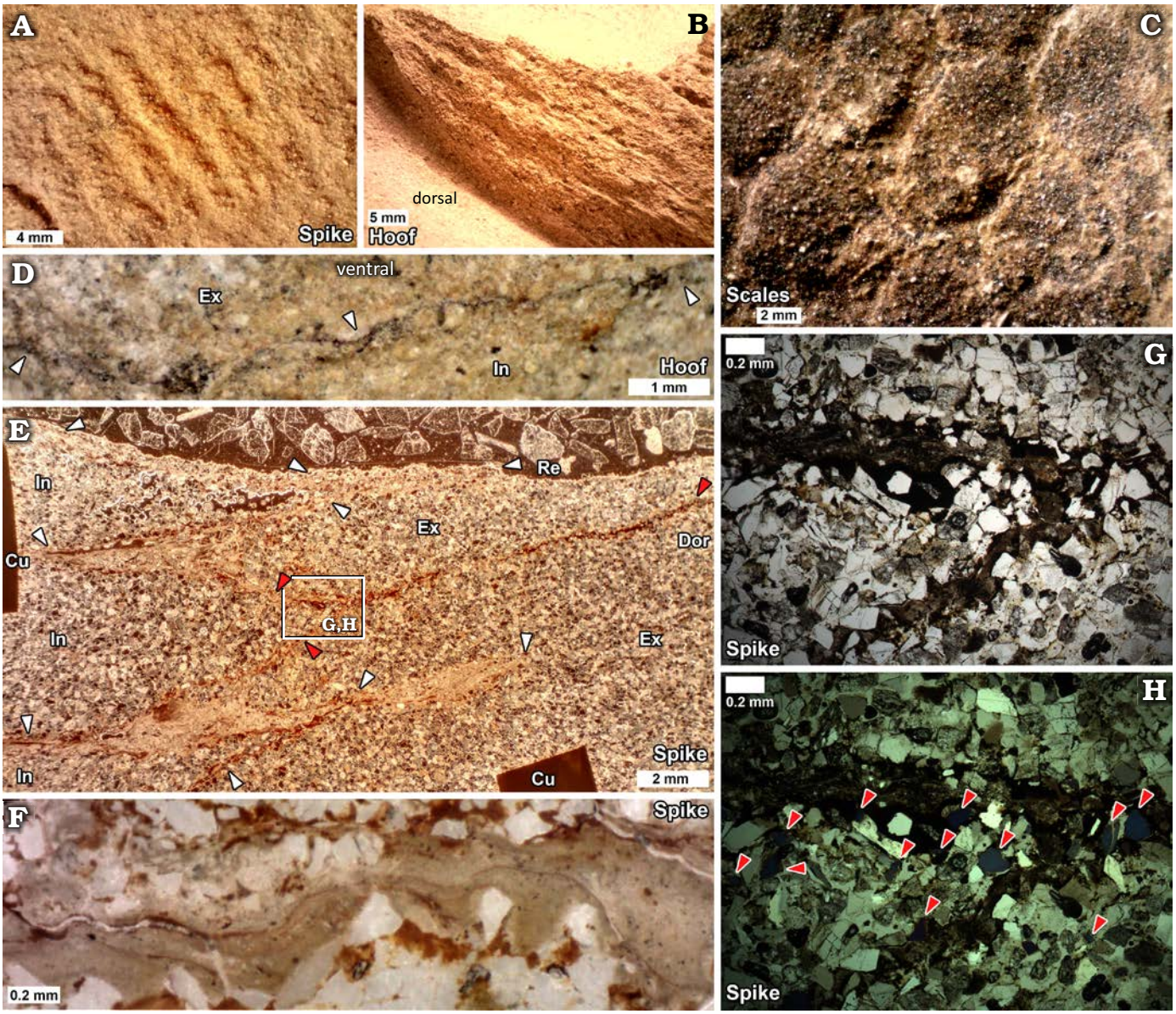


Fig. 4. Light microscopy of the early adult *Edmontosaurus annectens* (Marsh, 1892) "mummy" (UCRC PV30 from Wyoming, USA, Late Cretaceous). **A**–**F**. Digital light microscopy of the surfaces and manually prepared cross sections (A–D) and epoxy-embedded thin sections (E, F) of the spikes, hooves, and scales. **A**. Ridges on the lateral surface of a spike (three positions posterior to the primary thin-sectioned spike). **B**. Grooves and striations on the manually prepared hoof of the right pedal digit IV along its dorsal surface. **C**. Scales preserved on the associated, yet disarticulated integument rendering block found between the legs, showing rosette-like packing and dark material staining the surface. **D**. Manually prepared cross section of the ventral, thin, clay template (indicated by white arrows) of the hoof on right pedal digit III. **E**. Epoxy-embedded transverse thin section of two intersecting tail spikes, whose clay templates are indicated by white arrows for the more anterior spike and red by the inserting, more posterior spike (slide L9L 005 PE, posterior end). Prepared surface to the top, dorsal tips of spikes to the right. **F**. Epoxy-embedded transverse thin section of the clay template (running left to right) of a tail spike (slide L9L 001 AE, anterior end) where the slide was placed atop a white paper background to enhance contrast. **G**, **H**. Polarized light microscopy of the posterior spike seen inserting into the spike anterior to it in E (as indicated by white box), at the point where the clay template collapses into what were once internal cavities towards the dorsal apex of the spike. Plane-polarized (G) vs cross-polarized (H) light with birefringent grains indicated with red arrows. Abbreviations: Cu, copper tape used to aid in identifying regions of interest during microscopy analysis; Ex, external sediment; In, internal sediment; Re, epoxy embedding resin beyond the prepared lateral surface of the tail spike (contains large grains added to assist in sectioning).

and tight shrinking of the skin around the bone in the scapular region; $A_3$, a more top-down view, showing extent of the dorsal crest and tight wrapping of skin around rib cage; $A_4$, close up of the deep wrinkles of the dorsal crest. **B**. Prepared specimen with the front portion of the skull reconstructed for exhibition. $B_1$, general view; $B_2$, orange, clayey layers resembling rip-up clasts below whiter clayey material under the left scapular and coracoids; $B_3$, fine sediment laminations alongside more clayey rip-up clasts internal to the high point on the rib cage; $B_4$, rip-up clasts beyond the dorsal edge of the midline dorsal crest; $B_5$, fine sediment laminations below the high-resting pelvis. Each orange and black tick mark on scale bars in $A_2$, $A_4$, $B_2$, and $B_4$ are 1 cm (except rounded edges of scale bar). The bottom row of green and white ruler in $B_1$ (resting on the jacket behind the skull) has 1 cm squares. Solid black bar on scale bars in $B_3$ and $B_5$ are 10 cm. Abbreviations: dw, deep wrinkles; fw, fine wrinkles; lam, sediment laminations; ru, rip-up clasts.

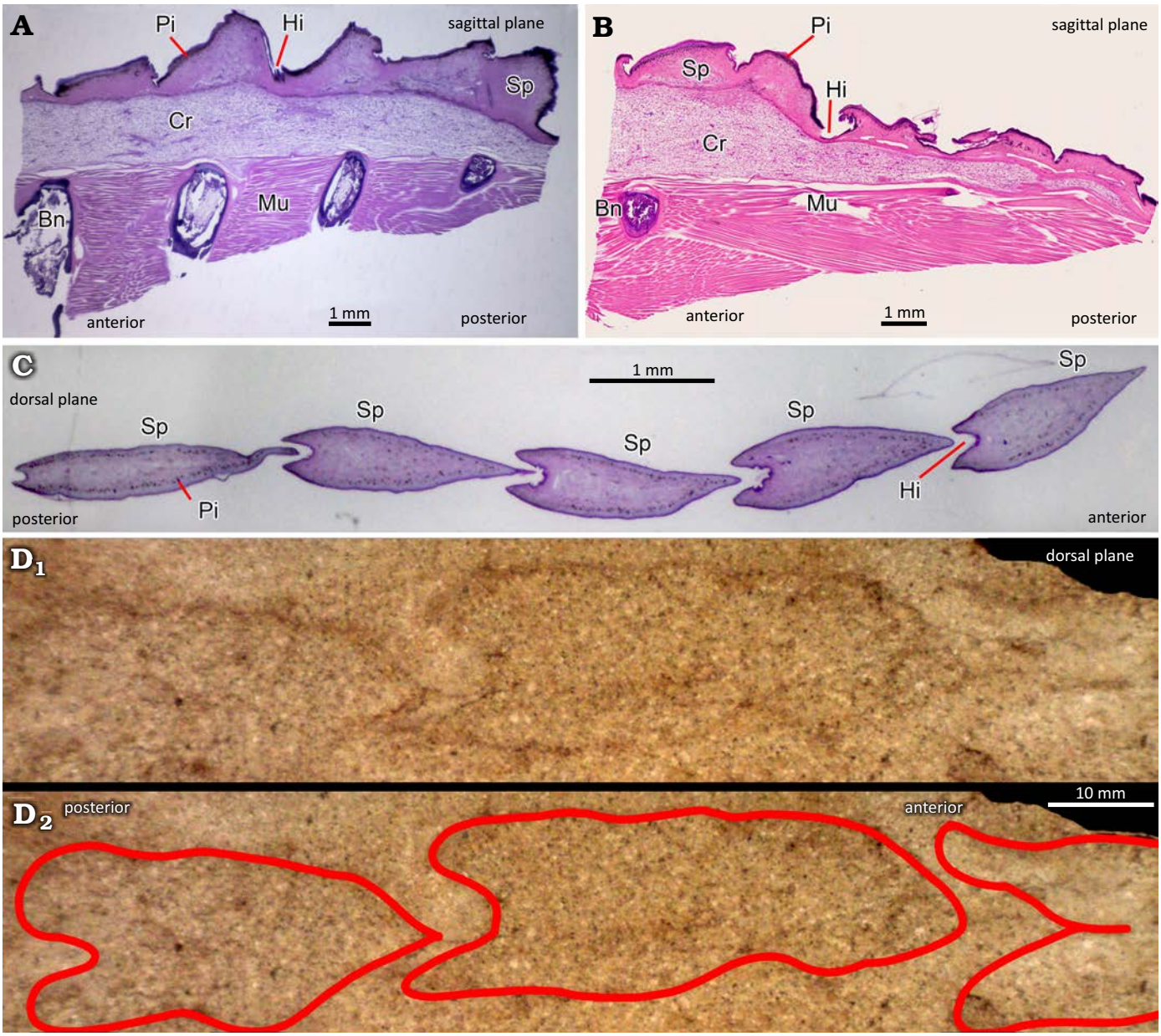


Fig. 5. Histological thin sections of *Gonocephalus doriae* (Peters, 1871) (FMNH H:249773, Borneo, Recent), midline spikes compared to a natural cross section of spikes from the early adult *Edmontosaurus annectens* (Marsh, 1892) "mummy" (UCRC PV30 from Wyoming, USA, Late Cretaceous). **A**–**C**. Staining with hematoxylin and eosin of three different thin sections of the *Gonocephalus doriae* midline crest. Posterior third of the dissected neck crest in sagittal plane viewed under Dino-Lite digital light microscopy from a more medial slice (**A**) and under a more powerful Nikon Eclipse LV150N optical microscope at Loyola University from a more lateral slice (**B**). Slide thickness 20 µm. **C**. Dorsal (i.e., frontal or coronal) plane view of five adjacent spikes, taken from the middle third dissected neck crest viewed under a Dino-Lite digital light microscope. Slide thickness 10 µm. **D**. Natural breakage in the UCRC PV30, showing dorsal (i.e., coronal or frontal) plane cross sections of the clay templates from three spikes; in $D_2$ individual spikes outlined in red. Anterior and posterior directions indicated. Abbreviations: Bn, bone of the cervical vertebrae; Cr, hypodermal tissue of the neck crest, identified as largely adipocytes and connective tissue; Hi, hinge region of the spikes where they imbricate/insert into the spike directly anterior; Mu, muscle of the neck; Pi, pigmented epidermis, identified as mostly melanophores; Sp, dermal tissue of the spike.

on an animal that is ~16.5 cm from snout to vent (Das 2004), while the *Edmontosaurus annectens* spikes are on the order of ~10 cm long anteroposteriorly on an animal that has been estimated to be up to 12 m long from snout to tail tip (Wosik and Evans 2022). As such, it is reasonable to think that the dinosaur's outermost epidermal layer would be thicker than that observed in *Gonocephalus doriae*, and that the integument rendering is not a direct replacement of that layer.

*Computed X-ray tomography*.—Both the micro-CT and hospital CT scans reveal that the integument rendering is consistently preserved as an extremely thin layer within a porous sand that is similar internally and externally (Fig. 7B, C, F). These scans even allow for the digital reconstruction of integument rendering still unexposed from the matrix (Fig. 7A, D). The appearance of high X-ray attenuation in the integument template compared to the sand

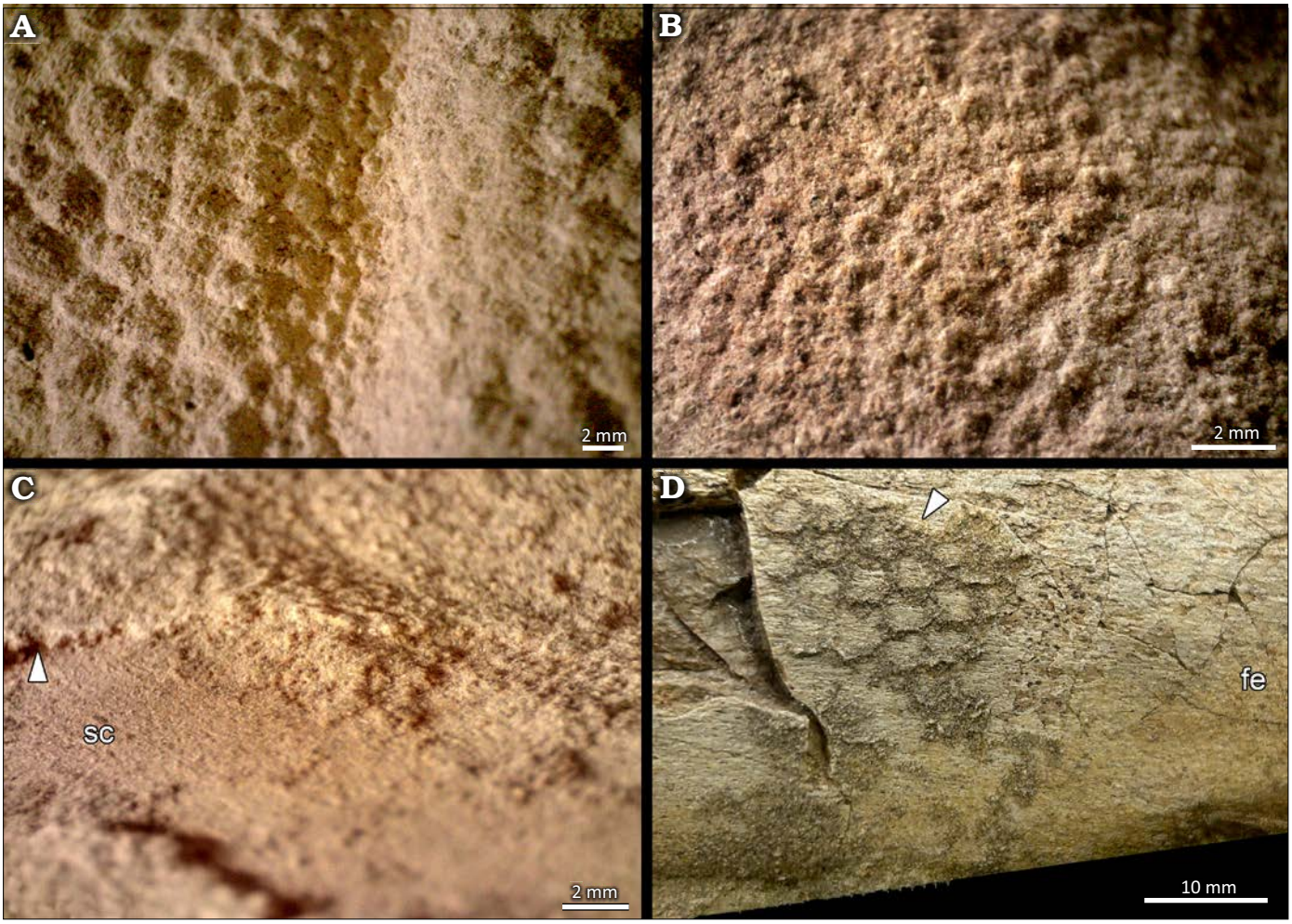


Fig. 6. Light microscopy of the late juvenile *Edmontosaurus annectens* (Marsh, 1892) "mummy" (UCRC PV31 from Wyoming, USA, Late Cretaceous). **A**. Small scales present inside of the deep wrinkle of the midline dorsal crest. **B**. Extremely small scales at the base of the tail. **C**. Natural cross section of integument rendering (indicated by white arrow) at the edge of a region of broken integument rendering on the scapula. **D**. "Honeycomb' scale preservation (arrow) on the femur presumably due to loss of the high point of each templated scale, retaining only the template of the lower hinge region. Abbreviations: fe, femur; sc, scapula.

matrix could derive from (i) elevated concentrations of elements such as Fe, Mn, or S in the integument template (see below) as well as (ii) large, uncemented pores in the sand matrix (i.e., high attenuation is influenced by electron density, not just atomic number). CT scanning of the tail tip at a region anterior to a large concretion produces relatively high amounts of noise and poor resolution of the X-ray (Fig. 7E), possibly consistent with elevated iron content as one nears the concretion.

*Laser-stimulated fluorescence photography.*—LSF photography of the AQ (anterior quarter) 150-µm thin section from the early adult *Edmontosaurus annectens* spike shows that the integument template appears as slightly darker brown compared to the tanner internal and external sand matrix (Fig. 8$A_2$, $A_3$). There is no strong fluorescence from the integument template that one might expect from phosphate. Furthermore, one can see small amount of this dark brown material dispersed sporadically though the matrix (Fig. 8$A_1$).

*Portable X-ray fluorescence.*—The integument rendering of the early adult *Edmontosaurus annectens* (UCRC PV30) "mummy" was examined with pXRF to determine the concentrations of various trace elements and compare those concentrations with the nearby sediment matrix (Table 3). In general, the fossil integument rendering is enriched in various trace elements compared to the surrounding sand matrix, including Zn, Ni, and Fe, although it might be slightly depleted in K in this pXRF analysis and/or specific sampling location. In particular, the fossil is greatly enriched in Mn and S. Note that we expect pXRF to show lower sensitivity (i.e., higher limits of detection) for lighter elements (e.g., O, Al, Si) compared to EDS (Mu and Stowe 2024), hence why pXRF struggled to detect these elements detected by EDS.

*Synchrotron XRF.*—Synchrotron XRF possesses a much more powerful X-ray source than the pXRF model. These results (Fig. 9) on the integument rendering of early adult UCRC PV30 from the small skin block that separated be-

Table 3. Portable XRF averaged results (number of spectra, n, within each average reported), compared as differences and percent changes (values below the limit of detection were coded as 0.00 for the purposes of averaging; ppm presented here to the nearest hundredth, based on this analytical precision; percent change rounded to the nearest whole number) between the early adult UCRC PV30 *Edmontosaurus annectens* integument rendering and associated sediment matrix from three regions of the specimen: a flaked sample of spike fragment with sediment on the underside, the small block of integument rendering between the hip and tail jacket that separated during excavation, and the large block of disarticulated and isolated integument rendering that was found between the legs and consolidated heavily with organic polymers to stabilize it. For the integument rendering on this final region (large skin block), we also present a comparison between the fossil integument rendering and a region on the integument rendering surface of the block that was covered with a thick layer of glue in order to try to isolate the signature of the glue. N/A indicates a division by zero (i.e., non-detection of an element in the sediment or glue) when calculating percent change.

| Value | Difference (ppm): fossil –sediment | Difference (ppm): fossil –sediment | Difference (ppm): fossil–sediment | Difference (ppm): fossil –thick glue | % change: sediment to fossil | % change: sediment to fossil | % change: sediment to fossil | % change: thick glue to fossil |
|---|---|---|---|---|---|---|---|---|
| Sample | spike fragment | small skin block | large skin block: heavy consolidant | large skin block: heavy consolidant | spike fragment | small skin block | large skin block: heavy consolidant | large skin block: heavy consolidant |
| Number of spectra | 2 fossil 2 sediment | 3 fossil 2 sediment | 3 fossil 4 sediment | 3 fossil 1 glue | 2 fossil 2 sediment | 3 fossil 2 sediment | 3 fossil 4 sediment | 3 fossil 1 glue |
| Mo | 8.36 | 6.77 | -0.96 | -3.40 | 155 | 111 | -26 | -56 |
| Zr | 396.25 | 23.18 | 219.99 | 334.73 | 179 | 6 | 102 | 334 |
| Y | 11.74 | 0.48 | 8.88 | 9.91 | 86 | 3 | 71 | 87 |
| Sr | 10.23 | 25.40 | 78.75 | 83.64 | 11 | 23 | 73 | 82 |
| U | 0.00 | -3.86 | 1.09 | 2.50 | N/A | -58 | 78 | N/A |
| Rb | 5.37 | -6.42 | 1.99 | 3.93 | 21 | -20 | 7 | 15 |
| Th | 7.68 | -2.17 | 6.14 | 6.93 | 165 | -25 | 88 | 112 |
| Pb | 39.77 | 14.00 | 15.58 | 16.01 | 345 | 109 | 126 | 135 |
| As | 131.08 | 12.53 | 17.10 | 21.58 | 708 | 400 | 382 | N/A |
| Zn | 262.88 | 111.29 | 70.83 | 76.85 | 632 | 219 | 204 | 267 |
| Cu | 40.34 | 6.33 | 24.68 | 25.85 | N/A | 18 | 92 | 100 |
| Ni | 47.40 | 170.07 | 130.38 | 139.33 | N/A | 903 | 418 | 627 |
| Co | 329.31 | -56.51 | 0.00 | 0.00 | N/A | -100 | N/A | N/A |
| Fe | 32084.07 | 24172.94 | 15283.87 | 19819.88 | 265 | 147 | 98 | 180 |
| Mn | 621.84 | 6782.82 | 6121.98 | 6190.63 | 810 | 1502 | 2007 | 2619 |
| Cr | 47.29 | 51.66 | 22.04 | -2.62 | N/A | 135 | 57 | -4 |
| V | 36.37 | 25.98 | 13.09 | 20.86 | 74 | 72 | 29 | 56 |
| Ti | 132.23 | 149.75 | 455.90 | 1586.62 | 6 | 9 | 23 | 190 |
| Sc | 56.06 | -30.42 | 90.84 | 51.30 | N/A | -100 | 199 | 60 |
| Ca | 4536.58 | -14889.97 | 22293.90 | 35681.72 | 28 | -33 | 74 | 215 |
| K | -1547.40 | -1279.76 | -1875.02 | 4676.85 | -13 | -12 | -16 | 86 |
| S | 2935.77 | 303.40 | 4766.73 | 5543.72 | 1805 | 304 | 299 | 678 |
| Ba | -92.24 | -49.69 | 118.78 | 142.17 | -100 | -6 | 20 | 25 |
| Cs | 0.00 | 2.38 | 19.87 | 20.97 | N/A | 3 | 48 | 52 |
| Te | 0.00 | -4.17 | 29.34 | 29.75 | N/A | -4 | 61 | 63 |
| Sb | 0.00 | -13.97 | 24.43 | 12.31 | N/A | -19 | 131 | 40 |
| Sn | 0.00 | -6.15 | 9.29 | 9.85 | N/A | -18 | 71 | 78 |
| Cd | 0.00 | 0.59 | 7.49 | 15.91 | N/A | 2 | 89 | N/A |
| Ag | 0.00 | 0.05 | 5.39 | 10.32 | N/A | 0 | 109 | N/A |
| Pd | -2.27 | 0.00 | -2.67 | 0.00 | -100 | N/A | -100 | N/A |
| Nb | 5.67 | -0.47 | 4.85 | 5.75 | 46 | -3 | 46 | 59 |
| Bi | 12.51 | 0.00 | 15.20 | 15.20 | N/A | N/A | N/A | N/A |

tween the hip and tail jacket during excavation are generally consistent with the results from the pXRF as well as the analyses described below, with detection of elements such as K and Ca. Notably though, the sXRF shows colocalization and broad distribution of Fe and S across the integument rendering.

*Electron microscopy (BSE) and energy dispersive X-ray spectroscopy (EDS).*—Initial EDS results from the early adult *Edmontosaurus* (UCRC PV30) "mummy" spike fragment (Fig. 10C) reveal a C signature on its surface, consistent with the presence of applied organic consolidant or glue, and further supported with the observation from a basement scale that fell off from the ventral side of the epoxied spike block removed for thin sectioning which showed colocalized C and Cl signatures under EDS on its surface as would be expected after applying Epotek 301 (SOM 1).

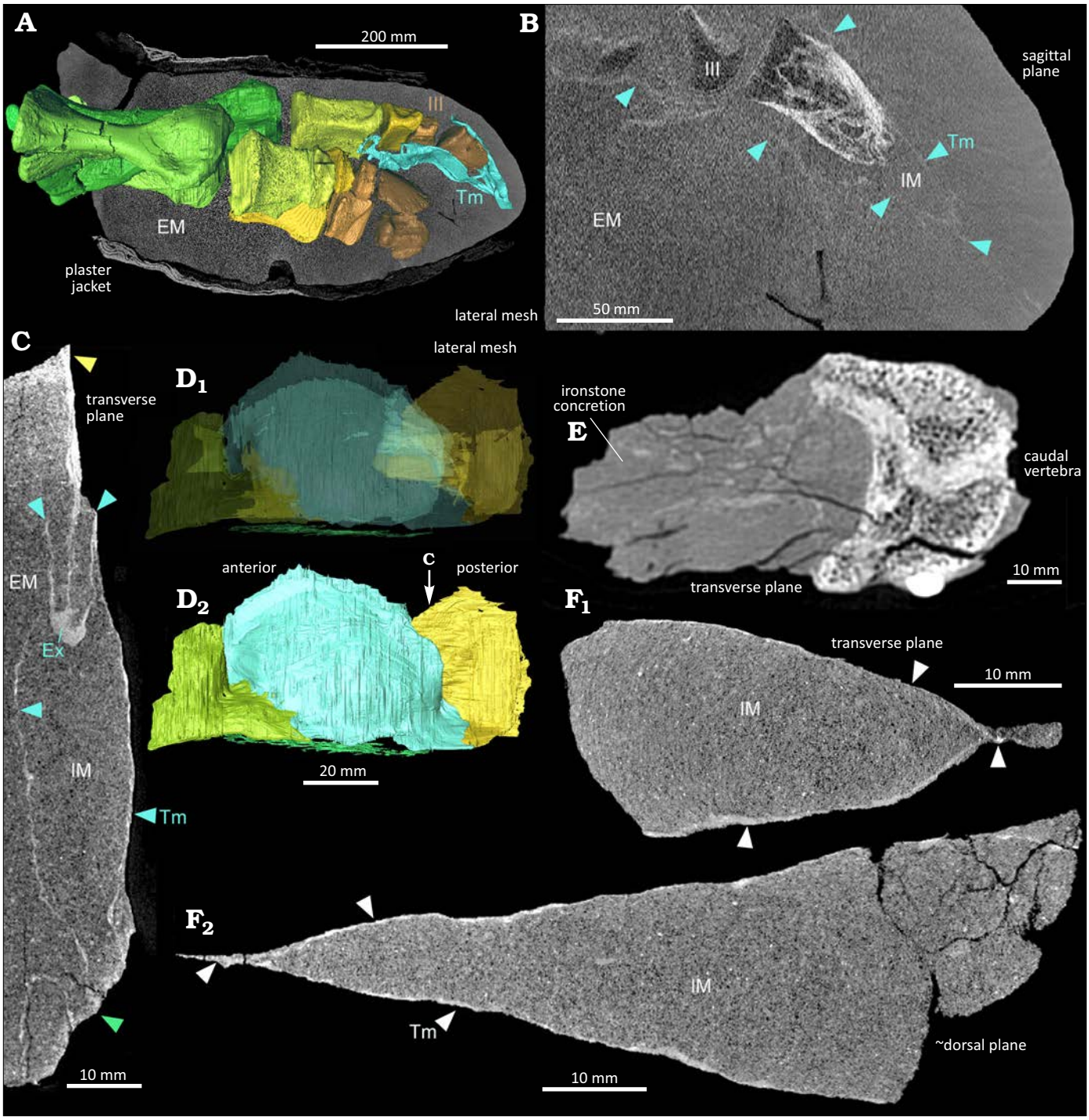


Fig. 7. CT scan data from the early adult *Edmontosaurus annectens* (Marsh, 1892) "mummy" (UCRC PV30 from Wyoming, USA, Late Cretaceous). **A**. Right pes in lateral view with integumentary clay template (hoof plus some skin) traced in blue around the distal end of digit III. **B**. Close-up of digit III sagittal plane slice showing the thin, yet visible clay template marked by blue arrows. **C**. Transverse section of the intersection of two spikes from the spike block that was later resin embedded and thin sectioned, showing excess clay in external nooks and collapses of internal nooks towards the dorsal apices of the spikes (arrows color coded according to colors in D indicate the specific spike [blue or yellow] or basement scales [bright green]). **D**. The lateral transparent ($D_1$) and opaque ($D_2$) meshes showing the posterior yellow spike inserting into the notch of the middle blue spike and green ventral, basement scales of the tail folded down (i.e., out of plane with the spikes) due to shrink wrapping of the skin of the tail. Anterior and posterior directions indicated, such that the surface facing the viewer is the unexposed left side in the unprepared matrix. Arrow in D shows the approximate location of the transverse slice C. **E**. Transverse section of the tail tip anterior to the concretion, showing the caudal vertebra and the noisy sediment matrix. **F**. Transverse ($F_1$) and approximately dorsal (i.e., frontal or coronal) ($F_2$) slices of the spike immediately anterior to the thin-sectioned spike block, which was manually prepared in three dimensions. The slices show no internal structure other than sandy matrix internal to the thin clay template (indicated by arrows). Abbreviations: III, pedal digit three; EM, external matrix; Ex, excess clay accumulation in external nooks; IM, internal matrix; Tm, clay template of integument.

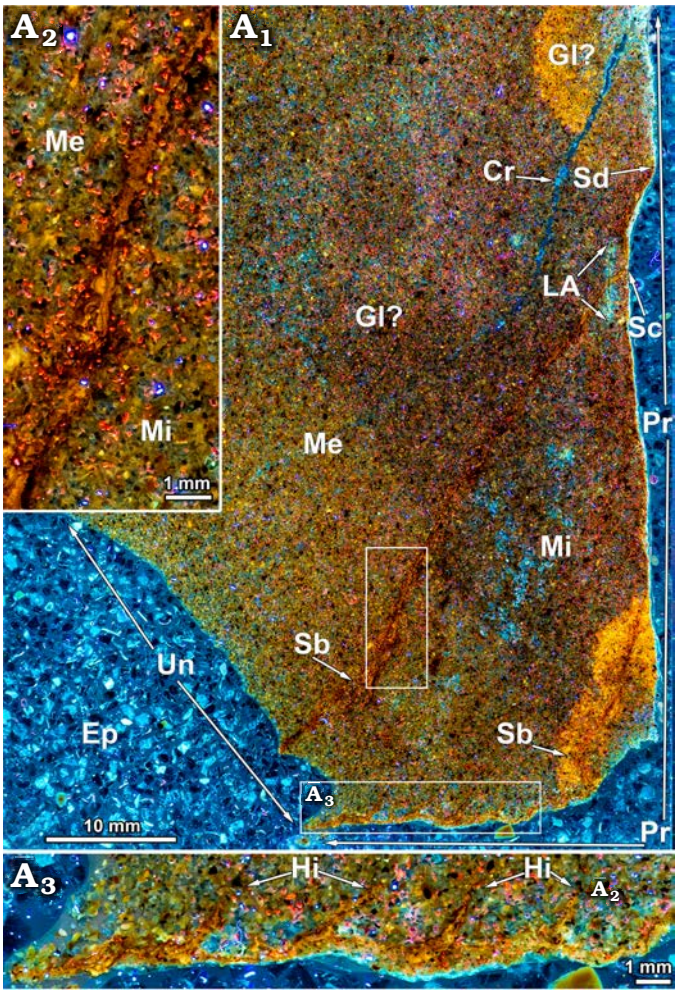


Fig. 8. The LSF photograph of the AQ (anterior quarter) 150-µm thin section of spike of early adult *Edmontosaurus annectens* (Marsh, 1892) "mummy" (UCRC PV30 from Wyoming, USA, Late Cretaceous). $A_1$, general view; $A_2$, prepared clay template of dorsal-most tail scales below the spike; $A_3$, unexposed clay template of spike. Abbreviations: Cr, crack in sediment matrix infilled with epoxy; Ep, epoxy embedding resin; Gl?, possible soaking of glues or other consolidants from the prepared surface down into the block; Hi, hinge region of scales; LA, artifact of laser preliminary test transect etched into the surface of the slide from LA-ICP-MS; Me, matrix external to template; Mi, matrix internal; Pr, manually prepared surface of sampled block exposing integument rendering; Sb, basal limit of midline spike above the scales of the tail; Sc, point of collapse of the dorsal portion of the spike; Sd, dorsal extent of spike's clay template; Un, unprepared surface of sampled block.

The results from the early adult UCRC PV30 spike thin section (Fig. 10A) suggest that this C is not localized to the fossil integument rendering layer compared to the sediment matrix, nor does the integument template contain any significant amounts of C within it. Instead, in thin section, C is clearly localized to the pore spaces and cracks in the integument template, deriving from the epoxy resin the sample was embedded in. Likewise, the integument template cross section is not particularly strong in S, which would be expected from original corneous β-proteins (i.e., β-"keratins"). Cl is also present in and mostly localized to the pore spaces, although weaker in its EDS signal than is C. Thus this Cl likely derives mostly from an epoxy resin precursor (Householder and Boyd 2023, 2024).

In thin section, the fossil integument rendering itself appears under BSE as a thin, low porosity, laminated layer compared to the porous sand (Fig. 10B), and EDS shows it to be particularly enriched in Al, Si, O, and Fe. O is present in all the sand grains and the integument template. While Si is prevalent in both the integument template and most of the sand grains (i.e., consistent with quartz and feldspars), Al is present in the integument template and only some of the sand grains (i.e., consistent with just the feldspars). Al, Si, and O in the integument template are indicative of aluminosilicates (consistent with its laminated and denser structure compared to the sand matrix). As for common cations between aluminosilicate clay layers, Ca is present with a more limited signal in the integument template and in some of the sand grains (i.e., consistent with carbonate grains). Other common aluminosilicate cations are likewise present with limited signal in the integument template and some of the sand grains (i.e., consistent with feldspars) including K, Na, and Mg.

Cu, an element that often chelates to fossil melanin and other fossil organics (Vinther 2015), is largely absent from the sample in the EDS signal. Furthermore, the integument template is not enriched in P, as would be expected if the skin had authigenically phosphatized.

Based on averaging of elemental compositional profiles (raw counts of 15 auto-assigned elements by Aztec software in each spectrum calculated as percentages) of fossil spectra from five regions of interest and sand spectra from five regions of interest (two internal, three external), the integument template is notably depleted in C (found in the porous spaces of the sand from the embedding epoxy) and possibly enriched in Na, Mg, Al, K, Ca, and Fe (SOM 1). Note that these regions of interest are not equally sized. Furthermore, the average internal and external sand elemental composition are very similar to each other.

The late juvenile *Edmontosaurus* (UCRC PV31) "mummy" integument rendering shows a < 500-µm clayey (i.e., platy, fine grain) layer (perhaps ~200–250 µm) above a layer of internal sandy matrix with large silica-rich grains (Fig. 11A), itself originally atop the bone of the scapula. As in the early adult, this layer is enriched in various elements consistent with aluminosilicate clays, such as Al. The late juvenile perhaps shows a more prominent Ca signal in its integument rendering than the early adult (Fig. 11B, C), but the Ca does not colocalize with P (i.e., it is not phosphatized skin). P is actually most prevalent on the sandy surface directly in contact with the bone. The Ca-rich region of the integument rendering layer could represent Ca interlayer cations associated with clays, such as montmorillonite or illite (Carroll 1959). This Ca-rich region could also be partly consistent with calcite—containing O, with somewhat crystalline structure of fine grains, although the C signature is limited and may therefore represent surface consolidants—as well as minor amounts of dolomite in some regions (i.e., where Mg occasionally colocalizes with the Ca; SOM 1).

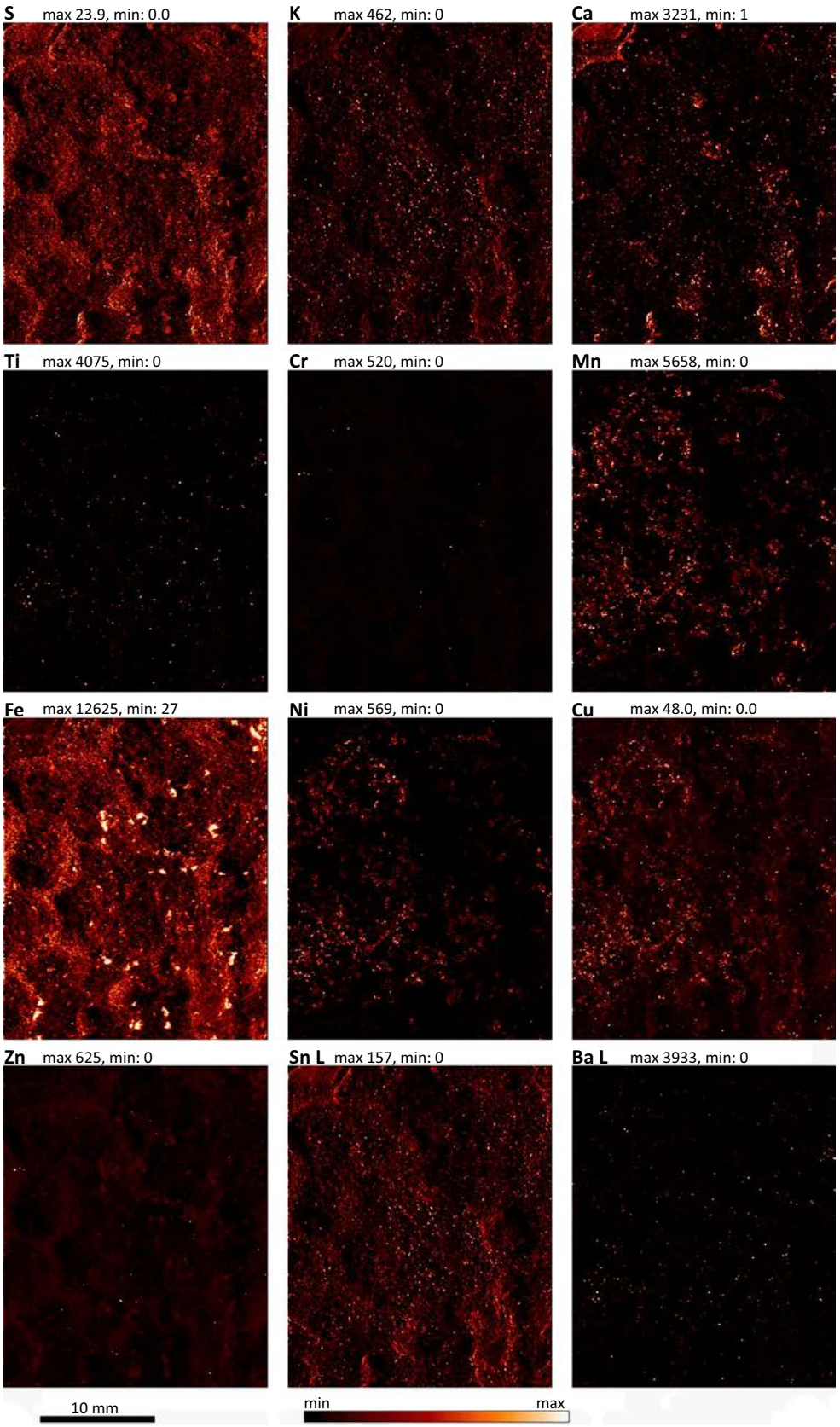


Fig. 9. Synchrotron XRF maps from the integument rendering of early adult *Edmontosaurus annectens* (Marsh, 1892) "mummy" (UCRC PV30 from Wyoming, USA, Late Cretaceous). The very top left semicircular region in the scan is the boundary between the preserved region of integument rendering and start of the visible matrix. Results show colocalization broadly across the mapped region of the integument rendering of Fe and S. For Sn and Ba, L-line emissions are shown. L lines are characteristic X-rays produced when electrons fill vacancies in an atom's L shell.

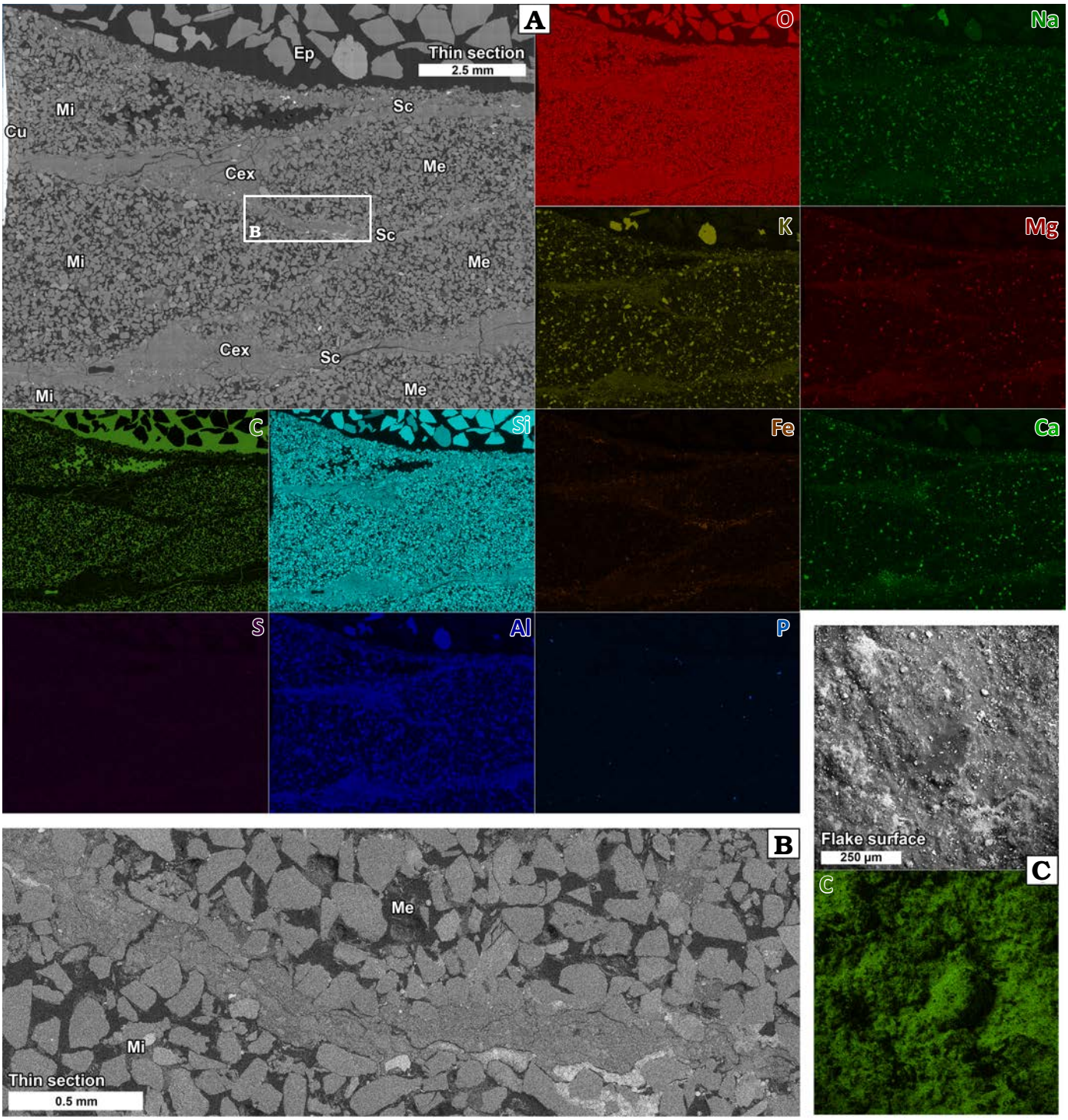


Fig. 10. BSE and EDS results from the early adult *Edmontosaurus annectens* (Marsh, 1892) "mummy" (UCRC PV30 from Wyoming, USA, Late Cretaceous); tail spike samples and surrounding sediment. **A**. BSE image of transverse thin section through two imbricating spikes with corresponding EDS elemental maps showing aluminosilicate composition of the clay template, paucity of organics or phosphates in the template, and the sandy matrix composition. Images are oriented in line with burial position of the carcass: prepared lateral surface at top, unprepared lateral surface to bottom, dorsal direction to right, ventral direction to left. **B**. Close-up BSE image of the clay template in A, showing fine-grain nature of the clay template running from top-left to bottom-right of panel relative to sandy matrix. **C**. A flake sampled from a tail spike ($C_1$, BSE surface; $C_2$, corresponding carbon EDS map), showing organic contamination of the prepared surface. Abbreviations: Cex, excess, external clay accumulation; Cu, copper tape applied to the slide to assist in electron imaging; Ep, epoxy embedding resin (large silicate grains in the external epoxy were added during the embedding process to improve thin sectioning); Me, matrix external to the clay template; Mi, matrix internal to the clay template; Sc, spike's clay template collapse point.

If Ca is coming from calcite, the carcass could have experienced a bit of carbonate precipitation during subaqueous organic decay, followed by minor amounts of diagenetic dolomitization of calcite (Machel and Mountjoy 1986).

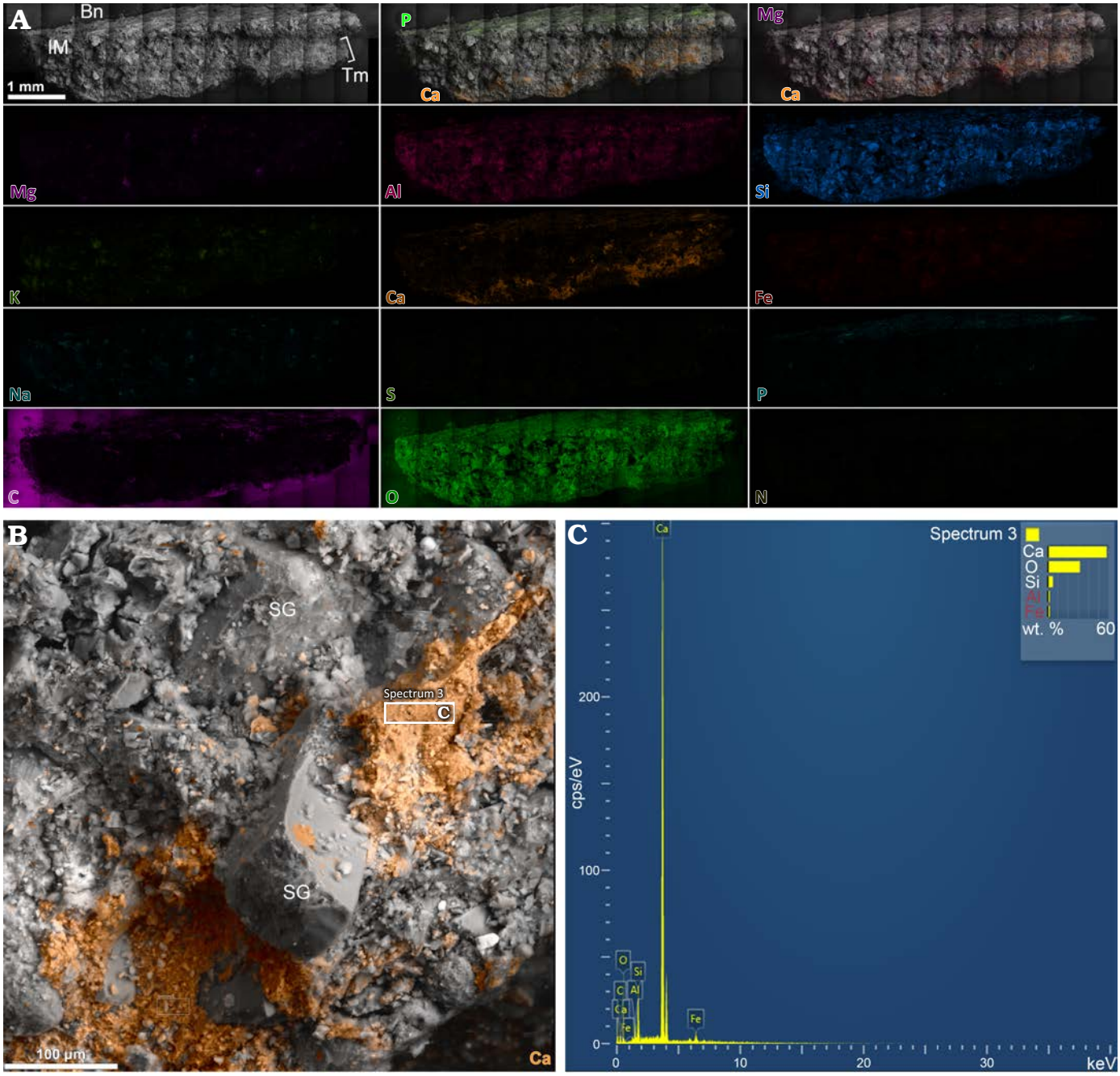


Fig. 11. BSE and EDS results from the late juvenile *Edmontosaurus annectens* (Marsh, 1892) "mummy" (UCRC PV31 from Wyoming, USA, Late Cretaceous); integument rendering and internal sediment above the scapula. **A**. BSE image showing the sample's cross section with surface contacting the scapula at the top, the clay template layer toward the bottom (bracketed), and the internal sediment matrix between. Alongside the BSE image are a series of EDS maps, showing lack of colocalization between Ca and P and limited colocalization between Ca and Mg. Individual elemental maps shown without overlaying onto the BSE image. Blocky sand grains of the matrix are Si rich. The clay template has a more platy, small-grained texture and is enriched in Al, Si, Ca, O. The sample is strongly depleted in elements that could derive from organics such as C (present in the underlying glue affixing it to the microscopy pin stub), S, and N, and is also depleted in P away from the surface in contact with the apatite bone (i.e., the Ca is not in the form of $CaPO_4$). **B**. BSE image showing the Ca fine granular or crystalline in texture, among more platy clays and large, blocky sand grains. **C**. EDS the spectrum from the boxed region shown in B, revealing that the Ca is dominant and associated with O and Si (i.e., the Ca could be associated with silicates, such as the clays). Abbreviations: Bn, surface in contact with bone of scapula; IM, internal matrix; SG, sand grain; Tm, clay template.

When examining the thin section of the early adult "mummy" spike, there are some patches of Fe along the edges of the integument template. The results from the dark staining materials on the early adult UCRC PV30 further elaborate on these patches (Fig. 12). Dark staining minerals on the fossil basement scales (Fig. 12A) reveal colocalization of Fe and O (i.e., consistent with iron oxides) and Mn and O (i.e., consistent with manganese oxides) between silicate grains, Mg and Ca grains (i.e., consistent with dolomite, and notably with limited P that does not obviously

colocalize with Ca), aluminosilicate clays. Occasionally, there is also colocalization of Fe and S (i.e., consistent with pyrite). Interestingly, samples of black (Fig. 12B) and orange (Fig. 12C) staining from the small skin block that separated between the tail and hip jacket, which was analyzed with synchrotron XRF in December 2017 and showed a broad, colocalized Fe and S signal (i.e., consistent with pyrite), now instead seemed to show more of a consistent Fe and O signal under EDS in July 2024, with only limited S, possibly suggesting some amount of pyrite oxidation (i.e., "pyrite disease"). However, sXRF penetrates deeper and has lower detection limits than EDS, so this difference could be analytical rather than temporal. The more orange stains from this small skin block still show some S signal, while the darker regions of this block only reveal Fe and Mn, as do dark stains sampled from the scales of the tail.

The sample taken from the large ironstone concretion from the tip of the tail (Fig. 13) has regions observed in BSE (Fig. 13D) with Fe and S localization, and others with Fe and O localization, suggestive of weathering of pyrite into iron oxides (Fig. 13A–C). Within this iron-rich matrix, angular Al- or Si-rich grains (i.e., consistent with feldspars and quartz, respectively) can be found, and they may not be as compacted as sand grains observed elsewhere in the integument rendering samples and matrix. They particularly seem to show greater spacing between grains than does the matrix external and internal to the thin-sectioned tail spikes—although comparison is complicated by the fact the ironstone fragment is a chipped off cross section, rather than a flat plane made through thin sectioning. A cracked surface under BSE shows C and O localization but is weaker in its Fe signal—meaning that this ultrascopic texture might represent fossil organic material (e.g., decay-labile plant matter) that nucleated the concretion rather than a carbonate matrix of the ironstone, or it could be the result of pyrite oxidation and iron depletion in the core of the concretion, leaving behind weathered, iron-depleted carbonate (Loope et al. 2012).

*Laser ablation-inductively coupled plasma-mass spectrometry.*—The LA-ICP-MS results (Table 4) suggest that the material of the fossil and matrix is not overall dense (compared to other types of materials), due to the production of visible holes/troughs along the path of laser ablation. Additionally, the samples had heterogeneity in elemental concentrations and overall signal intensity (counts per second) during ablation, as well as across analysis sites. The early adult UCRC PV30 spike flake is likely enriched in many minor/trace elements compared to the nearby external sand matrix when calculated as ppm of individuals elements, including Fe, Mn, Ca, K, Al, Mg, Na, but is relatively depleted in elements such as P compared to the matrix. Since Table 4 presents ppm rounded to the nearest whole number, it does not fully reflect the limit of detection of the LA-ICP-MS, which can be < 1 ppm for many, but not all, elements (SOM 1). Accordingly, our aim is to judge enrichment and depletion patterns in major/minor elements as opposed to trace levels

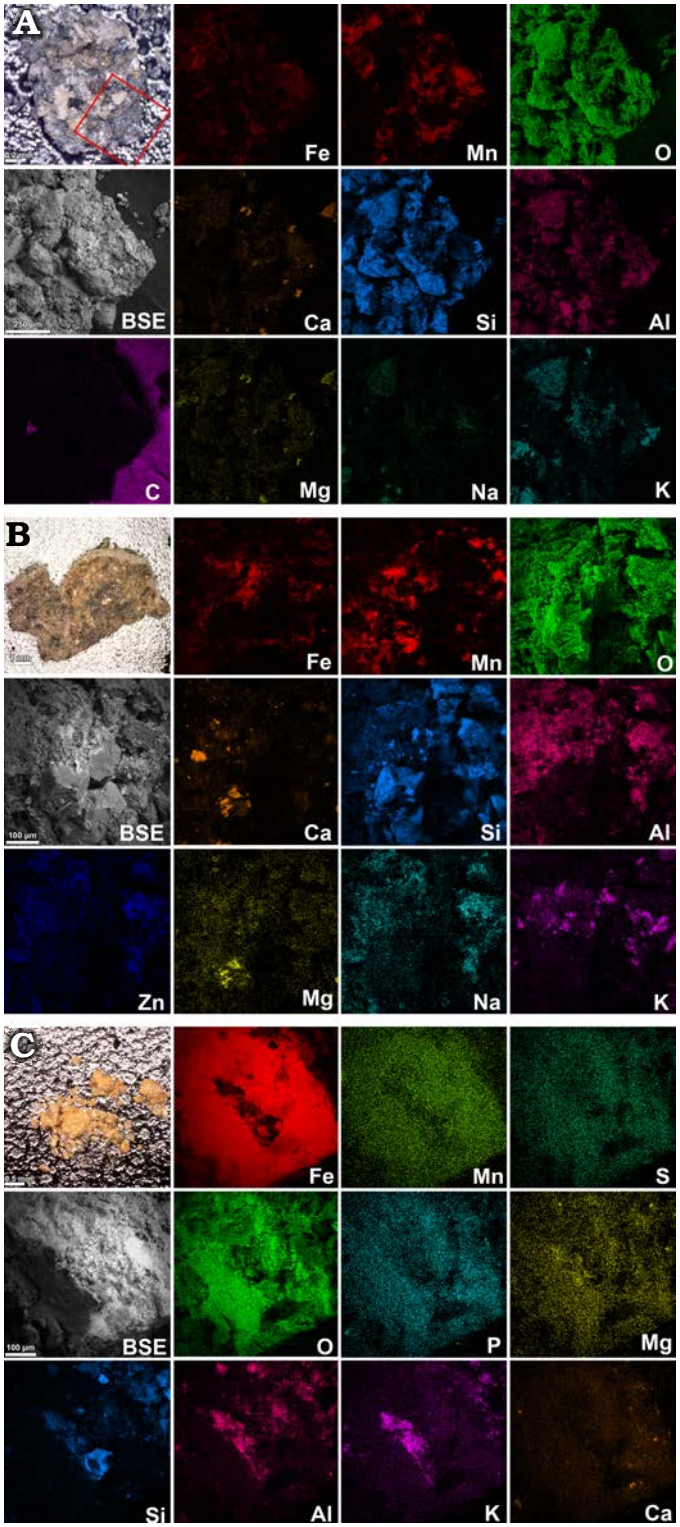


Fig. 12. Digital light microscopy ($A_1$–$C_1$), BSE ($A_2$–$C_2$), and EDS (30 kV beam voltage) of key elements ($A_3$–$A_{12}$, $B_3$–$B_{12}$, $C_3$–$C_{12}$) results from the dark black and orange staining material on the early adult *Edmontosaurus annectens* (Marsh, 1892) "mummy" (UCRC PV30 from Wyoming, USA, Late Cretaceous) integument rendering. **A**. Sample from dark black scale on ventral tail (BSE and EDS region of interest mapped onto light micrograph as a red box). **B**. Sample from dark black- (and orange-) stained integument rendering on base of tail. **C**. Sample from orange-stained integument rendering on base of tail. Samples in B, C taken from same block that was scanned with synchrotron XRF at Argonne National Laboratory (ANL) (see Fig. 9).

Table 4. LA-ICP-MS summary of the early adult *Edmontosaurus annectens* UCRC PV30 fossil spike and associated sediment matrix. Each sampling site is an average of a depth profile at that location from the laser. Si is the internal standard, with extremely consistent results for that element. All averages were then rounded to the nearest whole ppm, so this table sets a higher detection threshold (0.5 ppm) than that of the equipment. Light or dark grey indicate enrichment or depletion, respectively, of the element in the fossil after rounding.

| Elements | Average ppm (rounded) UCRC PV30 fossil spike flake (n = 10 sites) | Average ppm (rounded) UCRC PV30 sediment (n = 10 sites) | Elements | Average ppm (rounded) UCRC PV30 fossil spike flake (n = 10 sites) | Average ppm (rounded) UCRC PV30 sediment (n = 10 sites) |
|---|---|---|---|---|---|
| Si | 360301 | 367624 | Sb | 6 | 100 |
| Na | 6914 | 5282 | Cs | 4 | 3 |
| Mg | 7620 | 1872 | Ba | 503 | 280 |
| Al | 59711 | 40561 | La | 20 | 11 |
| P | 782 | 9261 | Ce | 34 | 25 |
| K | 16636 | 10901 | Pr | 4 | 3 |
| Ca | 10503 | 1156 | Ta | 1 | 0 |
| Mn | 502 | 64 | Au | 0 | 0 |
| Fe | 39216 | 8244 | Y | 14 | 6 |
| Pb | 112 | 205 | Bi | 1 | 0 |
| Li | 12 | 7 | U | 3 | 1 |
| Be | 2 | 3 | W | 1 | 1 |
| B | 31 | 68 | Mo | 17 | 27 |
| Sc | 11 | 7 | Nd | 16 | 7 |
| Ti | 2452 | 245 | Sm | 3 | 1 |
| V | 67 | 34 | Eu | 1 | 0 |
| Cr | 42 | 516 | Gd | 3 | 1 |
| Ni | 109 | 13 | Tb | 0 | 0 |
| Co | 69 | 5 | Dy | 3 | 1 |
| Zn | 328 | 189 | Ho | 1 | 0 |
| As | 262 | 73 | Er | 2 | 1 |
| Rb | 80 | 57 | Tm | 0 | 0 |
| Sr | 104 | 41 | Yb | 2 | 1 |
| Zr | 141 | 36 | Lu | 0 | 0 |
| Nb | 13 | 9 | Hf | 5 | 1 |
| Ag | 0 | 3 | Th | 8 | 4 |
| In | 0 | 3 | | | |

of rare earth elements. See SOM 1 for unrounded concentrations (i.e., raw data) of the less abundant elements, including rare earth elements, in Table 4.

*Time-of-flight secondary ion mass spectrometry.*—After sputtering the surface to clean it of surface residues, the early adult *Edmontosaurus annectens* (UCRC PV30) "mummy" spike fragment showed prominent TOF-SIMS peaks in the positive secondary ion spectrum that included: approximate m/z = 23, 27, 28, 39, and 56 (Fig. 14). These likely correspond, respectively, to many of the reported or expected secondary ion peaks from kaolinite or other clays: $^{23}Na^+$, $^{27}Al^+$, $^{28}Si^+$, $^{39}K^+$, and $^{56}Fe^+$ (Shahwan et al. 1999, 2004, although note different primary ion therein), with the $^{27}Al^+$ peak being the strongest in the spectrum. There are also positive secondary ion signals at approximately m/z = 7, 24, 29, 40, 41, 55, 57, and 60; likely consistent, respectively, with the atomic masses of: $^{7}Li^+$, $^{24}Mg^+$, $^{29}Si^+$, $^{40}Ca^+$, $^{41}K^+$, $^{55}Mn^+$, $^{57}Fe^+$, and $SiO_2^+$. In the negative secondary ion spectrum, secondary ion peaks include: approximate m/z = -16 and -17. These likely correspond, respectively, to reported secondary ion peaks from kaolinite: $^{16}O^-$ and $OH^-$ (Wang et al. 2013). Hydrocarbons on the surface of the fragment might be present as periodic peaks under m/z = 100 from $C_xH_y^+$ secondary ions or as the peak in the fossil at m/z = -26, corresponding to $C_2H_2^-$ (Nie and Jahangiri-Famenini 2022), which would be consistent with applied organic glues or consolidants or skin oil contaminants. Similar secondary ion spectra between raw and sputtered surfaces may reflect pervasive penetration of such glues or consolidants, although the positive spectra appear to show reduced relative intensity of peaks possibly related to $C_xH_y^+$ under m/z = 100 after sputtering, possibly indicating that these surface contaminants can be reduced through sputtering.

The nearby sediment matrix dorsal to the spike, after sputtering its surface, shows many similarities to the positive and negative secondary ion spectra of the spike fragment. However, the sand matrix analyzed through TOF-SIMS surface analysis of bulk fossil and matrix samples (i.e., not the thin section) is noticeably depleted in relative intensity of $^{23}Na^+$ compared to the fossil integument rendering, which may be consistent with Na cations

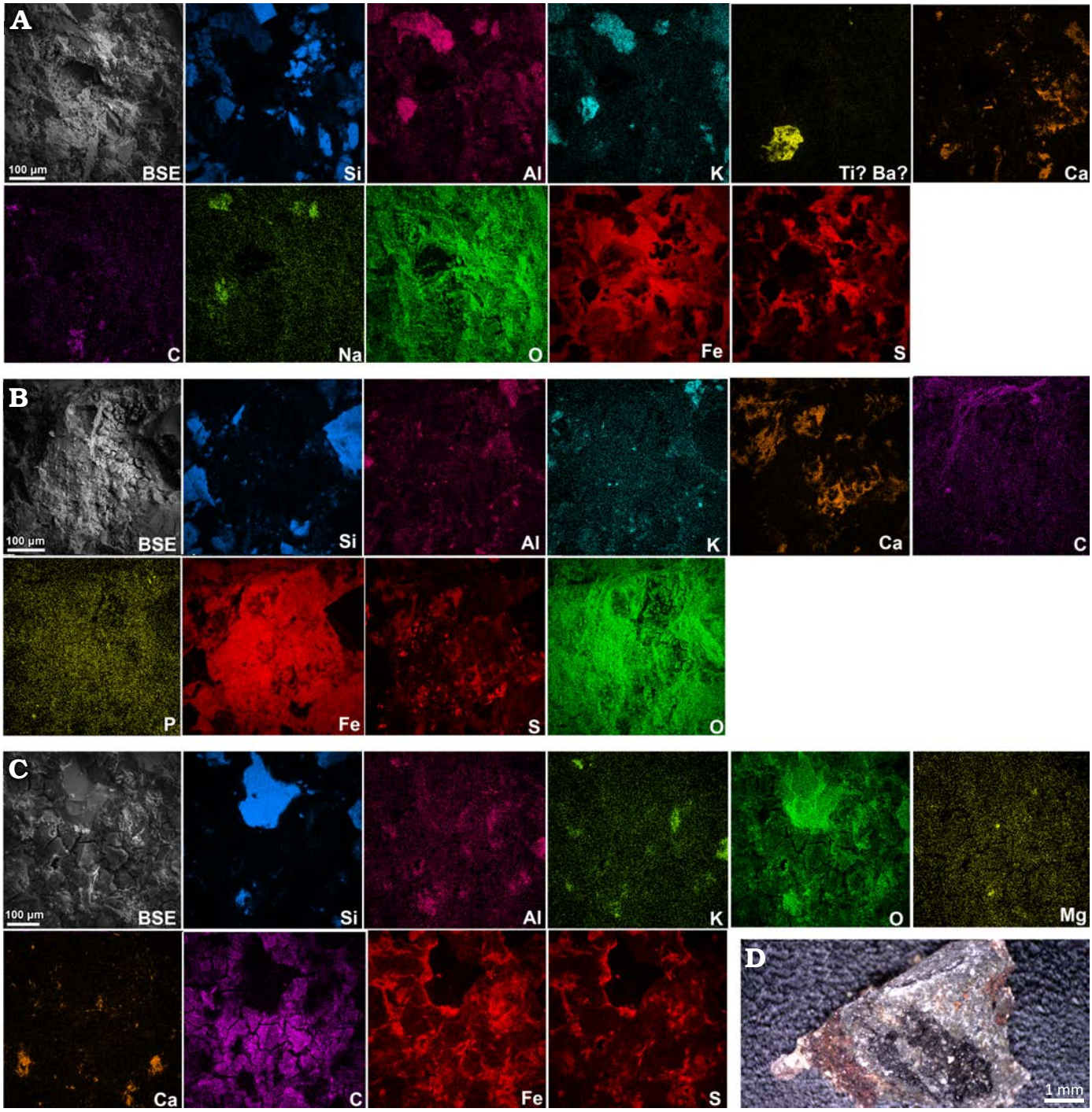


Fig. 13. Digital light microscopy (D), BSE, and EDS (30 kV beam voltage) of key elements results from the ironstone concretion at the tip of the tail of the early adult *Edmontosaurus annectens* (Marsh, 1892) "mummy" (UCRC PV30 from Wyoming, USA, Late Cretaceous). Three regions of interest (**A**–**C**) are shown alongside the sample itself (**D**). Note that what the Aztec software automatically identified as Ti is perhaps more likely to be Ba, since these elements can overlap in their EDS peaks.

associated with aluminosilicate clays that are otherwise low in concentration in the particular surrounding quartz, feldspar, and dolomite grains analyzed through bulk sediment surface analysis (see XRD results below). Note that EDS results of the early adult "mummy" spike thin section above show that some sediment grains are enriched in Na, not just the fossil clay layer. Also, the sputtering decreased the relative size of the $^{23}Na^{+}$ peak in both the fossil and the sediment, meaning that surface contaminants might be partly contributing to the signal (e.g., salt from human perspiration and contact).

Secondary ion maps of the thin section (L9L 005 PE, posterior end) containing two articulating spikes (i.e., from the posterior end of the embedded block) reveal feldspar

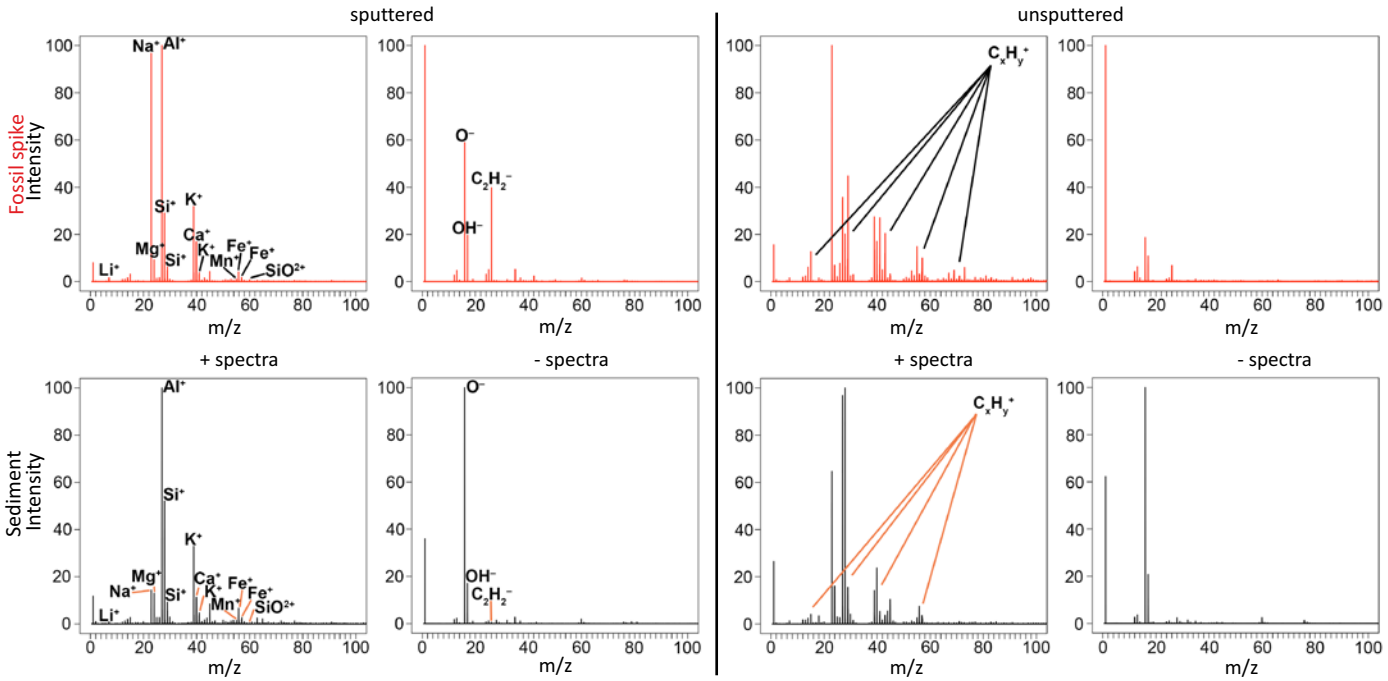


Fig. 14. Positive and negative secondary ion spectra from the fragment of the spike of early adult *Edmontosaurus annectens* (Marsh, 1892) "mummy" (UCRC PV30 from Wyoming, USA, Late Cretaceous), along with those of the nearby sediment matrix, both before and after sputtering. Key secondary ions indicated.

(e.g., colocalized $Al^+$, $K^+$, $Na^+$), quartz (e.g., $Si^+$), and some carbonates (e.g., $Ca^+$) grains in the sediment matrix (Fig. 15). The secondary ion maps for the integument template, as well as excess clay in the external nooks of the articulating spikes, show that the integument template itself is consistent with aluminosilicate clays, with enriched colocalized $Na^+$, $Al^+$, and $K^+$. Sand grains near or embedded in the integument template can be seen as highly enriched in $Si^+$ (consistent with quartz, for example) or enriched in colocalized $Ca^+$ and $Mg^+$ (consistent with dolomite). Minor amounts of $Fe^+$ or even trace $FeS^+$ can be detected in the spectra and mapped in close association with the integument template, consistent with iron oxides or pyrites.

*X-ray diffraction*.—XRD clay analysis at the University of Illinois Urbana-Champaign, USA (Table 5) shows that the sediment immediately adjacent to the fossil integument rendering layer in the AQ (anterior quarter) 150-µm thin section of the early adult *Edmontosaurus* (UCRC PV30) "mummy" has limited clay content (~6.2%, semi-quantitative % weight), and that clay is mostly illite and kaolinite with some chlorite. Most of the matrix consists of non-clay grains, consisting mostly of quartz (87.7%), with small amounts of feldspars (~5.5%) and even lesser dolomite (~0.5%).

The clay of the fossil spike itself, when a sampled flake is fractioned (< 2 µm) and particles oriented with ethylene glycol, was found to be predominantly kaolinite (~54.0%) with secondary illite (36.7%). In this clay fraction of the fossil spike, there are minor amounts of chlorite (~6.0%) and smectite (~3.3%).

X-ray powder diffraction at the University of Chicago, USA (Fig. 16) revealed that the ironstone concretion on the tip of the tail of the early adult UCRC PV30 is likely composed of pyrite and goethite (or similar iron oxide compounds). No obvious carbonate (e.g., siderite, calcite) was detected, meaning that the cracked C and O enriched texture detected in BSE/EDS likely derives from fossil organic material (e.g., fossil plants, or perhaps fossil melanin) which allowed for a greater extent of pyrite precipitation compared to the rest of the specimen, creating a sizeable concretion around the tip of the tail whose rind later oxidized (Gu et al. 2020; Taivalkoski et al. 2024). Although, some goethite can accumulate as concretions during late-stage weathering as well (Hurlbut and Klein 1985).

Table 5. XRD clay analysis of the early adult *Edmontosaurus annectens* (UCRC PV30 from Wyoming, USA, Late Cretaceous) showing semi-quantitative % weight of minerals (rounded to nearest tenth of a percentage). The bulk analysis of the external sediment immediately adjacent to the fossil (beam diameter 2.54 cm) contains non-clay grains, while the spike fragment was fractioned to obtain only clay sized particles (< 2 µm). * non-clay grains.

| Minerals | Thin section | Spike fragment |
|---|---|---|
| | 2.54 cm diameter circle of sediment immediately external to fossil layer | < 2 µm fraction (i.e., clay grains) analyzed |
| smectite | 0.0% | 3.3% |
| illite | 2.6% | 36.7% |
| chlorite | 1.2% | 6.0% |
| kaolinite | 2.4% | 54.0% |
| quartz* | 87.7% | NA |
| k-feldspar* | 1.7% | NA |
| p-feldspar* | 3.8% | NA |
| dolomite* | 0.5% | NA |

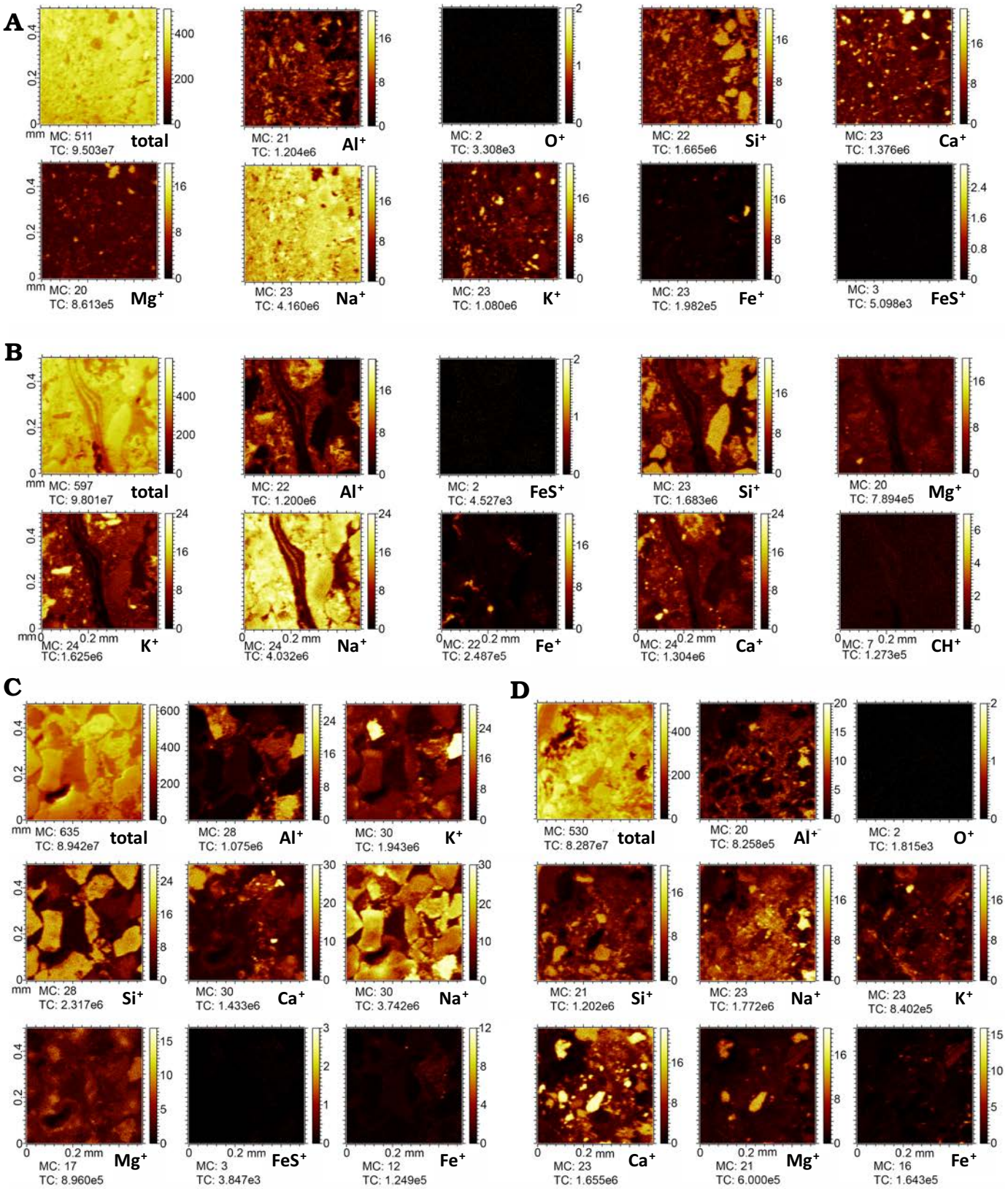


Fig. 15. Maps for key positive secondary ions in a thin section of the spikes of early adult *Edmontosaurus annectens* (Marsh, 1892) "mummy" (UCRC PV30 from Wyoming, USA, Late Cretaceous), auto-calibrated to common lightweight ions ($C^+$, $H^+$, $O^+$). Four regions of interest are included (clockwise from top left): **A**, excess clay accumulated in the external void space of the intersecting spikes on the right side (away from prepared surface) of the L9L 005 PE (posterior end) thin section; **B**, the fossil's clay template along its right (away from prepared surface) flange of the L9L 005 PE (posterior end) thin section; **C**, the external sediment matrix; **D**, the fossil's clay template along its prepared surface side. Map units in millimeters. Abbreviations: MC, maximum count; TC, total count.

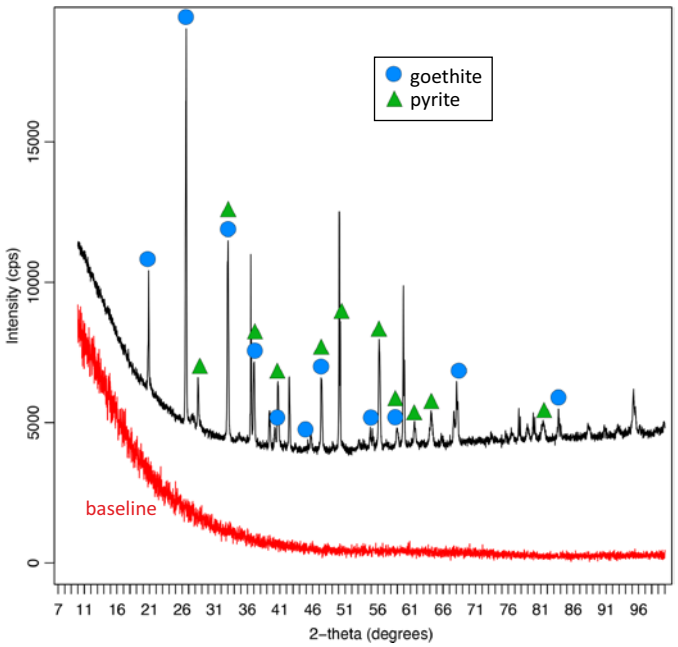


Fig. 16. XRD of the powdered ironstone concretion at the tip of the tail of the early adult *Edmontosaurus annectens* (Marsh, 1892) "mummy" (UCRC PV30 from Wyoming, USA, Late Cretaceous). Red spectrum is the zero-background sample holder (single crystal silicon) upon which the sample of concretion was analyzed. Results show characteristic diffraction peaks consistent with pyrite and goethite.

# Discussion

**Structural preservation of UCRC "mummy" integument**. —The UCRC *Edmontosaurus annectens* "mummies" preserve their integuments as extremely thin, pale, surficial templates, which appear as low porosity, laminated layers compared to the sand matrix under light microscopy and BSE. At times, only 200-µm thick, these layers are very unlikely to represent direct replacement of entire dermal histological layers, even the outermost epidermal "keratin", considering the large body size of early adult *Edmontosaurus annectens* (UCRC PV30). Still, fine surface details of the integument are preserved with high fidelity, including grooves on the surface of hoof sheaths and tail spikes, folds in skin crests, and even fine scales only ~0.5 mm in diameter. There is no internal structure preserved, as far as we can determine (Fig. 17). Occasionally, dark staining minerals appear on this thin integument rendering layer, as well as some instances of large concretions, but these are not ubiquitous, as exemplified by the late juvenile *Edmontosaurus annectens* (UCRC PV31) whose integument rendering is preserved with essentially no staining, concretions, or even many indicators of weathering in general. This structure is like that of other hadrosaur "mummies", including NDGS 2000 from the Hell Creek Formation, whose recently published CT scans not only show regions with high X-ray attenuation typical of ironstone concretions, but which also show no structural preservation internal to a very thin integument rendering layer (Drumheller et al. 2022).

There are a few non-collapsed, empty ovoid pockets visible in the sand matrix of the early adult *Edmontosaurus annectens* (UCRC PV30) spike cross sections (Fig. 17B, D), both internal and external to the integument rendering template. These pockets lack sand grains, and they are surrounded and sometimes crosscut by what appear to be thin layers of clay. There are various hypotheses that may explain these pockets. For example, they could possibly be due to organic material within the burial sand (i.e., unrelated to the *Edmontosaurus annectens* carcass, given their spatial distribution) that attracted surficial clay during decay, which was then able to survive diagenesis before ultimately being lost to recent subsurface weathering. Alternatively, these could have represented regions of carbonate mineral (e.g., calcite) that precipitated around decaying organic material (hence the associated clay-like layers also formed during decay), which survived diagenetic compaction and recently weathered away (Romero-Mujalli et al. 2019) to form a pocket. Otherwise, the clay could have deposited onto the surface of the now-lost carbonate as it weathered away (i.e., the clay is recent). However, if the voids were originally carbonate, then the observation that there are no sand grains within in the empty pocket is notable. The lack of sand grains may suggest a round object was present at the time of burial, for example biocalcite organisms worked into the fluvial sand during burial. Perhaps round organic objects were permineralized/replaced with calcite (Mähler et al. 2020), allowing survival through diagenesis. Another origin of the ovoid pockets could be that they were trace burrows, root casts, or *Microcodium*-like structures (Kabanov et al. 2008) that preserved calcareously to survive diagenesis (and were later lost to weathering), although the fact that they can occur internally to the integument rendering template and in tight association with narrow, highly complete spikes perhaps makes these explanations less likely. These hypotheses also beg the question as to whether there was more cementation in the matrix of the early adult UCRC PV30 matrix than currently survives (i.e., lost through weathering). In the suboxic zone of lake sediments, clays can also "inter-finger" with co-precipitated calcium phosphate during pre-compaction early diagenesis (Wacey et al. 2014); so another explanation for the ovoid pockets could be calcium phosphate grains subsequently lost through chemical weathering under acidic porewaters associated with soils. Note that this clay and phosphate interfingering is inconsistent with the hypothesis that the hadrosaur skin was first authigenically phosphatized during decay, since the clays of the template do not interfinger with what would have been the skin layer, but rather they accumulated external to the skin. Future work could determine if the putative clay in these ovoid pockets appears different in source than the early-deposited clay template of the skin or, less likely, if the clay template of the skin is actually late-deposited clay that replaced organic fossil melanin during weathering (see also Vinther 2020). The fact that the voids are both internal and external to the integument rendering template shows that they do not de-

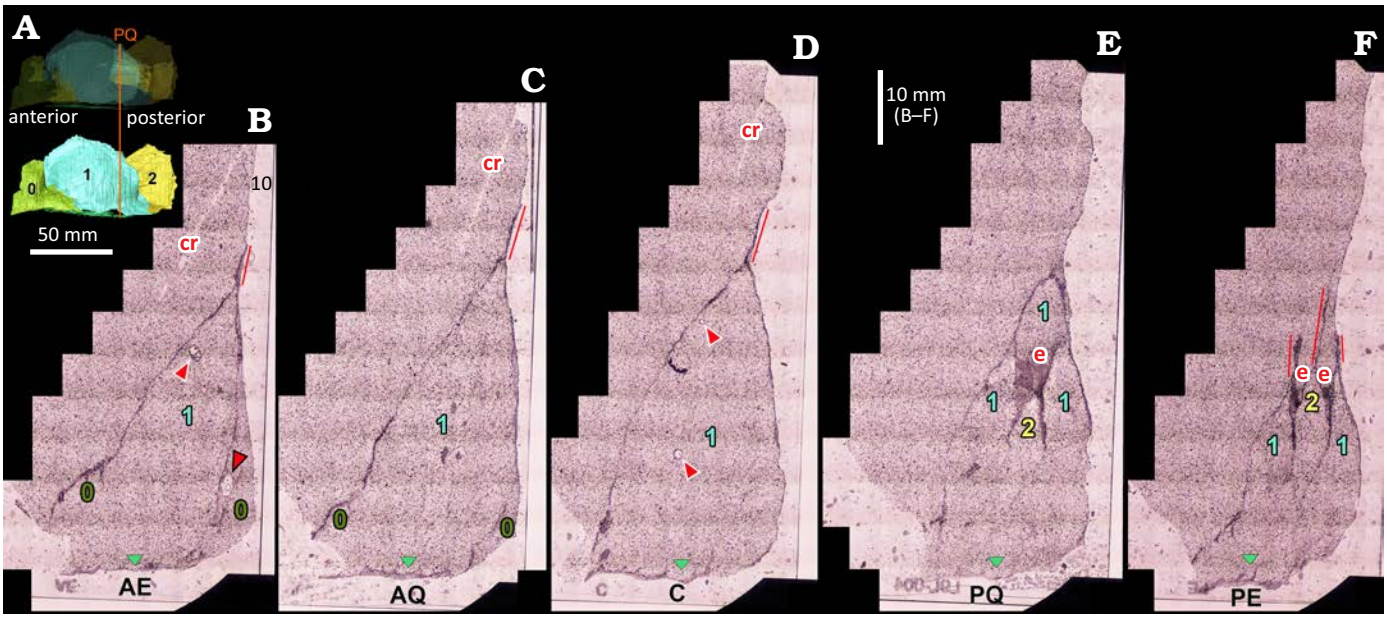


Fig. 17. Thin sections of the epoxy-embedded spike block of the early adult *Edmontosaurus annectens* (Marsh, 1892) "mummy" (UCRC PV30 from Wyoming, USA, Late Cretaceous), shown here as a CT mesh. **A**. The anterior partial spike (0) is in olive green, the complete middle spike (1) is in blue, and the posterior partial spike (2) is in yellow, while the basement scales of the tail that folds at a perpendicular angle to the dorsal-ventral axis of the spikes is in bright green. Thin sections (all scaled equally to each other) from left to right are anterior to posterior as follows: **B**, anterior end (AE, L9L 001); **C**, anterior quarter (AQ, L9L 002); **D**, center (C, L9L 003); **E**, posterior quarter (PQ, L9L 004); and **F**, posterior end (PE, L9L 005). Dorsal direction is to the top. The approximate location of the PQ section is shown in A as an orange line. In the thin sections, the spikes are numbered within their internal sediment matrix. The bright green arrows point to the basement scales of the tail. Red arrows with white borders are void spaces of the internal sediment matrix, while the red arrow with black border is a void space of the external sediment matrix. The red lines indicate the extent of the collapse of what were once internal cavities at the dorsal-most tips of the spikes. Section PQ shows spike 2 inserting into a notch and hood of spike #1, with sediment infiltrating into this notch/hood space and allowing for the accumulation of excess clay in what were once external cavities unfilled by sand. Abbreviations: cr, crack in the external sediment matrix; e, excess clay accumulated in what were once external cavities.

rive from the tissues of the hadrosaur. The clay integument template, which shows collapse internally vs. excess clay accumulation externally, formed before compaction. The fact the ovoid pockets contain empty space, unlike the clay template, suggests that they finished forming more recently, after compaction.

**Chemical preservation of UCRC "mummy" integument**.—Multiple, independent analyses all strongly suggest that the integument template is an aluminosilicate clay, consistent with its laminated, denser structure (relative to the sand matrix) and pale color. It is particularly strong in its Al, O, and Si signatures. This clay is predominantly kaolinite. Kaolinite does not have a net electrical charge (Nesse 2012) and so does not attract large cations between layers, and so the limited trace elements detected within the integument template may be associated with the other clay species detected in lesser quantities. It is also non-swelling since water molecules cannot enter between layers due to hydrogen bonding (Nesse 2012), meaning it can preserve fine structural details with high fidelity over time.

The integument rendering is clearly not preserved organically, and the carbon signal is only localized to fossil plant material (see below), surface consolidants from excavation and preparation, or embedding epoxy resin. Although some of the observed trace elements could hypothetically derive endogenously from vertebrate "keratins" (Baggott et al. 1988), the patterns observed are those expected from such an aluminosilicate clay composition (Shahwan et al. 1999, 2004). Furthermore, the surficial and external nature of the clay template might argue against an endogenous, histological source for these trace elements.

Dark stains associated with this clay layer of the fossil integument rendering appear to be iron sulfides that oxidize into iron oxides from weathering in situ and from exposure during curation. This means that pyrite might be primary and occurring during early subaqueous decay, while buried, with iron oxides being a secondary product from either oxidized pyrite or through precipitation at later taphonomic stages, during subsurface ground water weathering. The manganese oxides might also be precipitating in later taphonomic stages like subsurface weathering, as is seen in dendrite "pseudo-fossils" (Potter and Rossman 1979). The ironstone concretion at the tip of tail of the early adult *Edmontosaurus annectens* (UCRC PV30) "mummy" could have precipitated taphonomically early, microbially mediated during subaqueous decay (Cotroneo et al. 2016), as is thought to be common for fossil-encasing pyrite and siderite concretions (Allison and Pye 1994). The trapped but not tightly compacted sand grains (Gautier 1982) and different regions of pyrite versus iron oxide observed in the ironstone concretion sample removed could all be evidence for early

pyrite formation during decay, trapping sand grains within the concretion prior to heavy compaction, and later weathering of its associated pyrite into iron oxide (Loope et al. 2012). However, it is also possible for ironstone concretions to form later and after sediment compaction, such as in late diagenesis (Loope et al. 2011). Iron oxide is a common weathering product (Van der Burg 1969) and has been suggested as such for dinosaur "mummies" (Boyd et al. 2023). The lack of dark staining in the late juvenile *Edmontosaurus annectens* (UCRC PV31) "mummy" could mean the pore water was more sulfate-limited (or Fe-limited), at least compared to the patchy distribution of dark stains on the early adult specimen, during early microbially mediated decay (Gibson et al. 2023) and/or the specimen exhibited limited subsurface oxidative weathering to produce Fe- or Mn-oxides. Minimal pyrite precipitation could also indicate that anoxic microenvironments were relatively limited around the late juvenile compared to the early adult.

**Clay templating of soft tissue**.—The UCRC "mummy" hadrosaurs appear to show a form of taphonomic clay mineral templating, that is perhaps analogous to that seen in fossils from originally organic-walled organisms of the metamorphosed Cambrian Burgess Shale, Ediacaran Doushantuo and Dengying formations, and other pre-Mesozoic fossil deposits of exceptional preservation (Orr et al. 1998; Gaines et al. 2008; Page et al. 2008; Anderson et al. 2011). Especially relevant are fossils from those formations whose templates consist of kaolinite (Orr et al. 1998; Anderson et al. 2020, 2021), but also illite, chlorite, and smectite (Mapstone and McIlroy 2006), as we likewise detected in our early adult *Edmontosaurus annectens* "mummy" (UCRC PV30). Fascinatingly, these "mummy" dinosaurs represent examples of this taphonomic mode that is far younger and from metamorphically unaltered, terrestrial sediments. White Sea and South Australian Ediacaran fossils, as well as laboratory experiments, suggest that cementation of overlying sand is not required for this style of preservation (Bobrovskiy et al. 2019).

Volcanic-derived clays have been suggested to preserve Ediacaran soft-bodied fossils in the relatively unmetamorphosed Itajaí Basin of Brazil (Becker-Kerber et al. 2021). These particular clays are thought to be authigenically formed through alteration of pyroclastic sediments (after rapid burial events during eruptions) and driven by microbial activity. Microbes, they propose, may have led to early illitization and micrometer-scale in situ templating of the carcass surface, reminiscent of our observations from the two UCRC *Edmontosaurus annectens* "mummies". Becker-Kerber et al. (2021) also suggest that several different minerals can result in Ediacaran-style templating. Neoproterozoic (Tonian, ~950 Ma) marine Dolores Creek Formation (Yukon Territory, Canada) macroalgae fossils are also known to preserve via aluminosilicification and pyritization, with higher preservation fidelity associated with clay mineral coatings rather than iron oxide coatings, the latter interpreted as weathering products of pyrite (Maloney et al. 2022).

Torridon Group (Scotland, UK) organic-walled microfossils from ~1 Ga lakes can preserve via clays with high fidelity, even higher than when they are preserved via phosphates (Wacey et al. 2014). Wacey et al. (2014) note that their clays are iron-rich when in a narrow zone of direct contact with the cells and suggest that these enclosing clays derive from early-stage microbially mediated decay of labile organics in sulfate-limited environments. Even in freshwater environments, epilithic biofilms can be authigenically encrusted in fine-grained clays of Fe- and Al-silicate composition, with minor concentrations of K and no other trace metals (Konhauser et al. 1998). In addition to these authigenic precipitates, Konhauser et al. (1998) inferred that the large and reactive surface area of the biofilms could entrap/adsorb detrital kaolin, iron oxide, gibbsite ($Al(OH)_3$), quartz, and mica. Note that Fe enrichment could help contribute to the high X-ray attenuation of our early adult *Edmontosaurus annectens* "mummy" clay integument template as observed in CT scanning.

Post-burial, subaqueous decay of some of the most resistant tissues appears to yield clay templating, whereas more labile internal tissues/organs are largely lost prior to burial. In dinosaurs such as hadrosaurs, the most decay-resistant tissues would be predicted to consist primarily of the outermost integumental layer of heavily "keratinized"/cornified or pigmented epidermis. Indeed, Flinders-style preservation of Ediacaran fossils is thought to be promoted by prolonged conservation of organic material (Bobrovskiy et al. 2019). The prevalence of hadrosaurs among known "mummy" specimens (Davis 2014) is presumably influenced by taphonomic variables. Their environment was seasonally dry, and perhaps hadrosaurs were not just herbivores with high population sizes compared to other taxa, such as carnivores. Hadrosaurs may also have tended to frequent areas near seasonally flooding rivers where their "mummies" would ultimately be buried. When considering preservation at the molecular level, the preponderance of hadrosaur "mummies" could also partly be a result of their anatomy. Their scaly integument was likely more directly "keratinized", cornified, and pigmented than the skin of some other co-occurring taxa, particularly feathered theropods. However, hadrosaur dermal tissue was likely not thick (contra Davis 2014). Thin hadrosaur skin is evidenced by the fine folds in the integument rendering from desiccation and shrinkage, as well as the very small-sized scales relative to their body size. In other words, although their scaly skin might have had a "keratinized" and pigmented epidermis compared, for example, to feathered theropods, the epidermis and dermis was probably not thick in histological section.

The taphonomic process of clay templating has not always been accepted (e.g., Mapstone and McIlroy 2006), and some propose that clay templating is a result of metamorphism rather than being primary (Powell 2003). Even within the clay templating hypothesis, there are different possible molecular mechanisms that have been proposed. Anderson et al. (2023) note that it is unknown if preexisting kaolinite clays attach to

the carcass or if kaolinite clay precipitates de novo at the carcass. Experimental taphonomy has supported both de novo precipitation (Playter et al. 2017) and attachment (Martin et al. 2004). The induction of clay mineral precipitation might occur via the concentration of the elemental constituents of aluminosilicates (Darroch et al. 2012). Alternatively, kaolinite might bind well to decaying organic matter due to its edge sites area (10–20% of its surface area) and acidity (Theng 1974). Negatively charged microbial extracellular polymeric substances might also attract aluminosilicate cations, causing clay to flocculate onto the surface of carcasses through pore fluids (Simon Darroch, SMF personal communication 2024). Although kaolinite has a net neutral charge and no associated cations (Schulze 2005), the silica tetrahedral and alumina octahedral faces of kaolinite can develop electrical charges under certain pH conditions (Tombácz and Szekeres 2006; Gupta 2011; Zhu et al. 2016; Kumar et al. 2017). The biofilm could also be trapping clays through purely mechanical means, rather than electrochemical attraction.

Experiments modeling Neoproterozoic "death mask" Lagerstätten are helpful when it comes to this active area of research. Darroch et al. (2012) performed decay experiments of arthropod carcasses within freshwater and a predominantly sandy matrix, as well as in association with microbial mats. This experimental freshwater decay of arthropod larvae in an organic-rich sand under bacterial mats yielded an external mask of clay-like material, enriched in iron sulfides and common aluminosilicate signatures (i.e., Al, K, Fe, and Mg), above a negative relief of the decayed carcass (Darroch et al. 2012). These results are particularly relevant to our two UCRC *Edmontosaurus annectens* "mummies" in that the water was freshwater and the matrix was both sandy and organic rich. Other taphonomic experiments can induce pyrite accumulation in the sediment around experimentally decayed carcasses (Gibson et al. 2018) or iron sulfide and oxide veneers on carcasses (Gibson et al. 2023). The UCRC dinosaur "mummies" may have derived from a relatively sulfate- or iron-limited depositional environment, given their restricted pyrite/iron oxide veneers and predominance of clay in their integument templates (Gibson et al. 2023).

"Death masks" might occur in a variety of depositional settings. This taphonomic mode is unusual in terrestrial fluvial sands, given similar cases of preservation in marine benthic environments. Various depositional environments and microbial communities might therefore be capable of inducing "death masks" of varying compositions. Even during experimental decay of unburied shrimp atop of sediment, kaolinite substrate induced a black film of cryptocrystalline and anhedral aluminosilicates over the cuticles, preserving their morphology (Corthésy et al. 2025).

**Decay experiments of Slagter et al. (2024) induce kaolinite coatings across a range of burial conditions**.—A recent taphonomy experiment by Slagter et al. (2024) to investigate authigenic mineralization of Ediacaran-type preservation in medium- to fine-grained sandstones (either quartzose, clay-rich, or heterolithic silicastic) provides a good amount of insight into the mechanism behind the accumulation of clay as a template of soft tissues, further supporting hypotheses attributing its appearance during early decay. Using a range of sediments (various combinations of kaolinite, quartzose sand, and iron oxides $Fe_2O_3$), organisms (including marine invertebrates), and dissolved silica levels in water, they were able to produce authigenic clay and amorphous silica surficial coats on decaying organisms (with some accumulation in the nearby matrix pore spaces as well), while dissolved silica levels in solution gradually decreased. Specifically, they were able to yield authigenic kaolinite coatings when dissolved silica in the solution was 2 mM in substrates containing exogenous kaolinite: quartz + kaolinite, quartz + kaolinite + iron oxides, and kaolinite + iron oxides. Authigenic kaolinite coatings occurred over a range of dissolved silica levels (0.5–2 mM) when the substrate was pure kaolinite. In contrast, amorphous silica coatings instead predominated across other substrate types when initial dissolved silica concentrations were low (0.5–1 mM).

Slagter et al. (2024: 9) propose the following mechanism for this authigenic kaolinite coating: "Our results show that authigenic aluminosilicate minerals nucleate under high DSi [dissolved silica] concentrations (2.0 mM) in the presence of detrital kaolinite, likely facilitated by organic acid-mediated kaolinite dissolution and complexation with porewater Al in proximity to degrading macroorganism carcasses and biofilms, followed by decay-mediated increases in porewater dissolved Al availability. Moreover, drawdown of DSi was greater in experiments with kaolinite than those without, a finding consistent with extensive formation of authigenic aluminosilicate phases".

The authors also note that dissolved organic carbon around the organisms was lower in experiments whose substrates contained kaolinite than in those containing quartz, suggesting that kaolinite slows organic decay (Wilson and Butterfield 2014; McMahon et al. 2016) to produce higher-fidelity templates. The fact that Slagter et al. (2024) induced kaolinite coating under variable substrate and porewater conditions supports our hypothesis that a similar taphonomic process is occurring in our terrestrial "mummy" dinosaurs. The sand in which the *Edmontosaurus* was buried in would indeed provide a plentiful source of silica, which could lead to high dissolved silica concentrations in the porewater and favor authigenic kaolinite over amorphous silica (Derek Briggs, personal communication 2024).

Slagter et al. (2024) did not observe authigenic iron precipitation readily distinguishable from any detrital iron, even when the substrate contained iron oxide; although they note that their experiments did not maintain anoxia and that the sulfate level in solution was lower than that of modern seawater (i.e., their experiments used partially oxygenated and non-ferruginous water). They concur with authors such as Tarhan et al. (2015, 2018, 2019) that uranium isotopes, petrographic thin sections, patchy oxide distribution, and oxide concentration on weathered surfaces of some Ediacaran-type

fossils could imply a post-depositional origin of hematite stains late in their taphonomic history. However, they acknowledge that authigenic pyritization is consistent with the results of some decay experiments in sand and iron oxide substrates (Darroch et al. 2012; Gibson et al. 2018, 2023; Newman et al. 2019) as well as the discovery of pyritized Ediacaran fossils (Cai et al. 2010; Schiffbauer et al. 2020; Shore et al. 2021). Pyritization suggests high concentrations of reactive iron in sulfate-reducing environments around concentrated decay-labile organic matter (Raiswell and Berner 1985; Raiswell et al. 1993; Gibson et al. 2018), which could then oxidize into compounds such as hematite. Pyrite versus kaolinite precipitation, therefore, could reflect the availability of sulphate, iron, or anoxia in the porewater around decay-labile organics, or perhaps some of these iron compounds might be a result of later processes, as Slagter et al. (2024) suggest. When sulphate concentrations are low, iron silicates may be favored over iron sulfides (Wacey et al. 2014), something to consider given the patchy, sparse distribution of iron staining observed on the early adult "mummy" *Edmontosaurus annectens* (UCRC PV30). Future work on these specimens could search specifically for iron silicates (e.g., olivine, pyroxene), which would be of interest because they readily weather into clays and iron oxides (Wilson 2004). Thus, iron silicates precipitated onto the *Edmontosaurus annectens* carcass surface could have weathered and contributed to the clays and iron oxides of their integument templates as currently preserved.

**Clay template from kaolinization of 2:1 type clay?**—The net neutral charge of kaolinite and lack of associated cations (Schulze 2005) might complicate a hypothetical mechanism for clay templating involving an electrochemical attraction of clay cations to a negatively charged biofilm. However, this could be mitigated if a precursor clay with a net charge is attracted to the biofilm and decaying carcass interface that then undergoes kaolinization. Kaolinization of 2:1 type clays is known to occur through dissolution-crystallization at layer edges in near surface (i.e., supergene) environments under acidic $Al^{3+}$-rich conditions (Li et al. 2020). The high fidelity of the anatomical details of the clay template might indicate that a non-swelling clay (Akisanmi 2022; Rasool and Ahmad 2023), such as the net electrically charged (Sparks 2003) and cation-bearing (Akisanmi 2022) illite that we detected through XRD, would be the likely precursor clay (as experimentally demonstrated by Li et al. 2020) under such a hypothetical scenario. An illite precursor is possibly consistent with the XRD results from the sediment immediately external to the fossil integument rendering layer in thin section, which resulted in ~2.6% illite and only ~2.4% kaolinite (note, however, that this method is likely less accurate at quantifying clay species than XRD of the oriented clay-sized fraction). This process would initially produce interstratified kaolinite-illite through precipitation of kaolinite at the basal surface of the precursor illite that could be searched for in future research. However, illite can also form as a diagenetic product of kaolinite (Mantovani and Becerro 2010) and so it is difficult to rule out the reverse transformation currently (see below).

**Clay template from localized hydrolytic weathering of feldspar during decay?**—The limited clay concentration in the matrix surrounding the "mummy" dinosaurs, as seen through laser diffraction grain size analysis, microscopy, and XRD, the presence of some larger silicate grains within the clay layer, as seen through BSE, and the net neutral charge of kaolinite prompts one to consider another hypothesis, that hydrolytic weathering of surrounding feldspars in the sediment is the source of the kaolinite (White et al. 2001). Note that we are simply proposing this as an additional hypothesis for consideration, and we do not necessarily think this is the precise mechanism. In this hypothetical scenario, decaying organics might yield carbon dioxide that reacts with water to yield carbonic acid, which in turn reacts with feldspars in sand to produce kaolinite clay. These reactions might occur as follows when the desiccated skin that was shrunk around the bones is decayed by microbes while buried in water-logged fluvial sand rich in organic matter (e.g., alongside associated plant matter):

Respiration of organic material:

$$CH_2O \text{ (organics)} + O_2 \rightarrow H_2O + CO_2$$

Carbon dioxide dissolves in the pore water and leads to local acidification through the formation of carbonic acid, and hydrogen ions lower the pH, while diffusion through the highly porous, waterlogged sand produces a sharp pH gradient near the carcass surface:

$$CO_2 + H_2O \rightarrow H_2CO_3 \text{ (carbonic acid)}$$
$$H_2CO_3 \rightarrow HCO_3^- + H^+$$

Feldspars in the surrounding sand are weathered in acidic pore water to produce kaolinite clay at the site of intensive integument decay located at the interface with external biofilm, shown below using orthoclase potassium feldspar as an example:

$$4KAlSi_3O_8 \text{ (feldspar)} + 4H^+ + 2H_2O \rightarrow$$
$$2Al_2Si_2O_5(OH)_4 \text{ (kaolinite)} + 8SiO_2 + 4K^+$$

**Clay template from late-stage weathering?**—The Late Ordovician Soom Shale of South Africa can preserve soft tissues as illite, but there is uncertainty as to whether this clay forms early to replace tissues or if they are later diagenetic or metamorphic artefacts (Gabbott et al. 2017). Beyond an extreme metamorphic origin of the clay (Powell 2003), one could formulate a hypothesis that the clay and dark staining minerals come from weathering of either authigenic phosphate (Tazaki et al. 1987) or organic compounds derived from the organism (e.g., melanin or kerogen polymerized in situ of aliphatic lipids, Vinther 2020) and from precipitation of minerals through groundwater (as per Jakob Vinther, personal communication 2024). Mazon Creek concretions sometimes preserve fossils with a kaolinite overgrowth which is suggested to form post-lithification

of the concretion during late diagenesis or during weathering (Clements et al. 2019). A recent study of a Jehol Biota *Psittacosaurus* specimen suggests the presence of silicates in the sampled skin (Yang et al. 2024) in a fossil that would otherwise be expected to inorganically preserve its skin via authigenic phosphatization (Mayr et al. 2016; He et al. 2023). The feather fibers from *Shuvuuia deserti* likewise are predominantly calcium phosphate but might also contain some elemental signatures consistent with minor amounts of clay presence near the surface of the fiber (e.g., Si, Al, Mg, Na, K) and with pyrite (i.e., Fe, S) (Saitta et al. 2018a).

The Lance Formation is chronologically young (Late Cretaceous) and the Wyoming "mummy zone" is at the southeast margin of the Powder River Basin, was not buried sufficiently deep, and is thermally immature enough to confidently say it was not metamorphosed (Anna 2010), so only weathering need be considered (Jakob Vinther, personal communication 2024). The clay layer of the dinosaur appears to precipitate before sediment compaction (see section "Clay templating in three dimensions" below) as a thin, surficial template across the entire integument's external surface, based on the excess clay in the external nooks of the articulating spikes and the infilling sand internal to the clay. The clay layer does not appear to result from the weathering of what was originally melanin/kerogen derived from the tissue or of phosphate that had directly replaced the tissue. No evidence of extensive organic or phosphatic preservation was detected. For example, no Ca and P colocalization is apparent, nor does the fossil integument rendering layer possess a granular texture typical of accumulations of exposed melanosomes or even their mouldic impressions (e.g., Vinther 2015; Saitta et al. 2019a) or even a carbonaceous composition. If the clay derived from authigenically phosphatized skin, then one might expect the bones, also made of apatite, to be weathered as well, which they do not appear to be. Nor do the bones appear to directly bear a clay template themselves in addition to templating of the skin. A lack of original apatite is further consistent with the extreme thinness of the clay layer and the fact that no internal structures seem to be present. The exceptionally fine detail of surficial striations on spikes and hooves and tight shrinkage of the skin to the bones on the tail of the early adult *Edmontosaurus annectens*, as well as the fine midsagittal dorsal crest folds and even ~0.5 mm diameter scales on the late juvenile *Edmontosaurus annectens*, are consistent with early mineralization preserving high fidelity renderings of a desiccated "natural mummy" rather than altered, weathered remains with reduced fidelity. The loss and subsequent replacement or templating of phosphates or melanin might instead be expected to reduce fidelity. We don't see evidence of replacement or void cavities of what were originally histological layers. Instead, we see a detailed, extremely thin, external template surrounded by sand on both sides. Furthermore, if the clays were replacing melanin pigment preservation, then one would not expect such homogenous and extensive integument rendering preservation, including hinge regions of scales, rather than color patterning or counter shading.

While some of the dark staining minerals might derive from weathering (e.g., manganese oxides or iron oxides), the sparse dark staining on the UCRC *Edmontosaurus annectens* specimens, especially the late juvenile (UCRC PV31), suggests limited weathering. Further, the ironstone concretion at the tip of the early adult (UCRC PV30) tail and other dark stains on the specimen could have formed early as pyrite that later oxidized during weathering. We indeed detected instances of Fe and S colocalization in EDS and in sXRF. Sporadic precipitation of dark minerals and putative trace fossil burrows could be more consistent with limited anoxia in specific microenvironments around the carcass (e.g., in the places where pyrite precipitated) rather than more pervasive anoxia in a sand bar after burial that would lead to Jehol-like melanin preservation or authigenic phosphatization. Recall the cross-sectional pattern of clay collapse versus excess clay accumulation in the internal and external nooks of the spike, respectively. This pattern is consistent with clay deposition prior to sediment compaction, and the pattern is further seen in macroscopic lateral view of spikes, whereby the anterior margin of the spike forms a shelf under the posterior portion of the spike it inserts into. The observed spacing between sand grains in the tail tip ironstone concretion is further indicative of cementation prior to compaction (although this observation deserves to be replicated under thin section, beyond just a chipped off fragment). A *Tyrannosaurus rex* specimen (UCRC PV1) found in the same "Mummy Zone" of Wyoming preserves in a large carbonate concretion, retaining articulated bones, a large fossilized log of wood, and a sediment boundary (more carbonate cement dominated internally, more sand clasts externally) at what was originally the body cavity, consistent with early precipitation of cementing minerals during early decay in this environment and suggesting that porewater chemistry or levels of anoxia could vary between specimens in this locality (Lipkin et al. 2007; Sereno et al. 2026).

In summary, neither melanin/melanosomes nor phosphatized keratin would yield an external template if they were to be directly replaced by clay as a cast, and replaced phosphatized keratin might not be expected to occur in such an extremely thin layer (e.g., phosphatized coprolites are solid fossils). Although pigments can indeed be limited to the outermost layer of integument, would an animal roughly the size of an elephant have only a ~200-µm thick layer of cornified tissue in its hoof sheath? If clays derive from recent subsurface weathering, why are they preferentially occurring at the skin's surface rather than throughout the sediment matrix? Although weathered soil apatite grains have sometimes been observed to possess a film of clay particles, this process is still suggested to be linked to biofilms, allowing for apatite dissolution in the basic pH of soils (Heindel et al. 2018). Therefore, linking clay film accumulation to microbial biofilms would still make early-decay templating a more parsimonious hypothesis than one adding

an additional step of authigenic phosphatization, and again, we see no indication of prior phosphates.

As such, although we will of course remain open to the possibility that the clays could be secondary to melanin or to authigenic apatite that first replaced the integument, we do not currently find it likely that the clay template of integument on the two UCRC *Edmontosaurus annectens* "mummies" was produced through subsurface weathering. Instead, the fossils appear to represent early mineralization during subaqueous decay, possibly in the weeks or months after burial in fluvial sand. This interpretation is consistent with some interpretations of the Burgess Shale Formation, which found that kaolinite is preferentially found in the fossils, while the matrix shows a greater abundance of chlorite, a diagenetic product of kaolinite (Anderson et al. 2021). Anderson et al. (2021) hypothesized that this pattern indicates that early diagenetic interactions between the kaolinite and organic material prevented subsequent metamorphic alteration of the kaolinite in the fossils.

If weathering of melanin or calcium phosphate, which would have directly replaced the original tissue layer, can be ruled out based on the external nature of the template, it is again worth noting that iron silicates can form veneers on organic tissue under low sulphate concentrations (Wacey et al. 2014; Gibson et al. 2023). These iron silicates can readily weather into clays and iron oxides (Wilson 2004). In this scenario, weathering, either early- or late-stage, could have contributed to the current composition of the *Edmontosaurus* integument template.

**Associated plant fossils and uncertain tubular structures**.—In the early adult *Edmontosaurus annectens* (UCRC PV30) "mummy", fossil plant material is found in close association to the carcass (Fig. 18), such as under the tail (Fig. 18A, C, D) and foot (Fig. 18B), suggesting that the carcass and nearby plant matter were buried rapidly. This material is dark black and mostly crumbly, as might be expected from lignite to bituminous coal that is exposed to air (Schumacher and Juniper 2013). The fossil plant material (sampled from under the tail) shows a strong C and O signal under EDS (Fig. 18E), as expected. S is also present, and this could be organically bound, as typical of lignite, bitumen, and coal (Demirbaş 2002; Mousavi et al. 2022). The plant material also shows very little Cl in EDS (SOM 1), typical of less mature fossil plant material such as lignite or sub-bituminous coal (Yudovich and Ketris 2006). See Zazzeri et al. (2016) for coal-rank criteria. TOF-SIMS (Fig. 18F) reveals that this plant material shows many secondary ion peaks expected from fossil lignite to bituminous coal, such as $H^-$, $CH^-$, $O^-$, $OH^-$ (Pei et al. 2010) (negative spectrum reported here, after sputtering, since it contained more peaks than the positive spectrum). The plant matter, therefore, appears to be preserved as organic material in the range of lignite to bituminous coal. It also shows an appreciable amount of Ca in EDS, and Ca in lignite has been suggested to be bound to carboxyl groups (Zhang et al. 2021).

The Senckenberg *Edmontosaurus annectens* (SMF R 4036) "mummy" comes from the same area in Wyoming as the UCRC specimens. SMF R 4036 was also found with associated plant matter, which was originally interpreted to be stomach contents, but likely represents plant material buried rapidly along with the carcass (Uhl 2020; El Atfy and Uhl 2021). This organic plant matter buried along with the carcass, means that the pore water in which biofilm-induced clay templating took place was not organics-limited (Gibson et al. 2023), and the decay of more labile plant compounds might even have helped to produce localized environments near the carcass to promote pyrite or carbonate precipitation through anaerobic sulfate reduction or methanogenesis (Cotroneo et al. 2016).

The stark difference between organic preservation of plant material closely adjacent to the surficial, inorganic integument rendering template suggests that the mere presence of a biofilm is insufficient to produce the template. Active decay of organic material by a biofilm appears necessary, hence why there is a dichotomy between organic carbon loss and clay template production. The possibly woody plant material would have likely been far more decay-resistant (as well as resilient during subsequent diagenesis) than the desiccated skin tissue due to its lower water content and relatively recalcitrant lignin and cellulose (Velasco-Rodríguez et al. 2022). Bacteria are known to struggle to breakdown wood compared to other organisms, such as fungi—considered to be the primary decomposers of wood (Embacher et al. 2023).

In the late juvenile *Edmontosaurus annectens* (UCRC PV31) "mummy", structures possibly consistent with trace fossil burrows are found in close association to the carcass (Fig. 19$A_1$, $B_1$). These appear as white tubes containing sand grains with a caliche-like texture near the integument rendering and external to it (Fig. 19$A_2$, $A_3$, $B_2$). If so, these could be consistent with infilled burrows from scavenging of the carcass after burial or general sediment bioturbation, and further indication of the decay and ultimate loss of the specimen's organic material. Likewise, they would indicate a biologically active sediment, and one that was possibly oxygenated well-enough to support larger organisms at certain times and places. Trace fossils have been proposed in other "mummy" hadrosaurs before, such as in the Judith River Formation *Brachylophosaurus canadensis* (JRF 115H; Tweet et al. 2016), as well as pre-burial scavenging bite traces (Drumheller et al. 2022). However, an alternative identification of these tubular structures could be rhizoliths or "root casts" (Curran 2015) either from a paleosol formed after burial, again consistent with active biological decomposition of the carcass, or more recent soils, which would make them the only obvious sign of late-stage subsurface weathering in the UCRC PV31. However, the structures show limited branching, which might otherwise be expected from rhizoliths. Future analyses could help discern among these hypotheses.

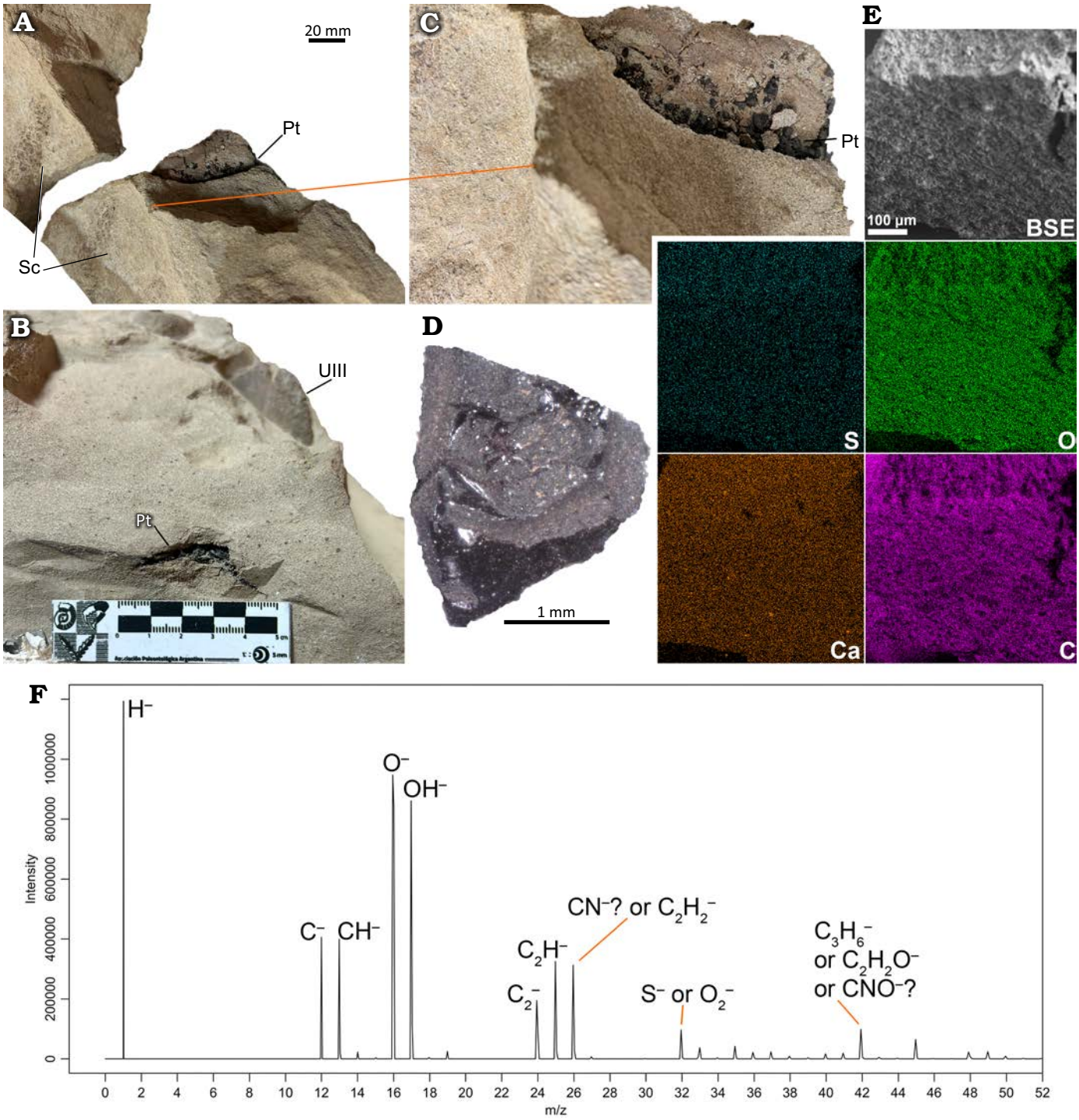


Fig. 18. Plant fossils associated with early adult *Edmontosaurus annectens* (Marsh, 1892) "mummy" (UCRC PV30 from Wyoming, USA, Late Cretaceous). **A**. Exposure of black plant material under the tail after removal of the three dimensionally prepared tail spike. **B**. Plant material under the right pes. **C**. Close up of the exposed plant material under the tail. **D**. The sampled plant material used for BSE, EDS, and TOF-SIMS. **E**. BSE ($E_1$) and EDS ($E_2$–$E_5$) maps from the surface of the sampled plant material, showing carbon richness. **F**. Negative TOF-SIMS spectrum of the sampled plant material from underneath the tail, auto-calibrated to common lightweight ions ($C^-$, $H^-$, $O^-$). No strong N was detectable in the EDS spectra (EDS does not easily detect light elements such as N), so N-bearing secondary ion identification in TOF-SIMS could be considered putative. Abbreviations: Pt, plant material; Sc, basement scales; UIII, ungual III.

**Clay templating in three dimensions**.—Regardless of the precise mechanism for clay templating, these "mummies" and other integumentary fossils are the first known examples of clay templating presented as a taphonomic mode in a dinosaur. Furthermore, given the predominance of kaolinite over illite in the early adult *Edmontosaurus annectens* (UCRC PV30) "mummy", one could hypothesize that a proportion of the authigenic or allochthonous kaolinite template that

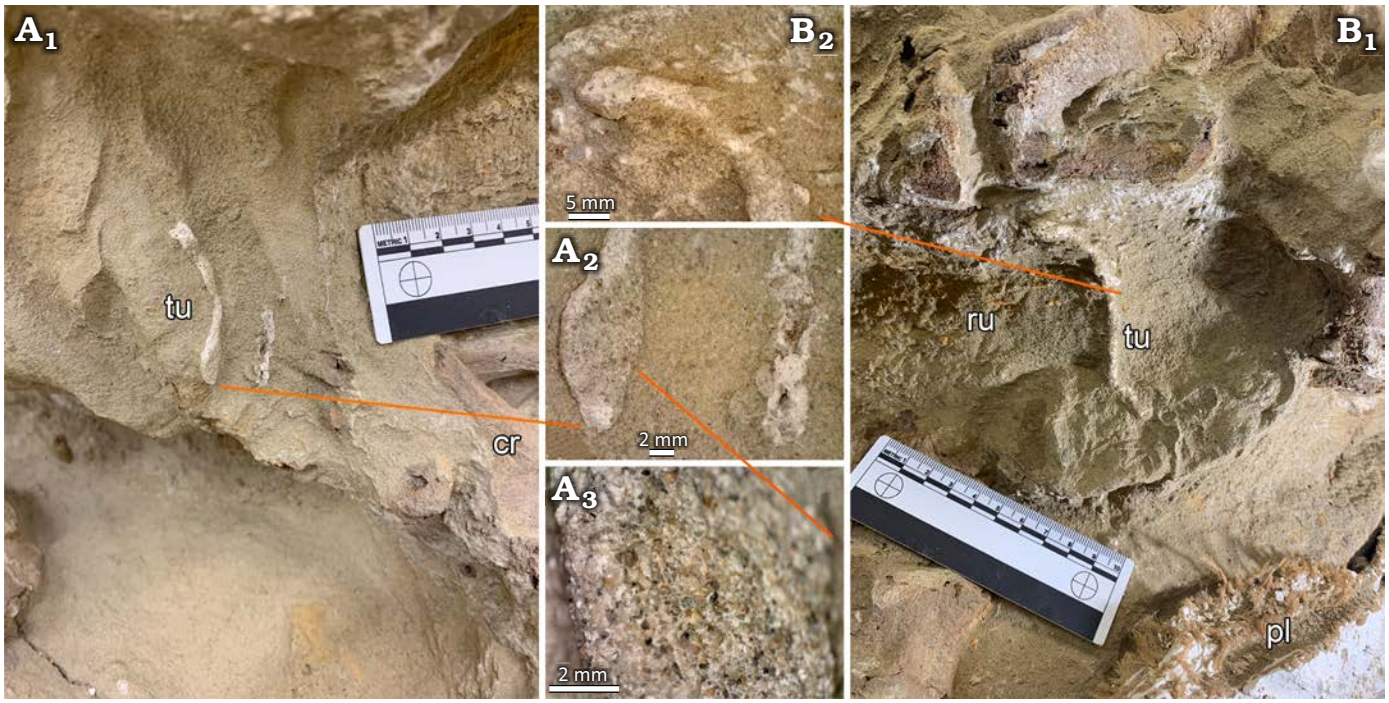


Fig. 19. Photography and light microscopy of tubular structures associated with late juvenile *Edmontosaurus annectens* (Marsh, 1892) "mummy" (UCRC PV31 from Wyoming, USA, Late Cretaceous). **A**. Tubular structures near the integument rendering template of the neck, dorsal to the left shoulder. **B**. Tubular structures dorsal to the right shoulder and nearby clay rip-up clast-like structures. $A_2$, $A_3$, $B_2$, close up digital light micrographs of the tubular structures, showing caliche-like composition with visible sand grains within a lightly colored cement. Putative clay rip-up clasts preserved as orange subspherical structures besides the tubular structure, consistent with high-energy rapid burial, unless these are instead laminations in the sediment of heterogenous composition/color through redox reactions. Abbreviations: cr, cervical rib; pl, plaster jacket; ru, rip-up clasts; tu, tubular structure.

formed during early microbial decay later underwent illitization during the diagenesis of sandstone at intermediate burial depth (e.g., 3–4 km, Mantovani and Becerro 2010), but the Lance Formation at the "mummy zone" locality was likely not buried deeply (Anna 2010). Alternatively, illitization has also been suggested to occur early in fossil templating due to microbial activity (Becker-Kerber et al. 2021). The minor amount (~6%) of detected chlorite in the fossil clay layer using XRD could also have derived from diagenetic alteration of kaolinite (Anderson et al. 2021).

The three-dimensional nature of clay templating in dinosaur "mummies" provides evidence that the clay formed during early decay, perhaps on the order of weeks or months after the preceding dry season/drought. The thin section of the early adult *Edmontosaurus* (UCRC PV30) in the region where one tail spike inserts into a posterior notch of the spike anterior to it shows a pattern of collapse and excess clay that suggests that the clay was deposited prior to compaction. First, when the carcass is buried, sand is unable to fully infiltrate the tight nooks on the internal concavities at the dorsal edges of the spikes, as well as in the external concavities at the site of spike articulation. Second, an external clay template forms as the organics of the skin decay and are lost, meaning that the external nooks where the spikes articulate are able to accumulate excess clay because they are void of sand. Third, the internal nooks void of sand, which were not filled with excess clay collapse during diagenetic compaction from the weight of overlying sediment with the carcass oriented on its side, leading to mediolateral compaction of what was a triangular template into a thin layer of clay at the dorsal edges of the spike lacking internal sand grains. The distal edges of the hoof sheaths also appear to be flattened.

The three-dimensionality of the clay template in "mummy" dinosaurs also raises interesting questions about the spatial orientation of biofilms and chemical/metabolic gradients in dinosaur "mummies" compared to other clay templated fossils. While most clay templated fossils appear to have a vertical polarity, with clays and pyrites deposited atop as a hyporelief of the carcass, dinosaur "mummies" are three-dimensional with all surfaces capable of preserving as a clay template. For the time being, we hypothesize that while a seafloor might have limited turbulence and slower sedimentation of finer grain sizes, allowing for the establishment of microbial communities with distinct metabolic pathways occurring in vertical layers (e.g., Maltby et al. 2018), dinosaur "mummies" were deposited rapidly under high-energy fluvial flows in shallow terrestrial settings, where biofilm growth is not vertically oriented on a bedding plane, but rather localized to all sides of the carcass. Microenvironments crucial to the accumulation of clays, pyrites, or carbonates would therefore be oriented radially around the carcass in a rapidly deposited fluvial sand, rather than oriented vertically in a less disturbed seabed.

**Taphonomic sequence for dinosaur "mummification".**—Our work allows for a taphonomic "mummification" sequ-

ence to be proposed for these dinosaurs (Table 6). Both UCRC *Edmontosaurus* "mummies" were found within a 10-kilometer radius of at least two other *Edmontosaurus annectens* "mummies" (AMNH 5060, SMF R 4036), a *Triceratops* "mummy" (HMNS 2006.1743), and an articulated *Tyrannosaurus rex* (UCRC PV1) with a sedimentologically preserved carcass boundary (Sereno et al. 2026). Climate models and oxygen isotopic data have suggested monsoonal conditions in the Late Cretaceous of North America (Fricke et al. 2010), consistent with cycles of drought and flooding; and even some Late Cretaceous North American dinosaur mass-mortality bone beds are thought to have been caused by droughts (Rogers 1990). Within a seasonally dry floodplain environment, taxa that are numerous (e.g., herbivores such as hadrosaurs and ceratopsians) and frequent this habitat are more likely to die within or near a dried riverbed during a dry season. Harsh conditions during a dry season may lower the rate of carcass scavenging or provide excess carcasses than can be readily scavenged due to drought-related mass mortality, allowing for the microbial/autolytic decay of most of the soft tissues, while the integument desiccated and shrank around the bones under exposure to air and sun. In some cases, scavenging that does occur may facilitate the release of body fluids through rupture of the abdominal cavity (Drumheller et al. 2022), alongside body cavity rupture through the expansion of decomposition gases produced by microbes heated by the sun (Moore et al. 2020), but the evidence for extensive integument preservation suggests that the conditions overall were scavenging-limited.

Taxa with scaly, "keratinized"/cornified and pigmented skin, especially those with "hard" ungual sheaths or rhamphotheca, would likely be more amenable to natural integument "mummification" through desiccation, as seen in hadrosaurs and ceratopsians from this region in Wyoming (Sereno et al. 2026). However, note that the small scales and skin folding seen in hadrosaur "mummies" suggests that, although their skin was scaly and therefore "keratinized"/cornified, the skin was likely histologically thin in cross section and pliable (contra Davis 2014). These taxa also tend to be herbivorous, and likely abundant in the ecosystem compared to large-bodied carnivores. Late Cretaceous, North American hadrosaurs are more often found in fluvial sandstone whereas ceratopsians are more often found in mudstone (Lyson and Longrich 2011), suggesting that hadrosaurs may have frequented riparian environments more often than ceratopsians. *Edmontosaurus* is also more likely to be preserved in multi-individual bonebeds (e.g., Siviero et al. 2020; Snyder et al. 2020), possibly consistent with large social groups, than is *Triceratops*. These features likely made hadrosaur carcasses the most available for "mummification" in the environment.

The desiccation of the skin prolongs its survival prior to ultimate degradation, as seen in more recent human "natural mummies" (Piombino-Mascali et al. 2017). Taphonomic studies of Quaternary (including modern) elephantid remains (Stuart and Larkin 2010; White and Diedrich 2012) support the idea that the *Edmontosaurus annectens* "mummies" did not spend more than one year exposed at the surface (i.e., more than one dry season-wet season cycle). At the cessation of the dry season in which they perished, rapid burial through monsoonal flooding would presumably have buried the carcass and any nearby plant material in fluvial sands with only minimal prior transport, as evidenced by the high degrees of preserved three-dimensional articulation. Crucially, to produce three-dimensional fossil integument rendering envelopes, as opposed to two-dimensionally flattened layers, sand (i.e., sediment with low compressibility) must be able to infiltrate the interior of the carcass/body cavity through prior rupture, beyond just burying the exterior of the carcass. The skin would have still been present at burial, and while the carcass was sub-aqueously buried in porous sands, it would have experienced further degradation in the waterlogged sediments. Microbes would have decomposed the skin organics and formed an external biofilm over weeks to months during this wet season and prior to the subsequent dry season, leading to high-fidelity clay templating either through localized attraction of clays already present in the sediment or through localized precipitation of clays de novo. Thus, the initial formation of templated dinosaur "mummies" is hypothesized to have largely occurred within a single year, with subsequent decay and diagenesis eventually eliminating any surviving organic material. Iron sulfides might also be produced alongside the clay template

Table 6. Hypothesized sequence of the main processes of dinosaur "mummy" taphonomy.

1. In life, all tissues present and body cavity sealed.
2. During drought, a deceased carcass settles to its side in or near a dry river channel after death. Microbial and autolytic decay occurs to remove the most labile tissues and ruptures the body cavity, while subaerial desiccation leaves a dried, shrunken husk of epidermis (possibly with crosslinking/polymerization of the skin) in under a year.
3. At the onset of monsoonal season, rapid burial of the carcass in fluvial, waterlogged sand occurs. Sand infiltrates the ruptured body cavity but cannot completely fill every external or internal crevice.
4. While buried and waterlogged, a microbial biofilm forms preferentially at the external surface of the skin, filling external cavities.
5. Due to active decay of the skin organics by the biofilm, clay (predominantly kaolinite) and some (e.g., anoxia-, iron-, or sulfate-limited) pyrite accumulate/precipitate at the interface of the skin and biofilm over weeks or months. This forms a template of the external surface of the skin, which is being eliminated in a subaqueous environment. Pyrite concretions form around close organic matter at the tip of the tail (e.g., less woody plant matter). Excess clay accumulates in external cavities, while internal cavities remain. Eventually, the biofilm dies off when digestible organics are spent.
6. Long-term diagenesis over millions of years occurs as the remains are buried more deeply. The sediment compacts to eliminate internal cavities, resulting in conjoining of clay layers well below the apical/dorsal tip of the spike.
7. Late-stage weathering oxidizes pyrite into iron oxides, which could form a rind around larger pyrite concretions. Manganese oxides precipitate.

as organics degrade in the presence of sulfate-reducing bacteria in anoxic microenvironments, and later weathered into iron oxides, perhaps even much later in their burial history.

We may have observed some "pyrite disease" in the thin layer of "mummy" integument rendering over the course of a few years under curatorial conditions, with Fe and S detected prominently years ago while Fe and O are detected more recently. In contrast, the more massive ironstone concretion at the tip of the tail still maintains a detectable signature of pyrite, perhaps suggesting that it was able to form an iron oxide rind with pyrite protected internally. Indeed, the rate of pyrite oxidation can be greatly slowed while buried but can occur in a matter of years when exposed to air (Gu et al. 2020). Manganese oxides can form from the oxidative weathering of Mn-bearing silicates or carbonates, sometimes in situ (Post 1999). Manganese and iron are often found together in the geologic record and can form dendritic patterns in bedding planes or fractures (Potter and Rossman 1979). The low compressibility of sand allows for the retention of any three-dimensionality of the infilled fossil integument rendering.

The thickness of the Lance Formation in this "mummy zone" region of eastern Wyoming (Connor 1992; Sereno et al. 2026) and the numerous exposures in this region likely contribute to the historical importance of this area in the discovery of dinosaur "mummies". If paleoclimate was monsoonal and prone to "mummification", then the part of the depositional basin (i.e., Powder River Basin) with the greatest subsidence and sedimentation (i.e., greatest thickness of the formation) would allow for even rare taphonomic events to accumulate in the fossil record over time.

**Powerful equipment does not necessarily lead to robust conclusions**.—Our model of dinosaur "mummification" is, in many ways, supportive of the insight made by Osborn (1911, 1912) over a century ago. Early observations of thin minerals responsible for preserving the fossil integument rendering are in stark contrast to more recent claims of extensive, exceptional organic preservation. These recent interpretations include "3D-preserved eumelanin-bearing bodies, dermal cells and blood vessel fragments in an organic matrix composed of protein fossilization products" (Fabbri et al. 2020: 185). Barbi et al. (2019: 1) describe a "band of carbon-rich layers" that are "topographically and morphologically congruent with the stratum corneum in modern reptiles" and that "these hosting carbonyl-rich layers are apparently composed of subcircular bodies resembling preserved cell structures". Manning et al. (2009: 3429) conclude the survival of "endogenously derived organics from the skin", even including unique amino acid composition. We consider it unlikely that dinosaur "mummification" follows such disparate modes of preservation as external mineral templating in some specimens, but histological and biomolecular preservation at the level of complete dermal layers, cells, and peptides in similarly preserved "mummies".

This then raises the following question: how could a century of technological advancement lead to conclusions that are, in our opinion, less in line with scientific reality? Modern microscopy, spectroscopy, and mass spectrometry methods are certainly powerful tools, but if data from a given method is taken in isolation, conclusions are often weaker than if multiple methods are used in conjugation to triangulate consistent patterns. Here, we attempted to address this concern by studying "mummified" dinosaur integument rendering with a greater number and diversity of analytical methods than most, if not all, previous studies on this topic.

**Alternative pathways?**—While the "mummy integument" in the UCRC specimens appear to be predominantly preserved via clay templating with associated iron and manganese compounds, we do not wish to rule out the possibility of taphonomic variation between dinosaur "mummy" specimens. Some might have more carbonate cementation in their surrounding matrix, compared to the essentially non-cemented sands of the UCRC *Edmontosaurus annectens* "mummies", and other "mummies" might have more ironstone concretions around the fossil, whereas the prepared regions of the early adult UCRC PV30 only show a sizeable ironstone concretion on the tip of the tail. Such cements likely reflect carbonate alkalinity during early microbial decay. Compared to the rather sparse dark staining on the UCRC specimens, other specimens might have more extensive pyrite precipitation on the fossil integument rendering due to higher iron and/or sulfate availability during early microbial decay and more prevalent anoxic microenvironments. Some specimens might be more heavily weathered in the subsurface later in their taphonomic history, with greater oxidation of pyrite into iron oxides or late-stage precipitation of iron oxides, carbonates, and manganese oxide dendrites.

We remain open to the possibility that other specimens might have fossilized skin via microbially mediated authigenic phosphatization early in their taphonomic history or even organic preservation of decay-resistant, diagenetically stable fossil melanin or, for example, of kerogen derived from in situ polymerization of fatty acids from integument lipids (Vinther 2020). Nevertheless, the UCRC specimens show no obvious indication themselves of such taphonomic modes.

# Conclusions

*Evidence wanting for preserved tissue structures and original biomolecules*.—From our sediment analysis, thin sectioning, and from multiple forms of microscopy, spectroscopy, and spectrometry, we conclude that original organic material is negligible or entirely absent within the integument rendering or adjacent sediment of our two *Edmontosaurus annectens* "mummies". Although there is inherent uncertainty when examining a limited number of specimens among many examples of fossilized dinosaur integument, our work here strongly suggests that dinosaur "mummies" are likely not predominantly preserved organically. They do not match expectations of carbonaceous soft

tissue preservation from either Konservat-Lagerstätten or from experimental simulations of diagenesis on modern vertebrate integuments under oxic, but microbial/autolytic decay-limited, conditions (Saitta et al. 2019a).

For large-bodied, non-avian Late Cretaceous dinosaurs preserved in fluvial settings in western North America, we are skeptical of the evidence offered to date for the preservation of internal tissue structures or endogenous biomolecules in the fossilized integument. Histological features, such as skin layers, cells, and vascular tracts, have yet to be convincingly identified, nor has there been suitable evidence for integument polypeptides or endogenous amino acids.

Although it may be tempting to assume organic preservation when encountering fossil integument rendering, "mummy" dinosaurs are not directly comparable in composition to deliberate or naturally occurring Holocene human mummies, such as those from ancient Egypt or Chile with organic remnants of skin (Lynnerup 2007). Nor are these dinosaurian remains similar in composition to subfossil mummy carcasses of various animals and other organisms from Pleistocene permafrost (Harington 2007) or lower latitude desiccated skins of recently extinct animals such as moa (Worthy 1989) or dodo (Warnett et al. 2021). Those far younger remains are organically preserved with relatively minimal alteration, but their proteins are still thermodynamically unstable over millions of years (Hedges 2002), even if their decomposition rate is radically slowed by natural or human-induced desiccation or by low temperatures and freezing (Rybczynski et al. 2013). For an example of the exceptional degree of organic preservation seen in permafrost, some Pleistocene permafrost organisms can even be reanimated from frozen states after thousands of years (e.g., ~46 Ka nematodes, Shatilovich et al. 2023). Instead, dinosaur "mummies" are true fossils in the sense that they are at chemical equilibria with their immediate burial environment, barring any late-stage weathering or erosion (Parry et al. 2018).

*Dinosaur "mummification" sequence in the Lance Formation.*—Most of the best-preserved dinosaur "mummies" pertain to the single "duckbill" species *Edmontosaurus annectens* (Sereno et al. 2026), which congregated in vast herds on a coastal floodplain along the western interior seaway, a margin subject to cyclic monsoonal climate (Fricke et al. 2010). Study of two newly described, exceptionally preserved "mummies" from the "mummy zone" in east-central Wyoming, with reference to others "mummies", provides evidence for a integument "mummification" sequence:

(i) Subaerial decay, deflation, and desiccation during dry-seasonal drought, resulting in wrinkling of the skin, limited scavenging, and death near or within dry riverbeds as well as stabilization of the integument akin to recent, natural mummies.

(ii) Rapid burial by wet-seasonal floodwaters in place or with limited transport, along with infilling of the breached carcass by sediment identical to that outside the carcass.

(iii) Biofilm formation and decay-mediated clay templating while buried in waterlogged sediment (possibly with associated pyrite precipitation or other ironstone concretion formation).

(iv) Eventual breakdown and elimination of organic integument through decay and diagenesis, along with diagenetic sediment compaction.

(v) Recent, groundwater-mediated weathering to oxidize pyrite into iron oxides or directly precipitate additional minerals (e.g., manganese oxides or iron oxides).

Future work will determine the generality of this taphonomic sequence in generating integumentary renderings in terrestrial settings.

*Clay templating in a terrestrial setting.*—We propose that decay of the last-surviving, outermost, corneous integument while buried in waterlogged sands might attract or induce the in situ precipitation of clay, with iron sulfides likewise being precipitated and iron oxides and manganese oxides likely produced during weathering. Dinosaur "mummies" undergo a taphonomic pathway whose early stages of desiccation are similar to those of naturally occurring African mammal "mummies" today, even if the ultimate mode of preservation differs radically. As initially observed by Osborn (1911, 1912), these dinosaurs died during cyclic droughts and desiccated subaerially, leaving behind leathery, shrunken skin wrapped tightly around the bones. The key to their ultimate preservation was sudden burial by floodwaters and infilling of the breached carcass by these same fluvial sands. Within these porous, waterlogged sediments, their organic material was microbially decayed while an inorganic template of the last-surviving integument simultaneously formed. Specifically, a biofilm on the carcass exterior attracted, or facilitated the accumulation of, a thin clay template. This template preserved the external, three-dimensional form of the integument as a "death mask".

The region in Wyoming described as a dinosaur "mummy zone" (Sereno et al. 2026) was likely one in which the paleoclimate promoted these sorts of dry and wet seasonal cycles. Ultimately, the mode of inorganic preservation of dinosaur "mummies" differs starkly from the organic preservation of recent natural mummies. Their three-dimensional, microbially mediated clay templating is, to our knowledge, the first known example of this type of soft tissue preservation in a dinosaur or in a terrestrial setting.

The integument rendering of the two UCRC "mummies" is predominantly preserved via aluminosilicate clay, with occasional metallic compounds near the clay (e.g., iron sulfides, iron oxides, and manganese oxides). These results are consistent with older fossil material as well as decay experiments in sands that preserve "death masks" of soft tissues, especially when associated with biofilms. Clay templating of soft tissues seems to occur as they microbially decay, with iron sulfides precipitated atop or with iron oxide and manganese oxides produced during oxidative weathering. This is also consistent with the closely associated fossil plant material observed here, along with fossil plants found

alongside other "mummy" dinosaurs, suggesting that the burial environment was not organics-limited.

Future research can search for direct evidence of a microbial biofilm within the clay template, such as bacterial hopanoids (e.g., Brocks et al. 2003) through gas or liquid chromatography and mass spectrometry methods. Although our study utilized many independent methods, additional approaches (e.g., FTIR, electron backscatter diffraction, transmission electron microscopy) could provide further insight into lingering questions. Thin sections and other approaches could investigate crystal morphology and growth to better describe the chronology of the clay templating and the Fe and Mn mineral precipitation (see Jauvion et al. 2020).

# Acknowledgements

We thank the following individuals for granting access to or providing support for laboratory equipment: Yarrow Axford, LGSA (NU), Peter J. Makovicky, white light scanning (University of Minnesota, Minneapolis, USA), Vishruth Venkat and Michael Coates, polarized light microscopy (both UC), Megan Whitney, optical microscopy (LU), Michael Pittman, LSF imaging (The Chinese University of Hong Kong), Gerard Olack, BSE/EDS (UC), and Martin Pentrak, XRD clay analysis (Illinois State Geological Survey, Champaign, USA), Luxi Li, sXRF analysis (ANL). Support for the project comes from private donation. Erin Fitzgerald (UC) assisted in the initial preparation of the UCRC specimens. We thank Kraig Derstler (Divide, CO, USA) and Marcus Erickson (Ventura County Science Center, Santa Paula, California, USA) for their role in collecting of the UCRC specimens. Terri Li, Xin Jiang, and Erica Markiewicz (all UC) assisted with dissection, embedding, and thin sectioning of *Gonocephalus doriae*. We thank the following for discussions over a range of topics in the manuscript: Susan Kidwell (UC) for extensive discussion of sedimentological analysis; Clint A. Boyd (NDGS) and Stephanie K. Drumheller (University of Tennessee-Knoxville, USA) for helpful discussion about other dinosaur "mummy" specimens; Justin Tweet (National Park Service, Cottage Grove, USA) for helpful discussion of trace fossils associated with "mummy" hadrosaurs; Simon Darroch (SMF), Christopher Mulligan (University of California, Davis, USA), Jakob Vinther (UB), Luke Parry (University of Oxford, UK), and Derek Briggs (YPMPU and University of Yale, New Haven, USA) for helpful discussion of taphonomic clay templating; Lorenzo Alibardi (University of Bologna, Italy) for helpful discussion about reptile scale histology. Finally, we thank Pierre Guériau (Muséum national d'Histoire naturelle Paris, France) and an anonymous referee for constructive journal reviews.

*Editor*: Eudald Mujal Grané

# References

Akisanmi, P. 2022. Classification of clay minerals. *In:* M. René (ed.), *Mineralogy*, 229–240. IntechOpen, London.

Alleon, J., Montagnac, G., Reynard, B., Brulé, T., Thoury, M., and Gueriau, P. 2021. Pushing Raman spectroscopy over the edge: Purported signatures of organic molecules in fossil animals are instrumental artefacts. *BioEssays* 43: 2000295.

Allison, P.A. and Pye, K. 1994. Early diagenetic mineralization and fossil preservation in modern carbonate concretions. *Palaios* 9: 561–575.

Anderson, E.P., Schiffbauer, J.D., and Xiao, S. 2011. Taphonomic study of Ediacaran organic-walled fossils confirms the importance of clay minerals and pyrite in Burgess Shale-type preservation. *Geology* 39: 643–646.

Anderson, R.P., Tosca, N.J., Cinque, G., Frogley, M.D., Lekkas, I., Akey, A., Hughes, G.M., Bergmann, K.D., Knoll, A.H., and Briggs, D.E. 2020. Aluminosilicate haloes preserve complex life approximately 800 million years ago. *Interface Focus* 10: 20200011.

Anderson, R.P., Tosca, N.J., Saupe, E.E., Wade, J., and Briggs, D.E. 2021. Early formation and taphonomic significance of kaolinite associated with Burgess Shale fossils. *Geology* 49: 355–359.

Anderson, R.P., Woltz, C.R., Tosca, N.J., Porter, S.M., and Briggs, D.E. 2023. Fossilisation processes and our reading of animal antiquity. *Trends in Ecology & Evolution* 38: 1060–1071.

Anna, L.O. 2010. Geologic assessment of undiscovered oil and gas in the Powder River Basin Province, Wyoming and Montana. *In*: *U.S. Geological Survey Powder River Basin Assessment Team, Total Petroleum Systems and Geologic Assessment of Oil and Gas Resources in the Powder River Basin Province, Wyoming and Montana, Chapter 1*, 1–97. U.S. Geological Survey Digital Data Series DDS–69–U, Reston.

Arbour, V.M. and Evans, D.C. 2017. A new ankylosaurine dinosaur from the Judith River Formation of Montana, USA, based on an exceptional skeleton with soft tissue preservation. *Royal Society Open Science* 4: 161086.

Barbi, M., Bell, P.R., Fanti, F., Dynes, J.J., Kolaceke, A., Buttigieg, J., Coulson, I.M., and Currie, P.J. 2019. Integumentary structure and composition in an exceptionally well-preserved hadrosaur (Dinosauria: Ornithischia). *PeerJ* 7: e7875.

Barthel, K.W. 1970. On the deposition of the Solnhofen lithographic limestone (Lower Tithonian, Bavaria, Germany). *Neues Jahrbuch für Geologie und Paläontologie* 135: 1–18.

Baggott, D.G., Bunch, K.J., and Gill, K.R. 1988. Variations in some inorganic components and physical properties of claw keratin associated with claw disease. British Friesian cow. *British Veterinary Journal* 144: 534–542.

Becker-Kerber, B., El Albani, A., Konhauser, K., Abd Elmola, A., Fontaine, C., Paim, P.S., Mazurier, A., Prado, G.M., Galante, D., Kerber, P.B., and da Rosa, A.L. 2021. The role of volcanic-derived clays in the preservation of Ediacaran biota from the Itajaí Basin (ca. 563 Ma, Brazil). *Scientific Reports* 11: 5013.

Bell, P.R. 2014. A review of hadrosaurid skin impressions. *In:* D.A. Eberth and D.C. Evans (eds.), *Hadrosaurs*, 572–590. Indiana University Press, Bloomington.

Bell, P.R., Fanti, F., Currie, P.J., and Arbour, V.M. 2014. A mummified duck-billed dinosaur with a soft-tissue cock's comb. *Current Biology* 24: 70–75.

Bell, P.R., Hendrickx, C., Pittman, M., Kaye, T.G., and Mayr, G. 2022. The exquisitely preserved integument of *Psittacosaurus* and the scaly skin of ceratopsian dinosaurs. *Communications Biology* 5: 809.

Bertazzo, S., Maidment, S.C., Kallepitis, C., Fearn, S., Stevens, M.M., and Xie, H.N. 2015. Fibres and cellular structures preserved in 75-million-year-old dinosaur specimens. *Nature Communications* 6: 7352.

Blakey, P.R. and Lockwood, P. 1968. The environment of calcified components in keratins. *Calcified Tissue Research* 2: 361–369.

Blakey, P.R., Earland, C., and Stell, J.G.P. 1963. Calcification of keratin. *Nature* 198: 481–481.

Bobrovskiy, I., Krasnova, A., Ivantsov, A., Luzhnaya, E., and Brocks, J.J. 2019. Simple sediment rheology explains the Ediacara biota preservation. *Nature Ecology & Evolution* 3: 582–589.

Boyd, C.A., Drumheller, S.K., Householder, M., Saini-Eidukat, B., Nestler, J., and Ullmann, P. 2023. Geochemical examination of dinosaurian "mummies" from the Should Hell Creek Formation reveals a pathway for dermal tissue fossilization. *In*: D. Ehret and E. Fulwood (eds.), *Society of Vertebrate Paleontology 83rd Annual Meeting Program Guide*, 97–98. Society of Vertebrate Paleontology, Cincinnati, Ohio.

Briggs, D.E.G., Kear, A.J., Martill, D.M., and Wilby, P.R. 1993. Phosphati-

zation of soft-tissue in experiments and fossils. *Journal of the Geological Society* 150: 1035–1038.

Brill, R.H. 1999. *Chemical Analyses of Early Glasses.* Vol. 1, 335 pp.; Vol. 2, 553 pp. Corning Museum of Glass, Corning.

Brocks, J.J., Buick, R., Summons, R.E., and Logan, G.A. 2003. A reconstruction of Archean biological diversity based on molecular fossils from the 2.78 to 2.45 billion-year-old Mount Bruce Supergroup, Hamersley Basin, Western Australia. *Geochimica et Cosmochimica Acta* 67: 4321–4335.

Brown, C.M. 2017. An exceptionally preserved armored dinosaur reveals the morphology and allometry of osteoderms and their horny epidermal coverings. *PeerJ* 5: e4066.

Brown, C.M., Henderson, D.M., Vinther, J., Fletcher, I., Sistiaga, A., Herrera, J., and Summons, R.E. 2017. An exceptionally preserved three-dimensional armored dinosaur reveals insights into coloration and Cretaceous predator-prey dynamics. *Current Biology* 27: 2514–2521.

Cai, Y.P., Hua, H., Xiao, S.H., Schiffbauer, J.D., and Li, P. 2010. Biostratinomy of the late Ediacaran pyritized Gaojiashan Lagerstätte from southern Shaanxi, South China: Importance of event deposit. *Palaios* 25: 487–506.

Carpenter, K. 1987. Paleoecological significance of droughts during the Late Cretaceous of the Western Interior. *In:* P.M. Currie and E.H. Koster (eds.), *Fourth Symposium on Mesozoic Terrestrial Ecosystems, Short Papers*, 42–47. Tyrrell Museum of Palaeontology, Drumheller.

Carpenter, K. 2007. How to make a fossil: Part 2: Dinosaur mummies and other soft tissue. *The Journal of Paleontological Science* 7: 1–23.

Carroll, D. 1959. Ion exchange in clays and other minerals. *Geological Society of America Bulletin* 70: 749–779.

Chinsamy, A. and Raath, M. A. 1992. Preparation of fossil bone for histological examination. *Palaeontologia Africana* 29: 39–44.

Christiansen, N.A. and Tschopp, E. 2010. Exceptional stegosaur integument impressions from the Upper Jurassic Morrison Formation of Wyoming. *Swiss Journal of Geosciences* 103: 163–171.

Clements, T., Purnell, M., and Gabbott, S., 2019. The Mazon Creek Lagerstätte: a diverse late Paleozoic ecosystem entombed within siderite concretions. *Journal of the Geological Society* 176: 1–11.

Connor, C.W. 1992. The Lance Formation: petrography and stratigraphy, Powder River basin and nearby basins, Wyoming and Montana. *U.S. Geological Survey Bulletin B* 1917-I: 17.

Corthésy, N., Saleh, F., Antcliffe, J.B., and Daley, A.C. 2025. Kaolinite induces rapid authigenic mineralisation in unburied shrimps. *Communications Earth & Environment* 6: 4.

Cotroneo, S., Schiffbauer, J.D., McCoy, V.E., Wortmann, U.G., Darroch, S.A.F., Peng, Y., and Laflamme, M. 2016. A new model of the formation of Pennsylvanian iron carbonate concretions hosting exceptional soft-bodied fossils in Mazon Creek, Illinois. *Geobiology* 14: 543–555.

Covington, A.D. 2009. *Tanning Chemistry: The Science of Leather*. xxxi + 483 pp. Royal Society of Chemistry, London.

Curran, H.A. 2015. Sinuous rhizoliths mimic invertebrate trace fossils on upper Pleistocene caliche surfaces, San Salvador Island, Bahamas. *In:* D. McIlroy (ed.), *Ichnology: Papers from ICHNIA III, Miscellaneous Publication 9*, 63–72. Geological Association of Canada, St. John's, Newfoundland.

Currie, P.J., Nadon, G.C., and Lockley, M.G. 1991. Dinosaur footprints with skin impressions from the Cretaceous of Alberta and Colorado. *Canadian Journal of Earth Sciences* 28: 102–115.

Darroch, S.A.F., Laflamme, M., Schiffbauer, J.D., and Briggs, D.E.G. 2012. Experimental formation of a microbial death mask. *Palaios* 27: 293–303.

Das, I. 2004. *Lizards of Borneo: A Pocket Guide.* 89 pp. Natural History Publications (Borneo), Kota Kinabalu.

Davis, M. 2014. Census of dinosaur skin reveals lithology may not be the most important factor in increased preservation of hadrosaurid skin. *Acta Palaeontologica Polonica* 59: 601–605.

Demirbaş, A. 2002. Desulfurization of lignite and coal using alkaline solution from biomass ashes. *Energy Exploration & Exploitation* 20: 371–378.

Drumheller, S.K., Boyd, C.A., Barnes, B.M., and Householder, M.L. 2022. Biostratinomic alterations of an *Edmontosaurus* "mummy" reveal a pathway for soft tissue preservation without invoking "exceptional conditions". *PLOS ONE* 17: e0275240.

Earland, C., Blakey, P.R., and Stell, J.G.P. 1962. Studies on the structure of keratin IV. The molecular structure of some morphological components of keratins. *Biochimica et Biophysica Acta* 56: 268–274.

El Atfy, H. and Uhl, D. 2021. Palynology and palynofacies of sediments surrounding the *Edmontosaurus annectens* mummy at the Senckenberg Naturmuseum in Frankfurt/Main (Germany). *Journal of Applied & Regional Geology/Zeitschrift der Deutschen Gesellschaft für Geowissenschaften (ZDGG)* 172: 127.

Embacher, J., Zeilinger, S., Kirchmair, M., Rodriguez-R, L.M., and Neuhauser, S. 2023. Wood decay fungi and their bacterial interaction partners in the built environment—a systematic review on fungal bacteria interactions in dead wood and timber. *Fungal Biology Reviews* 45: 100305.

Fabbri, M., Wiemann, J., Manucci, F., and Briggs, D.E. 2020. Three-dimensional soft tissue preservation revealed in the skin of a non-avian dinosaur. *Palaeontology* 63: 185–193.

Fricke, H.C., Foreman, B.Z., and Sewall, J.O. 2010. Integrated climate model-oxygen isotope evidence for a North American monsoon during the Late Cretaceous. *Earth and Planetary Science Letters* 289: 11–21.

Gabbott, S.E., Browning, C., Theron, J.N., and Whittle, R.J. 2017. The late Ordovician Soom Shale Lagerstätte: an extraordinary post-glacial fossil and sedimentary record. *Journal of the Geological Society* 174: 1–9.

Gaines, R.R., Briggs, D.E., and Yuanlong, Z. 2008. Cambrian Burgess Shale-type deposits share a common mode of fossilization. *Geology* 36: 755–758.

Gautier, D.L. 1982. Siderite concretions; indicators of early diagenesis in the Gammon Shale (Cretaceous). *Journal of Sedimentary Research* 52: 859–871.

Gibson, B.M., Schiffbauer, J.D., and Darroch, S.A. 2018. Ediacaran-style decay experiments using mollusks and sea anemones. *Palaios* 33: 185–203.

Gibson, B.M., Schiffbauer, J.D., Wallace, A.F., and Darroch, S.A. 2023. The role of iron in the formation of Ediacaran "death masks". *Geobiology* 21: 421–434.

Gratuze, B. 1999. Obsidian characterization by laser ablation ICP-MS and its application to prehistoric trade in the Mediterranean and the Near East: sources and distribution of obsidian within the Aegean and Anatolia. *Journal of Archaeological Science* 26: 869–881.

Gu, X., Heaney, P.J., Reis, F.D.A., and Brantley, S.L. 2020. Deep abiotic weathering of pyrite. *Science* 370: eabb8092.

Gupta, V. 2011. *Surface Charge Features of Kaolinite Particles and Their Interactions*. 210 pp. Ph.D. Thesis, The University of Utah, Salt Lake City.

Harington, C.R. 2007. Vertebrate records—Late Pleistocene mummified mammals. *In:* S.A. Elias (ed.), *Encyclopedia of Quaternary Science*, 3197–3202. Elsevier, Oxford.

He, X., Zhao, T., Hu, J., Li, X., Wang, X., Zheng, X., and Pan, Y. 2023. Taphonomic properties of the foot claw sheath from an Early Cretaceous bird specimen *Confuciusornis sanctus*. *Cretaceous Research* 144: 105453.

Hedges, R.E. 2002. Bone diagenesis: An overview of processes. *Archaeometry* 44: 319–328.

Heindel, R.C., Lyons, W.B., Welch, S.A., Spickard, A.M., and Virginia, R.A. 2018. Biogeochemical weathering of soil apatite grains in the McMurdo Dry Valleys, Antarctica. *Geoderma* 320: 136–145.

Hendrickx, C., Bell, P.R., Pittman, M., Milner, A.R., Cuesta, E., O'Connor, J., Loewen, M., Currie, P.J., Mateus, O., Kaye, T.G., and Delcourt, R. 2022. Morphology and distribution of scales, dermal ossifications, and other non-feather integumentary structures in non-avialan theropod dinosaurs. *Biological Reviews* 97: 960–1004.

Holthaus, K.B., Eckhart, L., Dalla Valle, L., and Alibardi, L. 2018. Evolution and diversification of corneous beta-proteins, the characteristic

epidermal proteins of reptiles and birds. *Journal of Experimental Zoology Part B: Molecular and Developmental Evolution* 330: 438–453.
Horner, J.R. 1984. A "segmented" epidermal tail frill in a species of hadrosaurian dinosaur. *Journal of Paleontology* 58: 270–271.
Householder, M. and Boyd, C.A. 2023. The impact of adhesives, consolidants, and solvents on geochemical data: An example using X-ray fluorescence. *In*: D. Ehret and E. Fulwood (eds.), *Society of Vertebrate Paleontology 83rd Annual Meeting Program Guide*, 221–222. Society of Vertebrate Paleontology, Cincinnati, Ohio
Householder, M.L. and Boyd, C.A. 2024. Reframing the question: are reversable adhesives also removable? *In*: D. Ehret (ed.), *Society of Vertebrate Paleontology, Program of Abstracts*, 265–266. Society of Vertebrate Paleontology, Minneapolis, Minnesota.
Hurlbut, C.S. and Klein, C. 1985. *Manual of Mineralogy 20th Edition.* vi + 596 pp. Wiley, New York.
Jauvion, C., Bernard, S., Gueriau, P., Mocuta, C., Pont, S., Benzerara, K., and Charbonnier, S. 2020. Exceptional preservation requires fast biodegradation: thylacocephalan specimens from La Voulte-sur-Rhône (Callovian, Jurassic, France). *Palaeontology* 63: 395–413.
Jones, J., Mirzaei, M., Ravishankar, P., Xavier, D., Lim, D.S., Shin, D.H., Bianucci, R., and Haynes, P.A. 2016. Identification of proteins from 4200-year-old skin and muscle tissue biopsies from ancient Egyptian mummies of the first intermediate period shows evidence of acute inflammation and severe immune response. *Philosophical Transactions of the Royal Society A: Mathematical, Physical and Engineering Sciences* 374: 20150373.
Kabanov, P., Anadón, P., and Krumbein, W.E. 2008. *Microcodium*: An extensive review and a proposed non-rhizogenic biologically induced origin for its formation. *Sedimentary Geology* 205: 79–99.
Kaye, T.G., Falk, A.R., Pittman, M., Sereno, P.C., Martin, L.D., Burnham, D.A., Gong, E., Xu, X., and Wang, Y. 2015. Laser-stimulated fluorescence in paleontology. *PLOS ONE* 10: e0125923.
Konhauser, K.O., Fisher, Q.J., Fyfe, W.S., Longstaffe, F.J., and Powell, M.A. 1998. Authigenic mineralization and detrital clay binding by freshwater biofilms: the Brahmani River, India. *Geomicrobiology Journal* 15: 209–222.
Kumar, N., Andersson, M.P., van den Ende, D., Mugele, F., and Sîretanu, I. 2017. Probing the surface charge on the basal planes of kaolinite particles with high-resolution atomic force microscopy. *Langmuir* 33: 14226–14237.
Li, S., He, H., Tao, Q., Zhu, J., Tan, W., Ji, S., Yang, Y., and Zhang, C. 2020. Kaolinization of 2: 1 type clay minerals with different swelling properties. *American Mineralogist* 105: 687–696.
Lingham-Soliar, T. 2014. Dinosaur Integument. *In*: T. Lingham-Soliar (ed.), *The Vertebrate Integument, Volume 1: Origin and Evolution*, 153–192. Springer, Berlin.
Lipkin, C., Sereno, P.C., and Horner, J.R. 2007. The furcula in *Suchomimus tenerensis* and *Tyrannosaurus rex* (Dinosauria: Theropoda: Tetanurae). *Journal of Paleontology* 81: 1523–1527.
Loope, D.B., Kettler, R.M., and Weber, K.A. 2011. Morphologic clues to the origins of iron oxide-cemented spheroids, boxworks, and pipelike concretions, Navajo Sandstone of south-central Utah, USA. *The Journal of Geology* 119: 505–520.
Loope, D.B., Kettler, R.M., Weber, K.A., Hinrichs, N.L., and Burgess, D.T. 2012. Rinded iron-oxide concretions: hallmarks of altered siderite masses of both early and late diagenetic origin. *Sedimentology* 59: 1769–1781.
Lynnerup, N. 2007. Mummies. *American Journal of Physical Anthropology* 134: 162–190.
Lyson, T.R. and Longrich, N.R. 2011. Spatial niche partitioning in dinosaurs from the latest Cretaceous (Maastrichtian) of North America. *Proceedings of the Royal Society B: Biological Sciences* 278: 1158–1164.
Machel, H.G. and Mountjoy, E.W. 1986. Chemistry and environments of dolomitization—a reappraisal. *Earth-Science Reviews* 23: 175–222.
Mähler, B., Janssen, K., Menneken, M., Tahoun, M., Lagos, M., Bierbaum, G., Müller, C., and Rust, J. 2020. Calcite precipitation forms crystal clusters and muscle mineralization during the decomposition of *Cambarellus diminutus* (Decapoda: Cambaridae) in freshwater. *Palaeontologia Electronica* 23: 1–17.
Mallison, H. 2014. Photogrammetry in paleontology—a practical guide. *Journal of Paleontological Techniques* 12: 1.
Maloney, K.M., Schiffbauer, J.D., Halverson, G.P., Xiao, S., and Laflamme, M. 2022. Preservation of early Tonian macroalgal fossils from the Dolores Creek Formation, Yukon. *Scientific Reports* 12: 6222.
Maltby, J., Steinle, L., Löscher, C.R., Bange, H.W., Fischer, M.A., Schmidt, M., and Treude, T. 2018. Microbial methanogenesis in the sulfate-reducing zone of sediments in the Eckernförde Bay, SW Baltic Sea. *Biogeosciences* 15: 137–157.
Manning, P. L. 2008. *Grave Secrets of Dinosaurs: Soft Tissues and Hard Science*. 316 pp. National Geographic Society, Washington, D.C.
Manning, P.L., Morris, P.M., McMahon, A., Jones, E., Gize, A., Macquaker, J.H., Wolff, G., Thompson, A., Marshall, J., Taylor, K.G., and Lyson, T. 2009. Mineralized soft-tissue structure and chemistry in a mummified hadrosaur from the Hell Creek Formation, North Dakota (USA). *Proceedings of the Royal Society B: Biological Sciences* 276: 3429–3437.
Mantovani, M. and Becerro, A.I. 2010. Illitization of kaolinite: The effect of pressure on the reaction rate. *Clays and Clay Minerals* 58: 766–771.
Mapstone, N.B. and McIlroy, D. 2006. Ediacaran fossil preservation: taphonomy and diagenesis of a discoid biota from the Amadeus Basin, central Australia. *Precambrian Research* 149: 126–148.
Marsh, O.C. 1892. Notice of new reptiles from the Laramie Formation. *American Journal of Science* 3: 449–453.
Martill, D.M., Bechly, G., and Loveridge, R.F. 2007. *The Crato Fossil Beds of Brazil: Window Into an Ancient World*. xvi + 625 pp. Cambridge University Press, Cambridge.
Martin, D., Briggs, D.E., and Parkes, R.J. 2004. Experimental attachment of sediment particles to invertebrate eggs and the preservation of soft-bodied fossils. *Journal of the Geological Society* 161: 735–738.
Mayr, G., Pittman, M., Saitta, E., Kaye, T.G., and Vinther, J. 2016. Structure and homology of *Psittacosaurus* tail bristles. *Palaeontology* 59: 793–802.
McMahon, S., Anderson, R.P., Saupe, E.E., and Briggs, D.E. 2016. Experimental evidence that clay inhibits bacterial decomposers: Implications for preservation of organic fossils. *Geology* 44: 867–870.
Moore, M.J., Mitchell, G.H., Rowles, T.K., and Early, G. 2020. Dead cetacean? Beach, bloat, float, sink. *Frontiers in Marine Science 7*: 333.
Morris, W.J. 1970. Hadrosaurian dinosaur bills: Morphology and function. *Contributions in Science of the Los Angeles County Museum of Natural History* 193: 1–14
Mousavi, M., Kabir, S.F., and Fini, E.H. 2022. Effects of sulfur phase transition on moisture-induced damages in bitumen colloidal structure. *Journal of Industrial and Engineering Chemistry* 107: 109–117.
Mu, S. and Stowe, D. 2024. Correlative X-ray microanalysis of a boron steel sample using micro-XRF and SEM-EDS. *Microscopy & Microanalysis* 30: 1.
Nesse, W.D. 2012. *Introduction to Mineralogy*. xvi + 495 pp. Oxford University Press, Oxford.
Newman, S.A., Daye, M., Fakra, S.C., Marcus, M.A., Pajusalu, M., Pruss, S.A., Smith, E.F., and Bosak, T. 2019. Experimental preservation of muscle tissue in quartz sand and kaolinite. *Palaios* 34: 437–451.
Nie, H.Y. and Jahangiri-Famenini, H.R. 2022. Time-of-flight secondary ion mass spectrometry analyses of self-assembled monolayers of octadecyltrimethoxysilane on $SiO_2$ substrate. *Applied Sciences* 12: 4932.
Orr, P.J., Briggs, D.E., and Kearns, S.L. 1998. Cambrian Burgess Shale animals replicated in clay minerals. *Science* 281: 1173–1175.
Osborn, H.F. 1911. A dinosaur mummy. *The American Museum Journal* 11: 7–11.
Osborn, H.F. 1912. Integument of the iguanodont dinosaur *Trachodon*. *American Museum of Natural History Memoir* 1: 33–54.
Page, A., Gabbott, S.E., Wilby, P.R., and Zalasiewicz, J.A. 2008. Ubiquitous Burgess Shale-style "clay templates" in low-grade metamorphic mudrocks. *Geology* 36: 855–858.

Parry, L.A., Smithwick, F., Nordén, K.K., Saitta, E.T., Lozano-Fernandez, J., Tanner, A.R., Caron, J.B., Edgecombe, G.D., Briggs, D.E., and Vinther, J. 2018. Soft-bodied fossils are not simply rotten carcasses-toward a holistic understanding of exceptional fossil preservation: exceptional fossil preservation is complex and involves the interplay of numerous biological and geological processes. *BioEssays* 40: 1700167.

Pautard, F.G.E. 1964. Calcification of keratin. *Progress in the Biological Sciences in Relation to Dermatology* 2: 227.

Pearce, N.J., Perkins, W.T., Westgate, J.A., Gorton, M.P., Jackson, S.E., Neal, C.R., and Chenery, S.P. 1997. A compilation of new and published major and trace element data for NIST SRM 610 and NIST SRM 612 glass reference materials. *Geostandards Newsletter* 21: 115–144.

Pei, L., Jiang, G., Baxter, L.L., and Linford, M.R. 2010. Analysis of Coal by Static Time-of-Flight Secondary Ion Mass Spectrometry (TOF-SIMS). *Surface Science Spectra* 17: 1–67.

Peters, W. 1871. Über neue Reptilien aus Ostafrica und Sarawak (Borneo), vorzüglich aus der Sammlung des Hrn. Marquis J. Doria zu Genua. *Monatsberichte der Königlichen Preussische Akademie des Wissenschaften zu Berlin* 1871: 566–581.

Piombino-Mascali, D., Gill-Frerking, H., and Beckett, R.G. 2017. The taphonomy of natural mummies. *In:* E.M.J. Schotsmans, N. Márquez-Grant, and S.L. Forbes (eds.), *Taphonomy of Human Remains: Forensic Analysis of the Dead and the Depositional Environment*, 101–119. Wiley, Oxford.

Pittman, M., Enriquez, N.J., Bell, P.R., Kaye, T.G., and Upchurch, P. 2022. Newly detected data from *Haestasaurus* and review of sauropod skin morphology suggests Early Jurassic origin of skin papillae. *Communications Biology* 5: 122.

Playter, T., Konhauser, K., Owttrim, G., Hodgson, C., Warchola, T., Mloszewska, A.M., Sutherland, B., Bekker, A., Zonneveld, J.P., Pemberton, S.G., and Gingras, M. 2017. Microbe-clay interactions as a mechanism for the preservation of organic matter and trace metal biosignatures in black shales. *Chemical Geology* 459: 75–90.

Post, J.E. 1999. Manganese oxide minerals: Crystal structures and economic and environmental significance. *Proceedings of the National Academy of Sciences* 96: 3447–3454.

Potter, R.M. and Rossman, G.R. 1979. Mineralogy of manganese dendrites and coatings. *American Mineralogist* 64: 1219–1226.

Powell, W. 2003. Greenschist-facies metamorphism of the Burgess Shale and its implications for models of fossil formation and preservation. *Canadian Journal of Earth Sciences* 40: 13–25.

Qvarnström, M., Niedźwiedzki, G., and Žigaitė, Ž. 2016. Vertebrate coprolites (fossil faeces): An underexplored Konservat-Lagerstätte. *Earth-Science Reviews* 162: 44–57.

Raiswell, R. and Berner, R.A. 1985. Pyrite formation in euxinic and semi-euxinic sediments. *American Journal of Science* 285: 710–724.

Raiswell, R., Whaler, K., Dean, S., Coleman, M.L., and Briggs, D.E.G. 1993. A simple three-dimensional model of diffusion-with-precipitation applied to localised pyrite formation in framboids, fossils and detrital iron minerals. *Marine Geology* 113: 89–100.

Rasool, M.H. and Ahmad, M. 2023. Understanding shale instability through the lens of clay mineralogy and zeta potential. *Geology, Earth & Marine Sciences* 5: 1–10.

Rogers, R.R. 1990. Taphonomy of three dinosaur bone beds in the Upper Cretaceous Two Medicine Formation of northwestern Montana: Evidence for drought-related mortality. *Palaios* 5: 394–413.

Romero-Mujalli, G., Hartmann, J., and Börker, J. 2019. Temperature and $CO_2$ dependency of global carbonate weathering fluxes—implications for future carbonate weathering research. *Chemical Geology* 527: 118874.

Roy, A., Pittman, M., Saitta, E.T., Kaye, T.G., and Xu, X. 2020. Recent advances in amniote palaeocolour reconstruction and a framework for future research. *Biological Reviews* 95: 22–50.

Rybczynski, N., Gosse, J.C., Richard Harington, C., Wogelius, R.A., Hidy, A.J., and Buckley, M. 2013. Mid-Pliocene warm-period deposits in the High Arctic yield insight into camel evolution. *Nature Communications* 4: 1550.

Saitta, E.T. and Vinther, J. 2019. A perspective on the evidence for keratin protein preservation in fossils: An issue of replication versus validation. *Palaeontologia Electronica* 22: 1–30.

Saitta, E.T., Fletcher, I., Martin, P., Pittman, M., Kaye, T.G., True, L.D., Norell, M.A., Abbott, G.D., Summons, R.E., Penkman, K., and Vinther, J. 2018a. Preservation of feather fibers from the Late Cretaceous dinosaur *Shuvuuia deserti* raises concern about immunohistochemical analyses on fossils. *Organic Geochemistry* 125: 142–151.

Saitta, E.T., Gelernter, R., and Vinther, J. 2018b. Additional information on the primitive contour and wing feathering of paravian dinosaurs. *Palaeontology* 61: 273–288.

Saitta, E.T., Kaye, T.G., and Vinther, J. 2019a. Sediment-encased maturation: a novel method for simulating diagenesis in organic fossil preservation. *Palaeontology* 62: 135–150.

Saitta, E.T., Liang, R., Lau, M.C., Brown, C.M., Longrich, N.R., Kaye, T.G., Novak, B.J., Salzberg, S.L., Norell, M.A., Abbott, G.D., Dickinson, M.R., Vinther, J., Bull, I.D., Brooker, R.A., Martin, P., Donohoe, P., Knowles, T.D.J., Penkman, K.E.H., and Onstott, T. 2019b. Cretaceous dinosaur bone contains recent organic material and provides an environment conducive to microbial communities. *Elife* 8: e46205.

Saitta, E.T., Rogers, C., Brooker, R.A., Abbott, G.D., Kumar, S., O'Reilly, S.S., Donohoe, P., Dutta, S., Summons, R.E., and Vinther, J. 2017. Low fossilization potential of keratin protein revealed by experimental taphonomy. *Palaeontology* 60: 547–556.

Saitta, E.T., Vinther, J., Crisp, M.K., Abbott, G.D., Wheeler, L., Presslee, S., Kaye, T.G., Bull, I., Fletcher, I., Chen, X., Vidal, D., Sanguino, F., Buscalioni, A.D., Calvo, J., Sereno, P.C., Baumgart, S.L., Pittman, M., Collins, M.J., Sakalauskaite, J., Mackie, M., Dal Bello, F., Dickinson, M.R., Stevenson, M.A., Donohoe, P., Heck, P.R., Demarchi, B. and Penkman, K.E.H. 2024. Non-avian dinosaur eggshell calcite can contain ancient, endogenous amino acids. *Geochimica et Cosmochimica Acta* 365: 1–20.

Schiffbauer, J.D., Selly, T., Jacquet, S.M., Merz, R.A., Nelson, L.L., Strange, M.A., Cai, Y., and Smith, E.F. 2020. Discovery of bilaterian-type through-guts in cloudinomorphs from the terminal Ediacaran Period. *Nature Communications* 11: 205.

Schulze, D.G. 2005. Clay minerals. *In:* D. Hillel (ed.), *Encyclopedia of Soils in the Environment*, 246–254. Elsevier/Academic Press, Boston.

Schumacher, G. and Juniper, L. 2013. Coal utilisation in the cement and concrete industries. *In:* D. Osborne (ed.), *The Coal Handbook: Towards Cleaner Production*, 387–426. Woodhead Publishing, Cambridge.

Sereno, P.C., Saitta, E.T., Vidal, D., Myhrvold, N., Ciudad Real, M., Baumgart, S.L., Bop, L.L., Keillor, T.M., Eriksen, M., and Derstler, K. 2026. Duck-billed dinosaur fleshy midline and hooves reveal terrestrial clay-template "mummification". *Science* 391: eadw3536.

Shahwan, T., Erten, H.N., Black, L., and Allen, G.C. 1999. TOF-SIMS study of Cs+ sorption on natural kaolinite. *Science of the Total Environment* 226: 255–260.

Shahwan, T., Erten, H.N., Black, L., and Allen, G.C. 2004. ToF-SIMS depth profiling analysis of the uptake of $Ba^{2+}$ and $Co^{2+}$ ions by natural kaolinite clay. *Journal of Colloid and Interface Science* 277: 23–28.

Shatilovich, A., Gade, V.R., Pippel, M., Hoffmeyer, T.T., Tchesunov, A.V., Stevens, L., Winkler, S., Hughes, G.M., Traikov, S., Hiller, M., and Rivkina, E. 2023. A novel nematode species from the Siberian permafrost shares adaptive mechanisms for cryptobiotic survival with *C. elegans* dauer larva. *PLoS Genetics* 19: e1010798.

Shore, A.J., Wood, R.A., Butler, I.B., Zhuravlev, A., McMahon, S., Curtis, A., and Bowyer, F. T. 2021. Ediacaran metazoan reveals lophotrochozoan affinity and deepens root of Cambrian Explosion. *Science Advances* 7: eabf2933.

Siviero, B.C., Rega, E., Hayes, W.K., Cooper, A.M., Brand, L.R., and Chadwick, A.V. 2020. Skeletal trauma with implications for intratail mobility in *Edmontosaurus annectens* from a monodominant bonebed, Lance Formation (Maastrichtian), Wyoming USA. *Palaios* 35: 201–214.

Slagter, S., Konhauser, K.O., Briggs, D.E., and Tarhan, L.G. 2024. Controls on authigenic mineralization in experimental Ediacara-style preservation. *Geobiology* 22: e12615.

Snyder, K., McLain, M., Wood, J., and Chadwick, A. 2020. Over 13,000 elements from a single bonebed help elucidate disarticulation and transport of an *Edmontosaurus* thanatocoenosis. *PLOS ONE* 15: e0233182.

Sparks, D.L. 2003. Inorganic Soil Components. *In:* D.L. Sparks (ed.), *Environmental Soil Chemistry (Second Edition)*, 43–73. Academic Press, San Diego, California.

Sternberg, C.H. 1909. *The Life of a Fossil Hunter*. 286 pp. Henry Holt and Company, New York.

Sternberg, C.M. 1970. Comments on dinosaurian preservation in the Cretaceous of Alberta and Wyoming. *Publications in Palaeontology*, *Ottawa: National Museums of Canada* 4: 3–4.

Stuart, A.J. and Larkin, N.R. 2010. Taphonomy of the West Runton mammoth. *Quaternary International* 228: 217–232.

Surmik, D., Boczarowski, A., Balin, K., Dulski, M., Szade, J., Kremer, B., and Pawlicki, R. 2016. Spectroscopic studies on organic matter from Triassic reptile bones, Upper Silesia, Poland. *PLOS ONE* 11: e0151143.

Szewciw, L.J., De Kerckhove, D.G., Grime, G.W., and Fudge, D.S. 2010. Calcification provides mechanical reinforcement to whale baleen α-keratin. *Proceedings of the Royal Society B: Biological Sciences* 277: 2597–2605.

Taivalkoski, A., Ranta, J.P., Sarala, P., Moilanen, M., Nikkola, P., and Soukka, T. 2024. Pyrite-goethite alteration in supergene oxidation processes in till: Elemental distribution and evaluation of goethite usability as a fingerprinting tool for vectoring mineral deposits. *Minerals* 14: 668.

Tarhan, L.G., Droser, M.L., and Gehling, J.G. 2015. Depositional and preservational environments of the Ediacara Member, Rawnsley Quartzite (South Australia): Assessment of paleoenvironmental proxies and the timing of "ferruginization". *Palaeogeography, Palaeoclimatology, Palaeoecology* 434: 4–13.

Tarhan, L.G., Planavsky, N.J., Wang, X., Bellefroid, E.J., Droser, M.L., and Gehling, J.G. 2018. The late-stage "ferruginization" of the Ediacara Member (Rawnsley Quartzite, South Australia): Insights from uranium isotopes. *Geobiology* 16: 35–48.

Tarhan, L.G., Hood, A.V.S., Droser, M.L., Gehling, J.G., Briggs, D.E.G., Gaines, R.R., Robbins, L.J., and Planavsky, N.J. 2019. Petrological evidence supports the death mask model for the preservation of Ediacaran soft bodied organisms in South Australia. *Geology* 47: e473.

Tazaki, K., Fyfe, W.S., and Dissanayake, C.B. 1987. Weathering of apatite under extreme conditions of leaching. *Chemical Geology* 60: 151–162.

Theng, B.K.G. 1974. *The Chemistry of Clay-Organic Reactions*. xii + 343 pp. John Wiley and Sons, New York.

Tombácz, E. and Szekeres, M. 2006. Surface charge heterogeneity of kaolinite in aqueous suspension in comparison with montmorillonite. *Applied Clay Science* 34: 105–124.

Tweet, J., Chin, K., and Ekdale, A.A. 2016. Trace fossils of possible parasites inside the gut contents of a hadrosaurid dinosaur, Upper Cretaceous Judith River Formation, Montana. *Journal of Paleontology* 90: 279–287.

Uhl, D. 2020. A reappraisal of the" stomach" contents of the *Edmontosaurus annectens* mummy at the Senckenberg Naturmuseum in Frankfurt/Main (Germany). *Zeitschrift der Deutschen Gesellschaft für Geowissenschaften* 171: 71–85.

Vandenbroucke, M. and Largeau, C. 2007. Kerogen origin, evolution and structure. *Organic Geochemistry* 38: 719–833.

Van der Burg, W.J. 1969. The formation of rattle stones and the climatological factors which limited their distribution in the Dutch Pleistocene. 1. The formation of rattle stones. *Palaeogeography, Palaeoclimatology, Palaeoecology* 6: 105–124.

Velasco-Rodríguez, Ó., Fil, M., Heggeset, T.M., Degnes, K.F., Becerro-Recio, D., Kolsaková, K., Haugen, T., Jønsson, M., Toral-Martínez, M., García-Estrada, C., and Sola-Landa, A. 2022. Characterization of microbial diversity in decayed wood from a Spanish forest: an environmental source of industrially relevant microorganisms. *Microorganisms* 10: 1249.

Vinther, J. 2015. A guide to the field of palaeo colour: Melanin and other pigments can fossilise: Reconstructing colour patterns from ancient organisms can give new insights to ecology and behaviour. *BioEssays* 37: 643–656.

Vinther, J., 2020. Reconstructing vertebrate paleocolor. *Annual Review of Earth and Planetary Sciences* 48: 345–375.

Wacey, D., Saunders, M., Roberts, M., Menon, S., Green, L., Kong, C., Culwick, T., Strother, P., and Brasier, M.D. 2014. Enhanced cellular preservation by clay minerals in 1 billion-year-old lakes. *Scientific Reports* 4: 5841.

Wang, S., Liu, Q., Tan, X., Xu, C., and Gray, M.R. 2013. Study of asphaltene adsorption on kaolinite by X-ray photoelectron spectroscopy and time-of-flight secondary ion mass spectroscopy. *Energy & Fuels* 27: 2465–2473.

Warnett, J.M., Williams, M.A., Wilson, P.F., and Smith, M.P. 2021. The Oxford Dodo. Seeing more than ever before: X-ray micro-CT scanning, specimen acquisition and provenance. *Historical Biology* 33: 2247–2255.

White, A.F., Bullen, T.D., Schulz, M.S., Blum, A.E., Huntington, T.G., and Peters, N.E. 2001. Differential rates of feldspar weathering in granitic regoliths. *Geochimica et Cosmochimica Acta* 65: 847–869.

White, P.A. and Diedrich, C.G. 2012. Taphonomy story of a modern African elephant *Loxodonta africana* carcass on a lakeshore in Zambia (Africa). *Quaternary International* 276: 287–296.

Wiemann, J., Fabbri, M., Yang, T.R., Stein, K., Sander, P.M., Norell, M.A., and Briggs, D.E. 2018. Fossilization transforms vertebrate hard tissue proteins into N-heterocyclic polymers. *Nature Communications* 9: 4741.

Wilson, L.A. and Butterfield, N.J. 2014. Sediment effects on the preservation of Burgess Shale-type compression fossils. *Palaios* 29: 145–154.

Wilson, M.J. 2004. Weathering of the primary rock-forming minerals: Processes, products and rates. *Clay Minerals* 39: 233–266.

Worthy, T.H. 1989. Mummified moa remains from Mt Owen, northwest Nelson. *Notornis* 36: 36–38.

Wosik, M. and Evans, D.C. 2022. Osteohistological and taphonomic life-history assessment of *Edmontosaurus annectens* (Ornithischia: Hadrosauridae) from the Late Cretaceous (Maastrichtian) Ruth Mason dinosaur quarry, South Dakota, United States, with implication for ontogenetic segregation between juvenile and early adult hadrosaurids. *Journal of Anatomy* 241: 272–296.

Xu, X., Zhou, Z., Wang, Y., and Wang, M. 2020. Study on the Jehol Biota: Recent advances and future prospects. *Science China Earth Sciences* 63: 757–773.

Yang, Z., Jiang, B., Xu, J., and McNamara, M.E. 2024. Cellular structure of dinosaur scales reveals retention of reptile-type skin during the evolutionary transition to feathers. *Nature Communications* 15*:* 4063.

Yudovich, Y.E. and Ketris, M.P. 2006. Chlorine in coal: A review. *International Journal of Coal Geology* 67: 127–144.

Zazzeri, G., Lowry, D., Fisher, R.E., France, J.L., Lanoisellé, M., Kelly, B.F., Necki, J.M., Iverach, C.P., Ginty, E., Zimnoch, M., and Jasek, A. 2016. Carbon isotopic signature of coal-derived methane emissions to the atmosphere: from coalification to alteration. *Atmospheric Chemistry and Physics* 16: 13669–13680.

Zhang, J., Tang, J., Liu, L., and Wang, J. 2021. The evolution of catalytically active calcium catalyst during steam gasification of lignite char. *Carbon* 172: 162–173.

Zhu, X., Zhu, Z., Lei, X., and Yan, C. 2016. Defects in structure as the sources of the surface charges of kaolinite. *Applied Clay Science* 124: 127–136.